АВТОМАТИКА
и
ТЕЛЕМЕХАНИКА

Volume 19, No. 3

March 1958

UNIVERSITY
OF MICHIGAN

MAY 4 - 1959

ENGINEERING
LIBRARY

SOVIET INSTRUMENTATION AND
CONTROL TRANSLATION SERIES

Automation and Remote Control

(The Soviet Journal *Avtomatika i Telemekhanika* in English Translation)

■ This translation of a Soviet journal on automatic control is published as a service to American science and industry. It is sponsored by the Instrument Society of America under a grant in aid from the National Science Foundation, continuing a program initiated by the Massachusetts Institute of Technology.

SOVIET INSTRUMENTATION AND CONTROL TRANSLATION SERIES

Instrument Society of America Executive Board

Henry C. Frost
President
Robert J. Jeffries
Past President
John Johnston, Jr.
President-Elect-Secretary
Glen G. Gallagher
Dept. Vice President
Thomas C. Wherry
Dept. Vice President
Philip A. Sprague
Dept. Vice President
Ralph H. Tripp
Dept. Vice President
Howard W. Hudson
Treasurer
Willard A. Kates
Executive Assistant—Districts
Benjamin W. Thomas
Executive Assistant—Conferences
Carl W. Gram, Jr.
Dist. I Vice President
Charles A. Kohr
Dist. II Vice President
J. Thomas Elder
Dist. III Vice President
George L. Kellner
Dist. IV Vice President
Gordon D. Carnegie
Dist. V Vice President
Glenn F. Brockett
Dist. VI Vice President
John F. Draffen
Dist. VII Vice President
John A. See
Dist. VIII Vice President
Adelbert Carpenter
Dist. IX Vice President
Joseph R. Rogers
Dist. X Vice President

Headquarters Office

William H. Kushnick
Executive Director
Charles W. Covey
Editor, ISA Journal
George A. Hall, Jr.
Assistant Editor, ISA Journal
Herbert S. Kindler
Director, Tech. & Educ. Services
Ralph M. Stotsenburg
Director, Promotional Services
William F. Minnick, Jr.
Promotion Manager

ISA Publications Committee

Nathan Cohn, *Chairman*
Jere E. Brophy, Enoch J. Durbin, George R. Feeley, Richard W. Jones, George A. Larsen, Thomas G. MacAnespie, John E. Read, Joshua Stern, Frank S. Swaney, Richard A. Terry

Translations Advisory Board of the Publications Committee

Jere E. Brophy, *Chairman*
T. J. Higgins, S. G. Eskin, G. Werbizky

■ This translation of the Soviet Journal *Avtomatika i Telemekhanika* is published and distributed at nominal subscription rates under a grant in aid to the Instrument Society of America from the National Science Foundation. This translated journal, and others in the Series (see back cover), will enable American scientists and engineers to be informed of work in the fields of instrumentation, measurement techniques and automatic control reported in the Soviet Union.

The original Russian articles are translated by competent technical personnel. The translations are on a cover-to-cover basis, permitting readers to appraise for themselves the scope, status and importance of the Soviet work.

Publication of *Avtomatika i Telemekhanika* in English translation started under the present auspices in April 1958 with Russian Vol. 18, No. 1 of January 1957. Translation of Vol. 18 has now been completed. The twelve issues of Vol. 19 will be published in English translation by mid-1959.

All views expressed in the translated material are intended to be those of the original authors, and not those of the translators, nor the Instrument Society of America.

Readers are invited to submit communications on the quality of the translations and the content of the articles to ISA headquarters. Pertinent correspondence will be published in the "Letters" section of the ISA Journal. Space will also be made available in the ISA Journal for such replies as may be received from Russian authors to comments or questions by American readers.

Subscription Prices:

Per year (12 issues), starting with Vol. 19, No. 1

General: United States and Canada	$30.00
Elsewhere	33.00
Libraries of non-profit academic institutions: United States and Canada	$15.00
Elsewhere	18.00
Single issues to everyone, each	$ 6.00

See back cover for combined subscription to entire Series.

Subscriptions and requests for information on back issues should be addressed to the:

Instrument Society of America
313 Sixth Avenue, Pittsburgh 22, Penna.

Translated and printed by Consultants Bureau, Inc.

Volume XIX No. 3 – March 1958

English Translation Printed February 1959

Automation and Remote Control

The Soviet Journal Avtomatika i Telemekhanika in English Translation

Avtomatika i Telemekhanika is a Publication of the Academy of Sciences of the USSR

EDITORIAL BOARD
as Listed in the Original Soviet Journal

Corr. Mem. Acad. Sci. USSR V. A. Trapeznikov, *Editor in Chief*
Dr. Phys. Math. Sci. A. M. Letov, *Assoc. Editor*
Academician M. P. Kostenko
Academician V. S. Kulebakin
Corr. Mem. Acad. Sci. USSR B. N. Petrov
Dr. Tech. Sci. M. A. Aizerman
Dr. Tech. Sci. V. A. Il'in
Dr. Tech. Sci. V. V. Solodovnikov
Dr. Tech. Sci. B. S. Sotskov
Dr. Tech. Sci. Ia. Z. Tsypkin
Dr. Tech. Sci. N. N. Shumilovskii
Cand. Tech. Sci. V. V. Karibskii
Cand. Tech. Sci. G. M. Ulanov, *Corresp. Secretary*
Eng. S. P. Krasivskii
Eng. L. A. Charikhov

See following page for Table of Contents.

Copyright by Instrument Society of America 1959

AUTOMATION AND REMOTE CONTROL

Volume 19, Number 3 March, 1958

CONTENTS

	PAGE	RUSS. PAGE
Analysis of Properties and Synthesis of Automatic Control Systems with Lag. Fan Chun-Wui	187	197
Increasing the Speed of Certain Automatic Control Systems by Means of Nonlinear and Computing Devices. G. M. Ostrovskii	199	208
Concerning a Possibility of Determining an Axial Hydrodynamic Force in a Valve. I. M. Krassov, and B. G. Turbin	210	217
The Theory of the Structure of Combiner Mechanisms. S. M. Iakovlev	214	221
The Transients in a Magnetic Amplifier Connected Via A Rectifier to an Inductive Load. L. V. Safris	220	228
The Calculation of a Choke Magnetic Amplifier Connected to a Single-Phase Bridge Rectifier. N. A. Kaluzhnikov	231	239
Contactless Determination of Specific Electrical Resistance. G. G. Iarmol'chuk	250	257
A Linear Induction Potentiometer for Industrial Use. O. I. Aven, S. M. Domanitskii, and Iu. M. Pul'er	261	268
Telemetering Compensation Device for Linear Transference. A. A. Kol'tsov and L. F. Kulikovskii	274	280

12-149244
S.O.

ANALYIS OF PROPERTIES AND SYNTHESIS OF AUTOMATIC CONTROL SYSTEMS WITH LAG

Fan Chun Wui

(Moscow)

A method of synthesizing compensating devices of servo systems [1-3] is extended to handle systems with lags. Curves are developed for synthesizing systems with lags and for analyzing their properties. Circle diagrams are constructed for the determination of the distortion function of the real frequency characteristics for different values of lag.

In most works concerned with automatic control systems containing lags, attention is principally directed towards the investigation of stability [4, 5].

In the present paper a method is presented for estimating the influence of lag on the properties of an automatic control system, a method which makes possible the synthesis of the proper compensating device by using the frequency characteristics of the system which would obtain were the lags not present.

1. Initial Relationships

It will be assumed that the stabilizing feedback path does not shunt any lag elements, and that the system under consideration is stable for sufficiently large gain [6].

We denote by KW(s) the transfer function of the open-loop system, excluding the lag element. Then, the transfer function of the closed system, having but one feedback path, will have the form:

$$\Phi_\tau(s) = \frac{KW(s)\,e^{-\tau s}}{1 + KW(s)\,e^{-\tau s}}, \qquad (1)$$

where τ is the lag time.

We introduce the following notation:

$$KW(j\omega) = U(\omega) + jV(\omega), \quad \Phi_\tau(j\omega) = P_\tau(\omega) + jQ_\tau(\omega).$$

Substituting $s = j\omega$ in Expression (1), we obtain the system's frequency characteristic:

$$\Phi_\tau(j\omega) = P_\tau + jQ_\tau = \frac{(U + jV)\,e^{-j\tau\omega}}{1 + (U + jV)\,e^{-j\tau\omega}}. \qquad (2)$$

We shall consider the real part of $\Phi_\tau(j\omega)$:

$$P_\tau = \frac{U^2 + V^2 + U\cos\tau\omega + V\sin\tau\omega}{1 + U^2 + V^2 + 2(U\cos\tau\omega + V\sin\tau\omega)}. \quad (3)$$

We introduce more notation:

$$F = \frac{U(\cos\tau\omega - 1) + V\sin\tau\omega}{(1+U)^2 + V^2}, \quad (4)$$

$$G = \frac{F}{1+2F} = \frac{U(\cos\tau\omega - 1) + V\sin\tau\omega}{(1+U)^2 + V^2 + 2U(\cos\tau\omega - 1) + 2V\sin\tau\omega}, \quad (5)$$

$$P = \mathrm{Re}\,\frac{KW(j\omega)}{1 + KW(j\omega)}. \quad (6)$$

After a simple transformation, Expression (3) may be written in the form

$$P_\tau = \frac{P+F}{1+2F} = P - G(2P-1). \quad (7)$$

As will become clear in the sequel, $G(\omega, \tau)$ of (7) can be considered as the distortion function.

Expression (7) gives the relationship between the real frequency characteristics of the system with, and without, lag. It is known that the real frequency characteristic completely determines the behavior of the system with a single step-wise action, and has also some bearing on the behavior of systems with other modes of action. The problem thus reduces to the study of the influence of lagging links on the nature of the variation of the real frequency characteristic. We shall assume that the form of the function $P(\omega)$ has been chosen to meet the qualitative conditions affecting the synthesis of the system when lag is not taken into account. In this case, the term $G(2P-1)$ completely depends on the function G.

The problem thus consists of the following:

1) to find the relationship between the distortion function $G(\omega, \tau)$ and the parameter τ, i.e., to find the quantitative change in the real frequency characteristic when a lag of time τ is present;

2) for a given value of τ, to carry out the synthesis of a compensating device which will allow the given qualitative demands on the system to be met.

Consider the function $G(\omega, \tau)$. After a slight transformation, we obtain from Expression (5)

$$\left[U + \frac{(2G-1)\cos\tau\omega + 1}{2G}\right]^2 + \left[V + \frac{(2G-1)\sin\tau\omega}{2G}\right]^2 = \frac{(2G-1)(\cos\tau\omega - 1)}{2G^2}. \quad (8)$$

For a given value, G = const; by changing the value of $\tau\omega$ we obtain the equations for a family of circles in the $KW(j\omega)$ plane. Holding $\tau\omega$ = const and varying G, we obtain another family of circles (Fig. 1-5).

2. Circle Diagrams for the Distortion Function $G(\omega, \tau)$.

We wish to dwell now on a question which has great practical interest. Let us assume that $G = G_a$ and $\tau\omega = \varphi_a$. Substituting these values in (8) we obtain a circle, A, on the $KW(j\omega)$ plane (Fig. 6). On the same plane we plot the frequency characteristic, $KW(j\omega)$. We assume that the circle A and the frequency characteristic $KW(j\omega)$ intersect in the points a and b, corresponding to the frequencies ω_a and ω_b. On the basis of the circle diagrams, Fig. 1-5, we have that, if the lag time of the system $\tau \leq \tau_a = \varphi_a/\omega_a$ then, in the frequency interval $0 < \omega < \omega_a$ the very important inequality holds:

$$|G| < |G_a|. \quad (9)$$

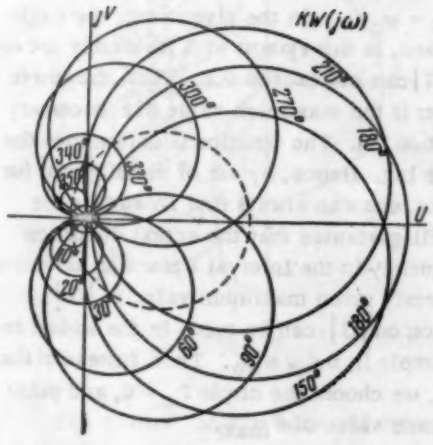

Fig. 1. Circle diagram for G = −0.1 and various values of $\tau\omega$.

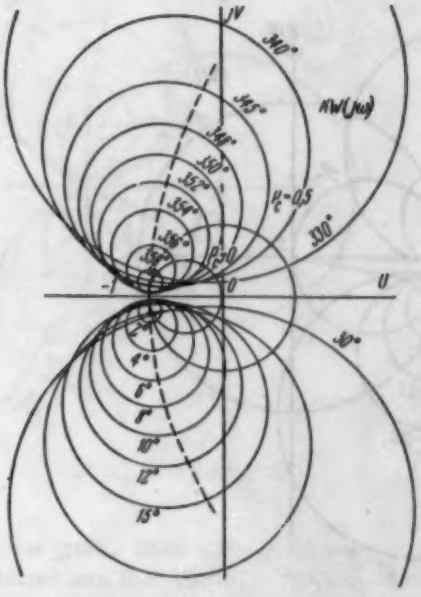

Fig. 2. The same as Fig. 1, but magnified four times.

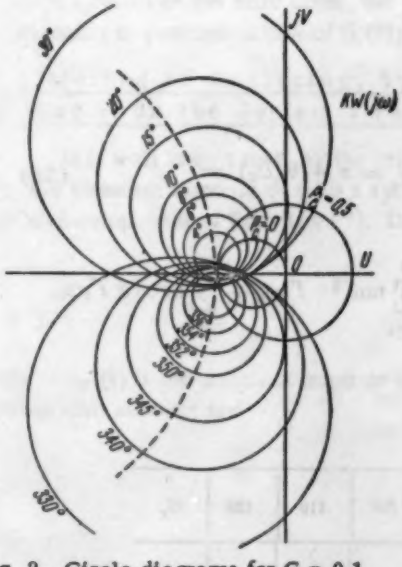

Fig. 3. Circle diagrams for G = 0.1.

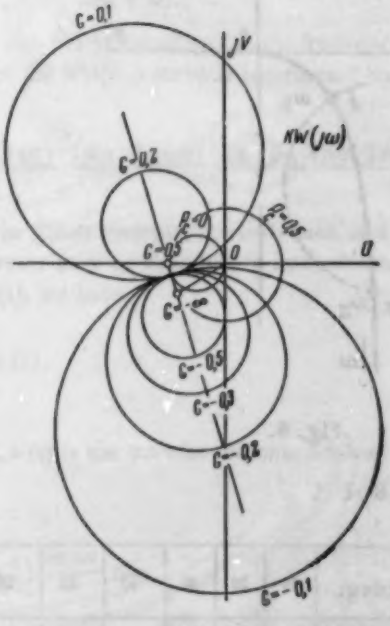

Fig. 4. Circle diagram for $\tau\omega = 30°$ and various values of G.

This inequality does not hold at point b. For $\tau \leq \varphi_a / \omega_b$ in the frequency interval $\omega_a < \omega < \omega_b$, $|G_a$ may be larger than $|G_a$, since all the remaining circles for $|G_a > |G_a$ and $\tau\omega < \varphi_a$ lie inside circle A. We shall call the point a the first point of intersection, and point b the second.

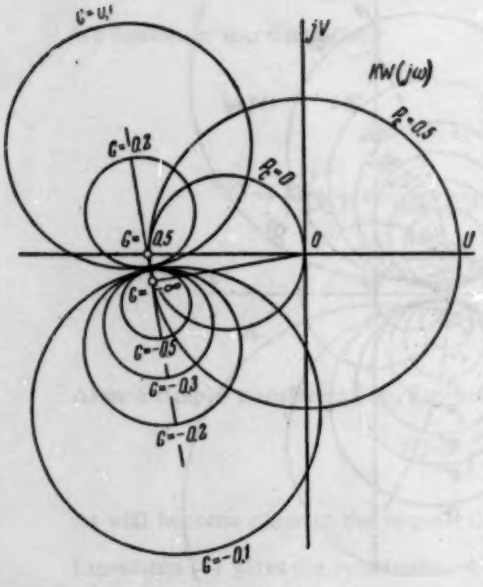

Fig. 5. Circle diagrams for $\tau\omega = 10°$.

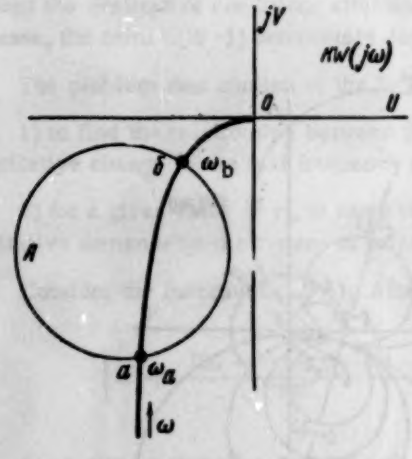

Fig. 6.

We consider the circle diagram for $G = -0.1$ (Fig. 7). On the $KW(j\omega)$ plane we construct the characteristic, $KW(j\omega)$, which is intersected at point C, corresponding to the cut-off frequency ω_c, by one circle of the proper radius. Through point C there passes just one circle of the family, G = const. We assume that point C is the first point of intersection. From this follows the obvious result: if the lag time in the system $\tau \leq \tau_c = \varphi_c/\omega_c$ (in the given case, the angle φ_c equals 6°) then, in this system with frequency $\omega < \omega_c$, the value of $|G|$ can not exceed 0.1. Thus, the lower is ω_c, the higher is the maximum value of τ necessary to satisy Condition (9). The function G determines the influence of the lag. Hence, by use of the diagram for the given system, one can always find an admissible τ_{max} which will guarantee that the actual distortion of the real frequency in the interval $0 \leq \omega \leq \omega_c$ does not exceed a previously given maximum value of $|G|$. Such a limitation on $|G|$ can be made in the widest intervals, for example in $0 \leq \omega \leq \omega_p$. Then, instead of the circle $P_c = 0.5$, we choose the circle $P_c = 0$, and point II determines some value of τ_{max}.

We consider now the obverse problem. If $KW(j\omega)$ and τ are given, then one may find the maximum value of the distortion coefficient, $|G|$, in, for example, the interval $0 \leq \omega \leq \omega_c$. For the solution of this problem, one may make use of Table 1.

Table 1 is entered with specific values of $\gamma_c = \pi + \theta(\omega_c)$ and $\varphi = \omega_c\tau$. The quantity γ_c can always be found from a known equation if $KW(j\omega)$ is known:

$$\gamma_c = \pi + \theta(\omega_c) = \tag{10}$$

$$= \pi - \nu\frac{\pi}{2} - \sum_{i=1}^{p} \tan^{-1} T_i\omega_c + \sum_{i=1}^{\mu} \operatorname{arc\,tg} T'_i\omega_c.$$

TABLE 1

γ_c deg.	10	20	30	40	50	60	70	80	90	100	110	120	G_c
	0.5	1	1.5	2	2.5	3	3.5	4	4.7	5.2	6.2	7.4	—0.05
	1	2	3	4	5	6	7.2	8,7	9.8	11.2	13	15	—0.10
	1.5	2.8	4	5.3	6.8	8.1	9.8	11,8	13.3	16	18	20.5	—0.15
φ, deg.	2	4	5.6	7	9	11	13	15,5	17.5	19.5	23	26	—0.20
	2.5	5	7,5	10	12.5	17.5	20	22	25.5	30	35	40	—0.30
	3.2	5.5	8.5	11.2	13.5	18.2	21.5	24	27.5	32	37	41	—0.40
	4	6	9.5	12.5	16	19	23	29	32.5	36.5	40	44	—0.50

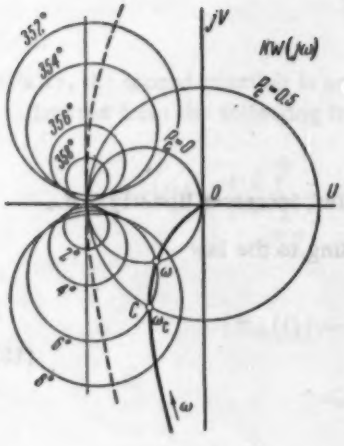

Fig. 7

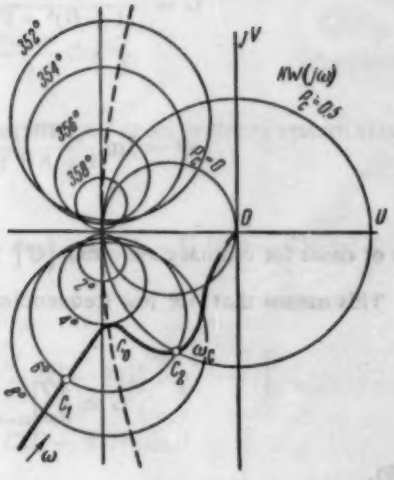

Fig. 8

The quantity $\omega_c \tau$ is known if the system lag time, τ, is given. From these parameters, it is possible to find G_c from Table 1. If point C is the first point of intersection, then the value of G_c is indeed $|G|_{max}$ in the given interval.

We now consider the case when point C of Fig. 7 is not the first point of intersection (Fig. 8). The frequency characteristic first intersects the circle at point C_1 and thereafter at point C_2. In this case, the cut-off frequency corresponds to point C_2. In order to satisfy the inequality $|G| \leq |G_a|$ for $0 \leq \omega \leq \omega_c$, it is necessary that τ be limited by the inequality $\tau \leq \varphi_{c0}/\omega_c$ instead of $\tau \leq \varphi_{c2}/\omega_c$, where φ_{c0} is the index of the circle tangent to KW(jω) at some point C_0 (in the given, $\varphi_{c0} = 4°$, $\varphi_{c2} = 6°$).

In first and second order static, and astatic, systems, G can not be positive for low frequencies, but for astatic systems of the third order, the low frequency portion of the KW(jω) curve is intersected by circles corresponding to positive values of G (Fig. 3).

3. Method of Analyzing, by Means of the Distortion Function G, the Influence of Lag τ on the System's Performance Quality

It is well known that, by the principle of superposition in linear systems, the influence of a lag element on the transient response of such a system with step-wise response may be determined immediately from the second component of Equation (7). Denoting this term by $\varepsilon(t)$, we have

$$x_\tau(t) = x(t) + \varepsilon(t),$$

where $x_\tau(t)$ is the transient response taking lag into account, $x(t)$ is the transfer response without lag being taken into account and

$$\varepsilon(t) = -\frac{2}{\pi}\int_0^\infty G(2P-1)\frac{\sin \omega t}{\omega}\, d\omega. \qquad (11)$$

We mention some properties of the distortion function G.

It is clear from Formula (5) that for sufficiently small values of $\tau\omega$, the function G may be written in the form

$$G = \frac{V\tau\omega}{(1+U)^2+V^2} = Q\tau\omega, \tag{12}$$

where

$$Q = \operatorname{Im}\frac{KW(j\omega)}{1+KW(j\omega)}.$$

In the majority of cases for ordinary systems, $|Q|$, for low frequencies, increases linearly, i.e., $Q \approx \left.\frac{dQ}{d\omega}\right|_{\omega=0} \omega$. This means that, for low frequencies, G varies according to the law

$$G \approx \left.\frac{dQ}{d\omega}\right|_{\omega=0} \tau\omega^2 \tag{13}$$

(cf. curve 2 on Fig. 9).

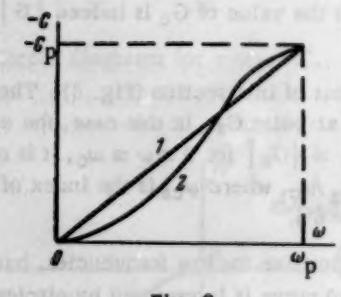

Fig. 9.

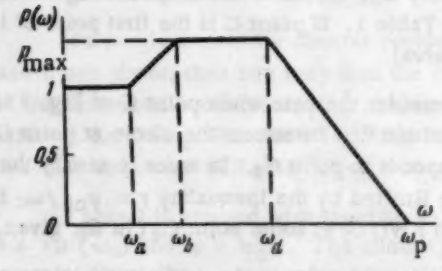

Fig. 10.

If it is known that, for $\omega < \omega_p$, $|G|$ is always less than a certain value, $|G_p|$ then, for $\omega \leq \omega_p$, the form of the function G is approximately as shown in Fig. 9 (curve 2).

In order to simplify the subsequent discussion without thereby introducing significant error, we shall assume, on the basis of the representation given above, that in the interval $0 \leq \omega \leq \omega_p$ G varies linearly, with slope given by $\tan\alpha = G_p/\omega_p$, i.e.,

$$G \approx \frac{G_p}{\omega_p}\omega \quad (\text{for } \omega \leqslant \omega_p). \tag{14}$$

We now find an approximate value for the second member of the transient function $\epsilon(t)$. It will be assumed that the real frequency characteristic, $P(\omega)$, is of the type shown in Fig. 10, the parameters of which, as determined by the conditions on its properties, may be the following [1]:

$$\chi = \frac{\omega_d}{\omega_p} \leqslant 0{,}8,\ \lambda = \frac{\omega_b}{\omega_p} \geqslant 0.5.\ \chi_a = \tag{15}$$

$$= \frac{\omega_a}{\omega_b} \geqslant 0.4.$$

On the basis of Equation (11), and taking Condition (14) into account, one may write

$$\varepsilon(t) = -\frac{2}{\pi}\int_0^{\omega_p}\frac{G_p}{\omega_p}\omega(2P-1)\frac{\sin\omega t}{\omega}d\omega - \tag{16}$$

$$-\frac{2}{\pi}\int_{\omega_p}^{\infty}G(2p-1)\frac{\sin\omega t}{\omega}d\omega.$$

Initially, the second member is negligible. As in the analysis of an ordinary system (Fig. 11), its value may be estimated from the following inequality [1]:

$$|\varepsilon_2(t)| = \left|\frac{2}{\pi}\int_{\omega_p}^{\infty} - G(2P-1)\frac{\sin\omega t}{\omega}d\omega\right| \leqslant 0.3|-G(2P-1)_{\min}|$$

or

$$|\varepsilon_{\tau 2}(t)| = \left|\frac{2}{\pi}\int_{\omega_p}^{\infty}\{P+[-G(2P-1)]\}\frac{\sin\omega t}{\omega}d\omega\right| \leqslant$$

$$\leqslant 0.3|\{P+[-G(2P-1)]\}_{\min}. \tag{17}$$

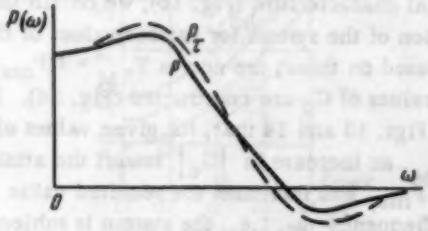

Fig. 11.

Moreover, it is known that the entire real frequency characteristic can be represented as a collection of a certain number of trapezoidal frequency characteristics, and (16) can be written in the form

$$-\frac{\varepsilon(t)}{G_p} = \frac{4}{\pi\omega_p}\sum_i\int_0^{\omega_p'}P_i\sin\omega t\,d\omega + \frac{2(\cos\omega_p t-1)}{\pi\omega_p t}, \tag{18}$$

where P_i is an elementary trapezoid of the collection.

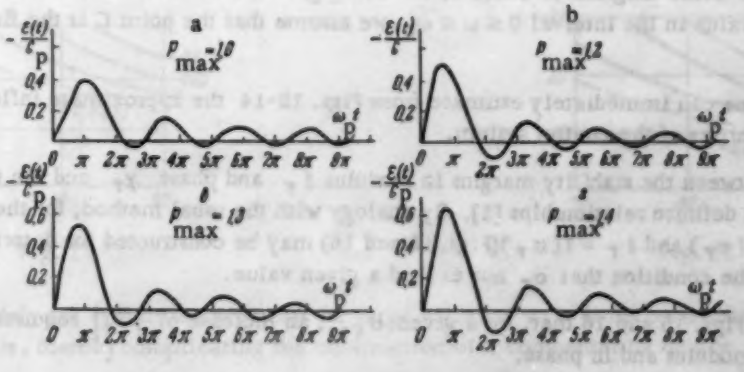

Fig. 12.

For the typical real frequency characteristic (Fig. 10), Expression (18) is written in the form

$$-\frac{\varepsilon(t)}{G_p}=\frac{2}{\pi}\left\{\frac{\cos\omega_p t-1}{\omega_p t}+\frac{2}{\omega_p t}P_{max}\left[1-\frac{\sin\omega_p t-\sin\chi\omega_p t}{(1-\chi)\omega_p t}\right]-\right.$$
$$\left.-\frac{2}{\omega_p t}(P_{max}-1)\left[1-\frac{\sin\omega_b t-\sin\chi_a\omega_b t}{(1-\chi_a)\omega_b t}\right]\right\}. \qquad (19)$$

Bearing in mind that (15) holds, and substituting the numerical values from (15) into Equation (19, we obtain the curve $-\epsilon(t)/G_p$ for different values of P_{max} (Fig. 12).

It is clear from Fig. 12 that, for $G_p < 0$, the quantity $-\epsilon(t)/G_p$ will be positive. In this case, the transient response $x_\tau(t)$ will be aggravated. Its overcompensation, σ_τ, will be approximately equal to the sum of the overcompensation of the function $x(t)$ and the maximum value of $\epsilon(t)$. Now the graph of $\sigma_M = f(P_{max})$, constructed in [1], may be reconstructed taking into account the effect of the lag, τ. We thus obtain the family $\sigma_{\tau M} = f(P_{max})$ for various values of G_c (Fig. 13). For $G_c = 0$, the curve $\sigma_{\tau M} = f(P_{max})$ coincides with the curve for the ordinary system without lag. We note that for positive values of G at low frequencies, the compensation in systems with lag is low compared to the same system without lag. But, in first and second order static and astatic systems, the value of G cannot in general be positive.

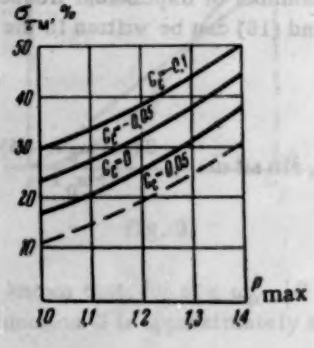

Fig. 13

Now we turn to the influence of lag on the magnitude of the regulation time, T. From the transfer function $x(t)$ [1, 3] and from $-\epsilon(t)/G_p$ for the corresponding typical characteristic (Fig. 10), we obtain the transfer function of the system for various values of the lag, $x_\tau(t)$. Based on these, the curves $T_{\tau M} = f(P_{max})$ for different values of G_c are constructed (Fig. 14). It is clear from Figs. 13 and 14 that, for given values of $\sigma_{\tau M}$ and $T_{\tau M}$, an increase in $|G_c|$ lowers the attainable value of P_{max} and increases the required value of the cutoff frequency ω_c, i.e., the system is subject to more stringent requirements. Thus, Figs. 12-14 give an approximate idea of the properties of a system with lag elements.

On the basis of what has gone before, we can assert the following sequence of analytical steps.

1. We determine ω_c from the given frequency characteristics, $KW(j\omega)$, not taking lag into account.

2. From either the circle diagram or Table 1, and being given τ, we determine the value of G_c which has the largest absolute value in the interval $0 \le \omega \le \omega_c$ (we assume that the point C is the first point of intersection).

3. Knowing G_c, one can immediately estimate from Figs. 12-14 the approximate influence of the lag on the fundamental properties of the control system.

It is known that between the stability margins in modulus l_τ and phase γ_τ and the magnitude of the compensation there exist definite relationships [1]. By analogy with the usual method, for the cases when $G \neq 0$ graphs of $\gamma_\tau = f(\sigma_\tau)$ and $l_\tau = f(\sigma_\tau)$ (Figs. 15 and 16) may be constructed for determining the necessary γ_τ and l_τ from the condition that σ_τ not exceed a given value.

We establish from Figs. 15 and 16 that, for a given $\sigma_{\tau M}$, an increase of $|G_c|$ requires an increase in the stability margins in modulus and in phase.

4. Method of Synthesizing Compensating Devices for Systems with Lag Elements

It is known that, to attain adequate accuracy in reproducing the controlling effect, g(t), which is different from unity, in the frequency interval $0 \leq \omega \leq \omega_g$, in which the frequency characteristic of the effect is itself sensibly different from zero, the system's frequency characteristic must satisfy the approximate equalities [1]:

$$P_\tau(\omega) \approx 1, \quad Q_\tau(\omega) \approx 0 \quad \text{for} \quad 0 \leqslant \omega \leqslant \omega_g, \ \omega_g < \omega_n. \tag{20}$$

From (7) and (20) we obtain

$$P(\omega) = \frac{1-G}{1-2G} \approx \frac{1-G_n\frac{\omega}{\omega_p}}{1-2G_n\frac{\omega}{\omega_p}} \quad \text{for} \quad 0 \leqslant \omega \leqslant \omega_g. \tag{21}$$

Expression (21) indicates the desirable form of the function $P(\omega)$ in the interval $0 \leq \omega \leq \omega_g$ with lag present in the system.

It is clear from (21) that, at low frequencies and with sufficiently low values of τ or G_p, the function $P(\omega) \approx 1$. Consequently, the desired logarithmic gain characteristic at low frequencies does not differ from the desired logarithmic gain characteristic of the ordinary system with the identical requirements on the accuracy of reproduction of the controlling signal.

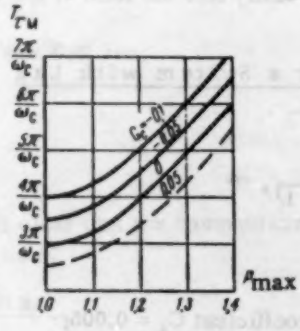

Fig. 14

The form of the desired logarithmic gain characteristic in the intermediate frequency range is determined by the basic requirements for stability margins and from the given desiderata for the system's properties for one step-wise controlling section. The desired logarithmic gain characteristic is found from Figs. 12-16 and Table 1. From the given values of $\sigma_{\tau M}$, $T_{\tau M}$ and τ, it is possible to determine, from Figs. 12-16, the values of ω_c, G_c and the necessary values of stability margins in modulus, l_τ, and in phase γ_τ. It is clear that, for the usual linear system, $G_c = 0$.

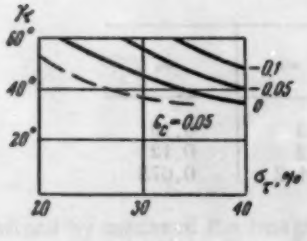

Fig. 15

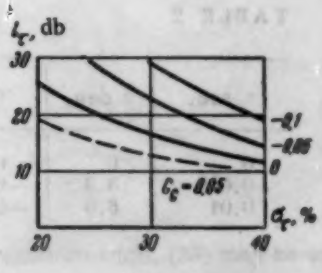

Fig. 16

In order to satisfy the system requirements for large values of τ, it is necessary that the modulus and phase margins be very large, thereby complicating the construction of a compensating device.

The form of the logarithmic gain characteristic at high frequencies does not esentially influence the system performance.

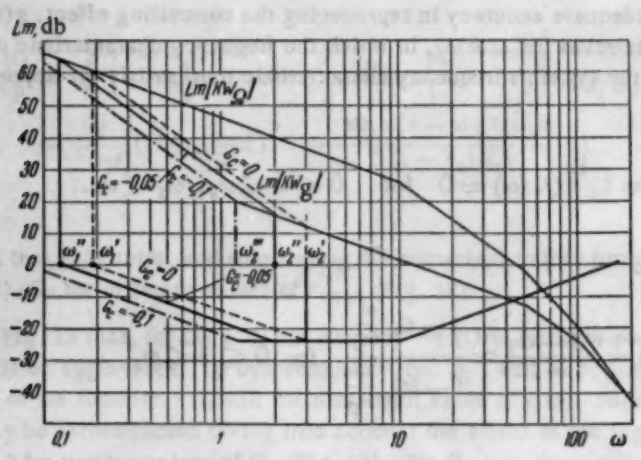

Fig. 17

In this manner we determine the desired logarithmic gain characteristic of the system with lag elements. After having thus determined the logarithmic gain characteristic, one may easily find the form of the compensating device.

Example of the Synthesis of a Compensating Device for a System with Lag

We assume that we are given an object with transfer function

$$KW_{\Omega}(s) = \frac{1}{s(0.1s+1)(0.02s+1)(0.01s+1)(0.005s+1)}\, e^{-\tau s} \qquad (22)$$

and that the given conditions on system properties may thus be stated:

a) the system must have first order astaticism, and a velocity error coefficient $C_1 = 0.005$;

b) the compensation, σ_τ, for one step-wise controlling action must not exceed 40%, and the transient response time, T, must not be greater than one second.

For the given values of control time and compensation, we choose, using Figs. 13 and 14, an approximate value of the cutoff frequency, $\omega_c = 11.5$. Further calculations will be made on the basis of three different values of $\tau = 0$, 0.005 and 0.01 sec. We find the values of $\varphi = \tau\,\omega_c$ for the stated values of τ (Table 2).

TABLE 2

τ, sec.	φ, deg.	G_c	$l_{1,2}$ db	γ_τ, deg.	ω_2	ω_1
0	0	0	±12	35	3	0.19
0.005	3.3	—0.05	±16	41	2	0.12
0.01	6.6	—0.1	±19	48	1.2	0.078

Above all, we must obtain the value of the distortion function $|G_c|$ from Table 1, entering the table with φ and γ_c. The magnitude of γ_c we choose, as is customary, approximately in the interval $20° \leq \gamma_c \leq 80°$. In this interval we seek the lowest value of $|G_c|$ (Table 2).

Knowing G_c and σ_τ it is possible, by using Figs. 15 and 16, immediately to determine the required stability margins both in phase and in modulus (cf. Table 2).

Using Formula (10) we find, as for the ordinary linear system, the greatest value of the conjugating frequency, ω_2, for which $\gamma_T \geq 35°$ ($G_C = 0$), $\gamma_T \geq 41°$ ($G_C = -0.05$) and $\gamma_T \geq 48°$ ($G_C = -0.1$).

The values of the mating frequencies ω_2 and ω_1 are given in Table 2.

It is easily verified that the stability margin in phase, for $\omega = \omega_C$, is satisfactory.

Figure 17 gives the desired logarithmic gain characteristics for $\tau = 0$, 0.005 and 0.01 sec. The same figure gives the logarithmic gain characteristics for the compensating device at low and intermediate frequencies. To avoid complications, the high-frequency portion of the compensating device's logarithmic gain characteristic was not corrected, which does not essentially influence the system's behavior.

Thus, we obtain the expressions for the frequency characteristic of the compensating devices:

for $\tau = 0$

$$KW_d(j\omega) = \frac{(0.33j\omega + 1)(0.1j\omega + 1)}{(5.26j\omega + 1)(0.0055j\omega + 1)}, \tag{23}$$

for $\tau = 0.005$ sec.

$$KW_d(j\omega) = \frac{(0.5j\omega + 1)(0.1j\omega + 1)}{(8.34j\omega + 1)(0.0055j\omega + 1)}, \tag{24}$$

for $\tau = 0.01$ sec.

$$KW_d(j\omega) = \frac{(0.83j\omega + 1)(0.1j\omega + 1)}{(12.8j\omega + 1)(0.0055j\omega + 1)}. \tag{25}$$

It is clear that the compensating devices for the first and second cases are more easily realized than in the third case.

Appendix

For greater accuracy in computing $\epsilon(t)$ and $x_T(t)$, it is necessary to determine the function G.

Using (4), we put F in the form

$$F = B + Q\sin\tau\omega, \tag{26}$$

where

$$Q = \mathrm{Im}\,\frac{KW(j\omega)}{1 + KW(j\omega)}, \tag{27}$$

$$B = \frac{U(\cos\tau\omega - 1)}{(1+U)^2 + V^2}, \tag{28}$$

with Q defined by means of the imaginary circle diagram. After transformation, (28) may be written as

$$\left[U + 1 + \frac{1 - \cos\tau\omega}{2B}\right]^2 + V^2 = \left[\frac{1 - \cos\tau\omega}{2B}\right]\left[2 + \frac{1 - \cos\tau\omega}{2B}\right]. \tag{29}$$

Letting D = (1-cos $\tau\omega$)/2B, we obtain from (29)

$$[U + (1 + D)]^2 + V^2 = D(2 + D). \qquad (30)$$

Equation (30) is the equation of the family of circles, symmetric with respect to the imaginary axis and with their centers on the real axis (Fig. 18).

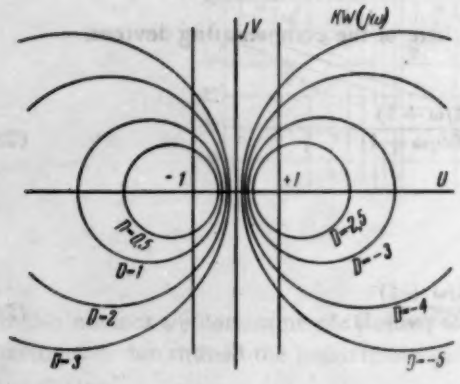

Fig. 18

If one constructs, on this same plane, the frequency characteristic of the open-loop system exclusive of the lag, then the points of intersection of the circles with this frequency characteristic give the curve $D(\omega)$. Knowing $D(\omega)$ and τ, one can speedily find $G(\omega)$ using the following relationships:

$$B = \frac{1 - \cos \tau\omega}{2D}, \qquad (31)$$

$$F = B + Q \sin \tau\omega, \qquad G = \frac{F}{1 + 2F}$$

SUMMARY

1. The introduction of the distortion function, G, allows the carrying out of the property analysis, and the synthesis, of compensating devices for automatic control systems with lag elements. The idea behind the method of introducing the function G is to establish an immediate connection between the frequency characteristic of the open-loop system exclusive of lag, the magnitude of the lag, τ, and the properties of the system. Knowing the frequency characteristics and the value of τ, one can, by this method, quickly determine the approximate characteristics of the transient response, $x_\tau(t)$, and also estimate, without complicated computations, the influence of the lag, τ, on the indicated control system properties.

2. The exposition of the method of synthesizing the compensating devices for systems with lag is based on the method for synthesizing compensating devices for ordinary linear systems [1]. For systems not possessing lag elements, we consider $G_c = 0$. The basic circumstance distinguishing systems with lag from those without is that the curves $T_{\tau M} = f(P_{max})$, $\sigma_{\tau M} = f(P_{max})$, $\gamma_\tau = f(\sigma_\tau)$ and $l_\tau = f(\sigma_\tau)$ are not identical.

LITERATURE CITED

[1] V. V. Solodovnikov, "Synthesis of compensating devices for servo systems with typical operation," Automation and Remote Control (USSR) 12, No. 5 (1951).

[2] V. V. Solodovnikov, "Synthesis of compensating devices for servo systems using optimum and typical logarithmic frequency characteristics," Automation and Remote Control (USSR) 14, No. 5 (1953).

[3] V. V. Solodovnikov, "On the use of trapeziodal frequency characteristics in the analysis of automatic control system properties," Automation and Remote Control (USSR) 10, No. 5 (1949).

[4] Ia. Z. Tsypkin, "Stability of feedback systems with lag," Automation and Remote Control (USSR) 7, No. 2-3 (1946).

[5] Ia. Z. Tsypkin, "Degree of stability of feedback systems with lag," Automation and Remote Control (USSR) 8, No. 3 (1947).

[6] M. V. Meerov, "On stabilizing systems containing lag elements," Automation and Remote Control (USSR) 14, No. 5 (1953).

Received June 5, 1957

INCREASING THE SPEED OF CERTAIN AUTOMATIC CONTROL SYSTEMS BY MEANS OF NONLINEAR AND COMPUTING DEVICES

G. M. Ostrovskii

(Moscow)

This article considers the questions involved in introducing nonlinear devices in certain automatic control systems in order to improve the quality of regulation given.

The basic results in the domain of using nonlinear devices in automatic control systems described by n'th order differential equation, with certain limitations on the variability of one or more coordinates, were obtained by A. A. Fel'dbaum [1, 2], A. Ia. Lerner [3] and L. S. Pontriagin, R. V. Gamkrelidze and V. G. Boltianskii [4]. In the present work, the method investigated in [5] is extended to cover certain automatic control systems described by n'th order differential equations.

Let the equation for the error $\underline{x}$ ($x = \theta_{in} - \theta_{out}$) of the system have the form:

$$x^{(n)} + a_1 x^{(n-1)} + \ldots + a_{n-1} x + a_n x = 0 \tag{1}$$

We assume that the parameters of the controlling portion vary within limits corresponding to values a_i:

$$\bar{c}_i \leqslant a_i \leqslant \bar{b}_i \qquad (i = 1, 2, \ldots, n-1). \tag{1a}$$

We choose the parameters $a_i = b_i$ so that the transient response will not be over-controlled, but will be characterized by a long control time. It will be assumed that, in this case, the characteristic equation of System (1) will have $\underline{n}$ real, negative and distinct roots; if the parameters $a_i = c_i$, the characteristics of the transient response are reversed.

If, by some nonlinear compensating device or another, we are able to arrange matters so that at the beginning of the transient response we have $a_i = c_i$, and at the end $a_i = b_i$ ($i = 1, 2, \ldots, n-1$), then this will assure high speed in attaining the equilibrium state at the beginning of the transient response, and a high degree of damping at the end. The system's compensating device must work in such a manner that, at a certain moment of time, the coefficients a_i rapidly change their values. It is clear that if this switch occurs too soon, the system will be subject to a long transient response, whereas if it occurs to late, the system will be heavily over-controlled.

One may formulate in the following way the problem which will be solved: at the first stage let the control system be described by the differential equation

$$x^{(n)} + c_1 x^{(n-1)} + \ldots + c_{n-1} x + x = 0, \tag{2}$$

and at the second stage, by the equation

$$x^{(n)} + b_1 x^{(n-1)} + \ldots + b_{n-1}\dot{x} + x = 0. \tag{3}$$

It is necessary to find the precise moment for transferring from Equation (2) to Equation (3) for which the system will not be over-controlled, but for which the control time will be a minimum. It is assumed that during the transition from Equation (2) to Equation (3), the first (n-1) derivatives of the output quantities vary smoothly.

We shall consider those systems which, for a unit excitation, have the following initial conditions:

$$x_0 < 0,\ \dot{x}_0 \geqslant 0, \ldots x_0^{(n-1)} \geqslant 0 \tag{4a}$$

or

$$x_0 > 0,\ \dot{x}_0 \leqslant 0, \ldots, x_0^{(n-1)} \leqslant 0. \tag{4b}$$

If the system has initial conditions of the form (4a), then a necessary and sufficient condition for monotonicity of the integral curve will be

$$\begin{aligned} F(x_1 x_2 \ldots x_n) = {} & \gamma_2\gamma_3 \ldots \gamma_n x_1 + (\gamma_2\gamma_3 \ldots \gamma_{n-1} + \gamma_2\gamma_3 \ldots \gamma_{n-2}\gamma_n + \ldots \\ & \ldots + \gamma_3\gamma_4 \ldots \gamma_n)\, x_2 + (\gamma_2\gamma_3 \ldots \gamma_{n-2} + \gamma_2\gamma_3 \ldots \gamma_{n-3}\gamma_{n-1} + \gamma_2\gamma_3 \ldots \\ & \ldots \gamma_{n-4}\gamma_{n-2}\gamma_{n-1} + \ldots + \gamma_4\gamma_5 \ldots \gamma_n)\, x_3 + \ldots + (\gamma_2\gamma_3 + \gamma_2\gamma_4 + \ldots \\ & \ldots + \gamma_2\gamma_n + \gamma_3\gamma_4 + \ldots + \gamma_3\gamma_n + \ldots + \gamma_{n-2}\gamma_{n-1} + \gamma_{n-2}\gamma_n + \\ & + \gamma_{n-1}\gamma_n)\, x_{n-2} + (\gamma_2 + \gamma_3 + \ldots + \gamma_n)\, x_{n-1} + x_n \leqslant 0, \end{aligned} \tag{5a}$$

where $x_1 = x$, $x_2 = \dot{x}_1, \ldots, x_n = \dot{x}_{n-1}$ (Cf. Appendix).

In the sequel it will be necessary for us to consider the hyperplane

$$F(x_1, x_2, \ldots, x_n) = 0. \tag{5b}$$

It will be assumed that, in $x_1, x_2, \ldots, x_n$ phase space, the initial points, determined by Conditions (4a), lie "beneath" Hyperplane (5b). We shall say that a point with coordinates $\overline{x}_1, \overline{x}_2, \ldots, \overline{x}_n$ lies "above" a surface, $x_n = f(x_1, x_2, \ldots, x_{n-1})$, if $\Psi(\overline{x}_1, \overline{x}_2, \ldots, \overline{x}_{n-1}) = \overline{x}_n - f(\overline{x}_1, \overline{x}_2, \ldots, \overline{x}_{n-1}) > 0$, and lies "below" this surface if $\Psi(\overline{x}_1, \overline{x}_2, \ldots, \overline{x}_{n-1}) < 0$.

The desired system will be such that $a_i = c_i$ so long as the phase point lies "below" Hyperplane (5b), and $a_i = b_i$ for all points lying on or above this hyperplane. Mathematically, this is written:

$$a_i = \begin{cases} c_i, & F(x, \dot{x}, \ldots, x^{(n-1)}) < 0, \\ b_i, & F(x, \dot{x}, \ldots, x^{(n-1)}) \geqslant 0. \end{cases} \tag{6}$$

We now consider the transient response with initial Conditions (4a).

Since, as was assumed, $F(x_0, \dot{x}_0, \ldots, x_0^{(n-1)} < 0$, then $a_i = c_i$ and the control system is described by the following differential equations:

$$\frac{dx_n}{dt} = -c_1x_n - c_2x_{n-1} - \ldots - x_1,$$
$$\frac{dx_{n-1}}{dt} = x_n,$$
$$\ldots\ldots\ldots\ldots\ldots\ldots \quad (7)$$
$$\frac{dx_1}{dt} = x_2.$$

We shall assume that the portion of the hyperplane

$$c_1x_n + c_2x_{n-1} + \ldots + x_1 = 0, \quad (8)$$

lying in the region $D(x_1 < 0, x_2 \geq 0, \ldots, x_n \geq 0)$ lies "above" the portion of Hyperplane (5b) lying in the same region. This can be attained by making c_1 sufficiently small. We shall prove that, during the switching process, the following inequalities will hold:

$$x_1 < 0, x_2 > 0, \ldots, x_n > 0. \quad (9)$$

In all cases these inequalities will hold until the phase point falls "below" Hyperplane (8) since, in this case, $\dot{x}_n > 0$.

To the extent that Hyperplane (5b) lies "below" Hyperplane (8), the sooner will the integral curve intersect Hyperplane (5b), this intersection occuring in region D. It is easily seen that the integral curve cannot enter the region $x_1 > 0$, being "below" Hyperplane (5b).

Indeed, while the phase point is "below" Hyperplane (5b), the inequality, $F(x_1, x_2, \ldots, x_{n-1}) < 0$, must hold. For, if the integral curve intersected the hyperplane $x_1 = 0$ then, at this point, we would have $x_1 = 0$, $x_2 > 0, \ldots, x_n > 0$, from whence $F(x_1, x_2, \ldots, x_n) > 0$, contradicting the above. Thus, the system cannot be over-controlled at the intersection of the integral curve with Hyperplane (5b).

After switching, the coefficients a_i will become equal to b_i, and the system will be heavily damped. Hence, the system, while tending towards an equilibrium state, will not be over-controlled (see Appendix).

If switching occurs too late, the system will certainly be over-controlled and, if too early, the system will be heavily damped during a long interval of time, thus increasing the duration of the transient response. In the case $x_0 > 0, \dot{x}_0 < 0, \ldots, x^{(n-1)} < 0$, a curve whose initial point lay "above" Hyperplane (5b) would never leave the semiplane $x_1 > 0$, i.e., $F(x_1, x_2, \ldots, x_n) \geq 0$. In order to obtain a device which would function correctly for both $\dot{x}_0 < 0$ and $\dot{x}_0 > 0$, it is necessary to take the sign of $\dot{x}$ into consideration. Thus, a control system will now be described by the following equation:

$$x^{(n)} + a_1x^{(n-1)} + \ldots + a_{n-1}\dot{x} + x = 0,$$

where

$$a_i = \begin{cases} c_i, & \dot{x}F(x, \dot{x}, \ldots, x^{(n-1)}) < 0 \\ b_i, & \dot{x}F(x, \dot{x}, \ldots, x^{(n-1)}) \geq 0 \end{cases} \quad (i = 1, 2, \ldots, n-1). \quad (10)$$

This means that, in an automatic control system, there must be included an analogue computing device which would generate the function $\dot{x}F(x, \dot{x}, \ldots, x^{(n-1)})$.

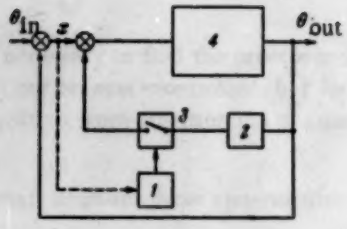

Fig. 1

The schematic for such a system is given in Fig. 1. At the input of the computing device, 1, there is impressed the error signal, x, and at its output appears the function $xF(x,\dot{x},\ldots,x^{(n-1)})$, controlling clutch 3; by means of a linear compensating device, 2, it is possible to change certain of the coefficients, a_i; the controlled object, 4, is also included in the system.

If clutch 3 is open, the subsidiary feedback path will not exist, and the system is described by Equation (2). If clutch 3 is closed, then certain a_i will become equal to b_i. Opening and closing of clutch 3 will depend on the sign of the function $xF(x,\dot{x},\ldots,x^{(n-1)})$.

It is clear that the output of the computing device may be fed to several clutches, controlling the work of several compensating devices.

We have cited a class of systems which, for unit initial excitation, have initial conditions of types (4a) and (4b). If the transfer function of the open system has the form: $W(p) = k/Q(p)$, where Q (p) is a polynomial, then the initial conditions will be $x_0 = -1, x_{20} = x_{30} = \ldots x_{n0} = 0$. If the open-loop transfer function has the form $W(p) = (Tp + 1)/Q(p)$, then the initial conditions will be $x_0 = -1, x_{20} = \ldots = x_{(n-1)0} = 0, x_n > 0$ [6].

The latter type of system underlies many systems of isodrome control (i.e., strict control of rotational speed under varying load conditions), used in the regulation of production processes.

It is easily seen that, in the first case, during an infinitesimally short interval of time, $x_n > 0, x_{n-1} > 0, \ldots x_2 > 0, x_1 < 0$. Indeed, integrating System (7) with the initial conditions $x_{10} = -1, x_{20} = \ldots = x_{n0} = 0$, over a sufficiently small period of time, we obtain

$$x_n = t > 0,$$
$$x_{n-1} = \frac{t^2}{2!} > 0,$$
$$x_{n-2} = \frac{t^3}{3!} > 0,$$
$$\ldots\ldots\ldots$$
$$x_1 = -1 + \frac{t_n}{n!} < 0,$$

where t is a small interval of time.

Reasoning further as in the proof of Inequality (9), we may show that the phase point must intersect Hyperplane (5b) and, once upon it, tends to an equilibrium state. The same reasoning is applicable to the second case. It is only necessary that the phase point, determined by the initial conditions lie "below" Hyperplane (5b), which can be attained by properly choosing the quantities $\gamma_2, \ldots, \gamma_n$. It should be mentioned that the applications of the method given are not restricted to these two classes of automatic control systems, or to systems characterized by initial Conditions (4a) and (4b). In each specific case when Conditions (4a) and (4b) do not hold, it is necessary to investigate the control system.

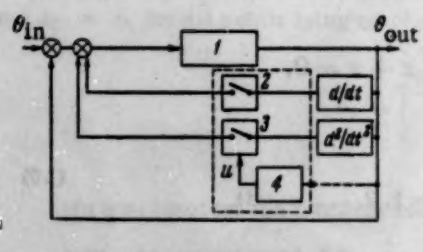

Fig. 2

We consider, by way of an example, a third order control system (Fig. 2). The invariant portion of system 1 consists of the regulated object and the executive mechanism. The transfer function of the open- looped system has the form:

$$W(p) = \frac{1}{T_3 p (T_1 p + 1)(T_2 p + 1)}. \tag{11}$$

For unit excitation of the given system, the initial conditions will be $x_0 = -1$, $\dot{x}_0 = 0$, $\ddot{x}_0 = 0$.

We denote by $\underline{n}$ the feedback loop's speed coefficient, and by m^2 its acceleration coefficient. In the case where there are no nonlinear compensating devices, consisting of clutches 2 and 3, in the link consisting of the subsidiary feedback loop and computing device 4, the system equation will be

$$[T_1 T_2 T_3 p^3 + (T_1 T_3 + T_2 T_3 + m^2) p^2 + (T_3 + n) p + k] \theta_{out} = k\theta_{in} \tag{12a}$$

If we introduce the nondimensional time

$$\tau = \sqrt[3]{\frac{k}{T_1 T_2 T_3}}\, t,$$

then Equation (12a) takes the form:

$$\dddot{\theta}_{out} + A\ddot{\theta}_{out} + B\dot{\theta}_{out} + \theta_{out} = \theta_{in} \tag{12b}$$

where

$$A = \frac{T_1 T_3 + T_2 T_3 + m^2}{\sqrt[3]{k T_1^2 T_2^2 T_3^2}}, \quad B = \frac{T_3 + n}{\sqrt[3]{k^2 T_1 T_2 T_3}}, \tag{13}$$

and the dots represent differentiation with respect to τ.

For $\underline{m} = \underline{n} = 0$, the coefficients A and B take the values:

$$A_0 = \frac{T_1 T_3 + T_2 T_3}{\sqrt[3]{k T_1^2 T_2^2 T_3^2}}, \quad B_0 = \frac{T_3}{\sqrt[3]{k^2 T_1 T_2 T_3}}. \tag{13a}$$

For some fixed $\underline{m}$ and $\underline{n}$, the coefficients A and B will take the values A_m and B_n.

The nonlinear compensating device will function in the following manner. Computing device 4 generates the function $\underline{u} = \Phi(x, \dot{x}, \ddot{x})$, where $\underline{x} = \theta_{in} - \theta_{out}$. The signal $\underline{u}$ is fed to clutches 2 and 3, which pass the signal through the subsidiary feedback loop if $\underline{u} \geq 0$, and inhibit it if $\underline{u} < 0$.

The control system will be described by the following equations:

$$\dddot{x} + A_0 \ddot{x} + B_0 \dot{x} + x = 0 \text{ for } u < 0, \tag{14a}$$

$$\dddot{x} + A_m \ddot{x} + B_n \dot{x} + x = 0 \text{ for } u \geq 0. \tag{14b}$$

Let the roots of the characteristic equation be $-\alpha, -\gamma \pm i\omega$ in case (14a), and $-\gamma_1, -\gamma_2, -\gamma_3$ in case (14b), with $\gamma_1 < \gamma_2 < \gamma_3$.

The function at the output of the computing device will have the form:

$$u = \Phi(x, \dot{x}, \ddot{x}) = \dot{x}[\gamma_2\gamma_3 x + (\gamma_2 + \gamma_3)\dot{x} + \ddot{x}].$$

Equation (14a) has the following solution:

$$x(\tau) = C_1 e^{-\alpha\tau} + C_2 e^{-\gamma\tau}\sin\omega\tau + C_3 e^{-\gamma\tau}\cos\omega\tau, \tag{15}$$

where

$$C_1 = \frac{\gamma^2 + \omega^2}{(\alpha-\gamma)^2 + \omega^2} x_0,\ C_2 = \frac{\alpha(\omega^2 - \gamma^2 + \alpha\gamma)}{\omega[(\alpha-\gamma)^2 + \omega^2]} x_0,\ C_3 = \frac{\alpha(\alpha - 2\gamma)}{(\alpha-\gamma)^2 + \omega^2} x_0,$$

and Equation (14b) has the solution:

$$\bar{x}(\tau) = B_1 e^{-\gamma_1\tau} + B_2 e^{-\gamma_2\tau} + B_3 e^{-\gamma_3\tau}, \tag{16}$$

where

$$B_1 = \frac{\gamma_2\gamma_3 x_1 + (\gamma_2 + \gamma_3)\dot{x}_1 + \ddot{x}_1}{(\gamma_2 - \gamma_1)(\gamma_3 - \gamma_1)},\quad B_2 = \frac{\gamma_1\gamma_3 x_1 + (\gamma_1 + \gamma_3)\dot{x}_1 + \ddot{x}_1}{(\gamma_1 - \gamma_2)(\gamma_3 - \gamma_2)},$$
$$B_3 = \frac{\gamma_1\gamma_2 x_1 + (\gamma_1 + \gamma_2)\dot{x}_1 + \ddot{x}_1}{(\gamma_1 - \gamma_3)(\gamma_2 - \gamma_3)}, \tag{17}$$

where $x_1, \dot{x}_1, \ddot{x}_1$ are the values of the coordinates and their first and second derivatives at the moment of switching.

If switching occurs on the surface $\Phi(x, \dot{x}, \ddot{x}) = 0$, in this case $B_1 = 0$, since the numerator of B_1 coincides with the quantity in brackets in the expression for $\Phi(x, \dot{x}, \ddot{x})$ for $x = x_1$, $\dot{x} = \dot{x}_1$ and $\ddot{x} = \ddot{x}_1$.

We find the expression for $\underline{u}$ by substituting the value of $\underline{x}$ from (15) in $\Phi(x, \dot{x}, \ddot{x})$.

$$u = (L_1 e^{-\alpha\tau} + L_2 e^{-\gamma\tau}\sin\omega\tau + L_3 e^{-\gamma\tau}\cos\omega\tau)\dot{x},$$

where

$$L_1 = C_1[\gamma_2\gamma_3 - \alpha(\gamma_2 + \gamma_3) + \alpha^2],$$
$$L_2 = \gamma_2\gamma_3 C_2 - (C_2\gamma + C_3\omega)(\gamma_2 + \gamma_3) + 2\gamma\omega C_3 + C_2(\gamma^2 - \omega^2),$$
$$L_3 = \gamma_2\gamma_3 C_3 + (\gamma_2 + \gamma_3)\alpha C_1 - \alpha^2 C_1. \tag{18}$$

Let us assign the numerical values: $T_1 = 35$ sec., $T_2 = 6.55$ sec., $T_3 = 3$ sec. and $k = 0.5$. Then $A_0 = 2.02$ and $B_0 = 0.54$. We set $x_0 = -1$.

The solution (15) has then the following form

$$x(\tau) = -0.112e^{-2\tau} - 0.319e^{-0.01\tau}\sin 0.707\tau - 0.888e^{-0.01\tau}\cos 0.707\tau.$$

Let the speed and acceleration coefficients of the feedback loop equal: $n = 4.55$ and $m = 15.8$. Then $A_m = 6$, $B_n = 8.5$. Hence, $\gamma_1 = 0.13$, $\gamma_2 = 2.0$, $\gamma_3 = 3.87$, $L_3 = -7.74$, $L_2 = 1.4$, $L_1 = 0$; the function $\underline{u}$ vanishes at time $\tau_1 = 1.97$. Hence, $x(\tau_1) = -0.46$, $\dot{x}(\tau_1) = 0.57$ and $\ddot{x}(\tau_1) = 0.21$. From (17) we get that $B_1 = 0$, $B_2 = 0.65$ and $B_3 = 0.19$.

The time, τ_2, during the course of which $\bar{x}(\tau)$ becomes less, in absolute value, than 0.06, will equal 1.17. Consequently, the time for the transient response equals $T = \tau_1 + \tau_2 = 3.14$.

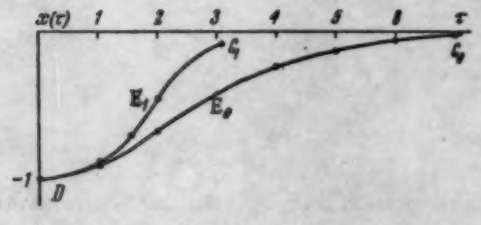

Fig. 3

In this case, the curve for the transient response (Fig. 3) is DE_1G_1. On arc DE_1 of the curve we have the solution to Equation (14a) and, on arc E_1G_1, the solution of Equation (14b).

For comparison, we take the curve DE_0G_0 of the transient response of a third order linear system in which $A = B = 3$ and, consequently, $\gamma_1 = \gamma_2 = \gamma_3 = 1$; the equation of the curve DE_0G_0 is: $x(\tau) = -\left(1 + \tau + \frac{\tau^2}{2}\right) e^{-\tau}$. In this case, the time for $|x(\tau)|$ to become less than 0.06 will equal 6. Thus, in the nonlinear system, the time of the transient response is almost twice as low.

We sought the moment of switching under the assumption that c_i and b_i were given. To give a rule which would unambiguously determine the coefficients c_i and b_i is difficult. However, it is possible to show that, in the first period, the smaller the coefficient c_i, the quicker does the system move. The coefficient b_i may be found by constructing, in the aperiodic region, curves of equal stability, using the method of Tsypkin and Bromberg, and choosing b_i by the curve corresponding to the least degree of stability.

Appendix

We consider the equation

$$x^{(n)} + b_1 x^{(n-1)} + b_2 x^{(n-2)} + \ldots + b_{n-1}\dot{x} + x = 0. \tag{A.1}$$

Assuming that the characteristic equation has n real, negative, distinct roots, $-\gamma_1 > -\gamma_2 > \ldots > -\gamma_n$, we find the necessary and sufficient condition that the integral curve of Equation (A.1) be monotonic for the initial conditions $x_0 < 0, \dot{x}_0 > 0, \ddot{x}_0 > 0, \ldots, x_0^{(n-1)} > 0$. We turn to the system of equations:

$$\begin{aligned} \frac{dx_n}{dt} &= -b_1 x_n - b_2 x_{n-1} - \ldots - x_1, \\ \frac{dx_{n-1}}{dt} &= x_n, \\ &\cdots\cdots\cdots \\ \frac{dx_1}{dt} &= x_2. \end{aligned} \tag{A.2}$$

We consider $x_1, x_2, \ldots, x_n$ phase space. In it there are, among the integral curves of System (A.2), the n lines:

$$\begin{aligned} x_1 &= -e^{-\gamma_i t}, \\ x_2 &= \gamma_i e^{-\gamma_i t}, \\ x_3 &= -\gamma_i^2 e^{-\gamma_i t}, \\ &\cdots\cdots\cdots \\ x_n &= (-1)^n \gamma_i^{n-1} e^{-\gamma_i t} \quad (i = 1, 2, \ldots, n). \end{aligned} \tag{A.3}$$

We conceive of the lines (A.3) as the axes of a new oblique coordinate system, $u_1, u_2, \ldots, u_n$, where we consider, as the u_1 axis, the line corresponding to γ_1, as the u_2 axis the line corresponding to γ_2, etc. As the

positive semi-axis of the u_1 axis, we take the semi-axis lying in the half-plane $x_1 < 0$. The formulae for passing from the $u_1, u_2, \ldots, u_n$ system to the $x_1, x_2, \ldots, x_n$ system have the form [7]:

$$\begin{aligned} x_1 &= -(u_1 + u_2 + \ldots + u_n), \\ x_2 &= \gamma_1 u_1 + \gamma_2 u_2 + \ldots + \gamma_n u_n, \\ x_3 &= -(\gamma_1^2 u_1 + \gamma_2^2 u_2 + \ldots + \gamma_n^2 u_n), \\ &\ldots\ldots\ldots\ldots\ldots\ldots \\ x_n &= (-1)^n (\gamma_1^{n-1} u_1 + \gamma_2^{n-1} u_2 + \ldots + \gamma_n^{n-1} u_n). \end{aligned} \tag{A.4}$$

In what follows, we shall need the expressions for u_1 and u_2 in terms of $x_1, x_2, \ldots x_n$. Solving System (A.4), we get

$$\begin{aligned} u_1 = -\frac{\prod\limits_{2\leqslant j<i\leqslant n}(\gamma_i - \gamma_j)}{\prod\limits_{1\leqslant j<i\leqslant n}(\gamma_i - \gamma_j)} [&\gamma_2\gamma_3\ldots\gamma_n x_1 + (\gamma_2\gamma_3\ldots\gamma_{n-1} + \gamma_2\gamma_3\ldots\gamma_{n-2}\gamma_n + \\ &+ \gamma_2\gamma_3\ldots\gamma_{n-3}\gamma_{n-1}\gamma_n + \ldots + \gamma_3\gamma_4\ldots\gamma_n) x_2 + \ldots + (\gamma_2\gamma_3\ldots\gamma_{n-i+1} + \\ &+ \gamma_2\gamma_3\ldots\gamma_{n-i}\gamma_{n-i+2} + \ldots + \gamma_3\gamma_4\ldots\gamma_{n-i+2} + \\ &+ \gamma_3\gamma_4\ldots\gamma_{n-i+1}\gamma_{n-i+3} + \ldots\gamma_4\gamma_5\ldots\gamma_{n-i+3} + \ldots + \gamma_{i+1}\gamma_{i+2}\ldots\gamma_n) x_i + \\ &+ \ldots + (\gamma_2\gamma_3 + \gamma_2\gamma_4 + \ldots + \gamma_2\gamma_n + \gamma_3\gamma_4 + \ldots + \gamma_3\gamma_n + \ldots + \gamma_{n-1}\gamma_n) x_{n-2} + \\ &+ (\gamma_2 + \gamma_3 + \ldots + \gamma_n) x_{n-1} + x_n]. \end{aligned} \tag{A.5}$$

The coefficient of x_i takes the form of a sum of products of (n-1) of the n roots, $|\gamma_i|$ For u_2 we obtain

$$\begin{aligned} u_2 = \frac{\prod\limits_{1\leqslant j<i\leqslant n^{(i+2;\, j+2)}}(\gamma_i - \gamma_j)}{\prod\limits_{1\leqslant j<i\leqslant n}(\gamma_i - \gamma_j)} [&\gamma_1\gamma_3\ldots\gamma_n x_1 + (\gamma_1\gamma_3\ldots\gamma_{n-1} + \gamma_1\gamma_2\ldots\gamma_{n-2}\gamma_n + \\ &+ \gamma_1\gamma_3\ldots\gamma_{n-3}\gamma_{n-1}\gamma_n + \ldots + \gamma_3\gamma_4\ldots\gamma_n) x_2 + \ldots + (\gamma_1\gamma_3\ldots\gamma_{n-i+1} + \gamma_1\gamma_3\ldots\gamma_{n-i}\gamma_{n-i+2} + \\ &+ \ldots + \gamma_3\gamma_4\ldots\gamma_{n-i+2} + \gamma_3\gamma_4 \ldots \gamma_{n-i+1}\gamma_{n-i+3} + \ldots + \gamma_4\gamma_5\ldots\gamma_{n-i+3} + \\ &+ \ldots + \gamma_{i+1}\gamma_{i+2}\ldots\gamma_n) x_i + \ldots + (\gamma_2\gamma_3 + \gamma_2\gamma_4 + \ldots\gamma_2\gamma_n + \gamma_3\gamma_4 + \ldots + \gamma_3\gamma_n + \\ &+ \ldots + \gamma_{n-1}\gamma_n) x_{n-2} + (\gamma_2 + \gamma_3 + \ldots + \gamma_n) x_{n-1} + x_n]. \end{aligned} \tag{A.6}$$

The $u_1, u_2, \ldots, u_n$ coordinate system will be normal [8], and in it the equations of the integral curves will have the form:

$$\begin{aligned} u_1 &= u_{10} e^{-\gamma_1 t}, \\ u_2 &= u_{20} e^{-\gamma_2 t}, \\ &\ldots\ldots\ldots \\ u_n &= u_{n0} e^{-\gamma_n t}. \end{aligned} \tag{A.7}$$

If $u_{10} = 0$ at the outset of the motion then, for all time, $u_1 = 0$, i.e., throughout the motion the integral curve will lie in the hyperplane $u_1 = 0$. We designate this hyperplane by the letter, L. We might make a similar statement for u_2, etc. It is easily seen that an integral curve which does not lie in any of the hyperplanes $u_1 = 0$, $u_2 = 0, \ldots, u_n = 0$, may intersect them only at the origin of coordinates.

Consider hyperplane L. We will show that, if the integral curve lies "above" hyperplane L, it will leave the half-space, $x_1 < 0$. If the integral curve lies "below" L and, at the initial moment, $x_1 > 0, x_2 > 0, \ldots, x_n > 0$, then it will not leave the half-space $x_1 < 0$. We get the equation of hyperplane L from (A.5) by setting u_1 equal to zero.

It is known that all integral curves of System (A.2), excluding those for which $u_1 = 0$, are tangent to the u_1 axis [8], being tangent to the positive semi-axis for $u_{10} > 0$, and to the negative semi-axis for $u_{10} < 0$.

Consider the integral curves whose initial points lie in region D "above" hyperplane L. Substituting the coordinate values for these points in the right side of Equation (A.5), we get $u_{10} < 0$. From (A.7) we then obtain that $u_1 < 0$ during the entire motion. Consequently, the integral curve will be tangent to the negative half of the u_1 axis, which lies in the half-space, $x_1 > 0$. The integral curve must of necessity then leave half-space $x_1 < 0$. We have thus proved the first part of our assertion. We now assume that the initial point lies in the region D "below" hyperplane L. Substituting the coordinates of this point in the expression for u_1, we find that $u_{10} > 0$, and that, therefore, $u_1 > 0$ throughout the motion. Consider the intersection of hyperplanes $u_1 = 0$ and $u_2 = 0$. For this purpose, we rewrite the equations for these surfaces in the following manner:

$$\begin{aligned} F(x_1, x_2, \ldots, x_n) = {} & \gamma_2\gamma_3\cdots\gamma_n x_1 + [\gamma_2\gamma_3\cdots\gamma_{n-1} + \cdots + \gamma_3\gamma_4\cdots\gamma_n]\, x_2 + \\ & + \cdots + [\gamma_2\gamma_3 + \gamma_2\gamma_4 + \cdots + \gamma_2\gamma_n + (\gamma_3\gamma_4 + \cdots + \gamma_{n-1}\gamma_n)]\, x_{n-2} + \\ & + [\gamma_2 + (\gamma_3 + \cdots \gamma_n)]\, x_{n-1} + x_n = 0, \end{aligned} \tag{A.8}$$

$$\begin{aligned} & \gamma_1\gamma_3\cdots\gamma_n x_1 + [\gamma_1\gamma_3\cdots\gamma_{n-1} + \cdots + \gamma_3\gamma_4\cdots\gamma_n]\, x_2 + \cdots + [\gamma_1\gamma_3 + \gamma_1\gamma_4 + \cdots \\ & \cdots + \gamma_1\gamma_n + (\gamma_3\gamma_4 + \cdots + \gamma_{n-1}\gamma_n)]\, x_{n-2} + [\gamma_1 + (\gamma_3 + \cdots + \gamma_n)]\, x_{n-1} + x_n = 0. \end{aligned} \tag{A.9}$$

In the coefficients of x_i in Equations (A.8) and (A.9), identical expressions are isolated within parentheses. Outside the parentheses are terms which differ only in that they have γ_1 in the second equation where they have γ_2 in the first. We multiply (A.8) by γ_1 and (A.9) by γ_2, and subtract the first from the second. With this, the terms outside the parentheses drop out, and the terms inside the parentheses may be written as:

$$\begin{aligned} & \gamma_3\cdots\gamma_n(\gamma_2 - \gamma_1)\, x_2 + \cdots + (\gamma_3\gamma_4 + \cdots \gamma_{n-1}\gamma_n)(\gamma_2 - \gamma_1)\, x_{n-2} + \\ & + (\gamma_3 + \cdots + \gamma_n)(\gamma_2 - \gamma_1) x_{n-1} + (\gamma_2 - \gamma_1)\, x_n = 0. \end{aligned}$$

We divide through by the common factor $(\gamma_2 - \gamma_1)$ to obtain

$$\gamma_3\cdots\gamma_n x_2 + \cdots + (\gamma_3\gamma_4 + \cdots + \gamma_{n-1}\gamma_n)\, x_{n-2} + (\gamma_3 + \cdots + \gamma_n)\, x_{n-1} + x_n = 0.$$

Since all the coefficients of this equation are positive, there is no solution for $x_2 > 0, \ldots, x_n > 0$. Hence, the hyperplanes $u_1 = 0$ and $u_2 = 0$ do not intersect in region D.

We now show that hyperplane $u_1 = 0$ is "above" hyperplane $u_2 = 0$ in region D. Consider the line parallel to the x_n axis:

$$x_1 = -a, \; x_2 = x_3 = \cdots = x_{n-1} = 0. \tag{A.10}$$

The points of intersection of this line with Hyperplanes (A.8) and (A.9) will be the points $B_1(-a,0,\ldots,0,\bar{x}_n)$ and $B_2(-a,0,\ldots,0,\bar{\bar{x}}_n)$, where $\bar{x}_n = \gamma_2\gamma_3\cdots\gamma_n a$ and $\bar{\bar{x}}_n = \gamma_1\gamma_3\cdots\gamma_n a$. We have $\bar{x}_n > \bar{\bar{x}}_n$, since $\gamma_2 > \gamma_1$. Hence, point B_1 lies above point B_2 on Line (A.10). Consequently, insofar as hyperplanes $u_1 = 0$ and $u_2 = 0$ do not intersect, hyperplane $u_1 = 0$ will be "above" hyperplane $u_2 = 0$ everywhere in region D. Consider now a point of hyperplane $u_1 = 0$ in region D. It lies "above" hyperplane $u_2 = 0$. From (A.6) we then obtain for this point

that $u_2 > 0$. We now show that, if the initial point lies in the region D "below" hyperplane L, then the integral curve starting at it will not leave the half-space $x_1 < 0$. We prove this by the use of mathematical induction. It is proved for equations of the second order in [5], hence we may assume that the assertion is also true for equations of order n

In this case, the initial point lies in the region $x_1 < 0, x_2 > 0, \ldots, x_n > 0$ "below" the hyperplane $u_1 = 0$. This region in $u_1, u_2, \ldots, u_n$ is given by the following inequalities:

$$\begin{gathered}
u_1 + u_2 + \cdots + u_n > 0, \\
\gamma_1 u_1 + \gamma_2 u_2 + \cdots + \gamma_n u_n > 0, \\
\gamma_1^2 u_1 + \gamma_2^2 u_2 + \cdots \gamma_n^2 u_n < 0, \\
\cdots\cdots\cdots\cdots\cdots \\
(-1)^{n-1}(\gamma_1^{n-2} u_1 + \gamma_2^{n-2} u_2 + \cdots + \gamma_n^{n-2} u_n) > 0, \\
(-1)^n (\gamma_1^{n-1} u_1 + \gamma_2^{n-1} u_2 + \cdots + \gamma_n^{n-1} u_n) > 0, \\
u_1 > 0.
\end{gathered} \tag{A.11}$$

An integral curve whose initial point lies in this region does not, according to the assumption, leave the half-space $x_1 < 0$, i.e., does not intersect the plane $u_1 + u_2 + \ldots + u_n = 0$.

We now consider a system of the (n+1)'st order. The region D is defined by the inequalities

$$\begin{gathered}
u_1 + u_2 + \cdots + u_{n+1} > 0, \\
\gamma_1 u_1 + \gamma_2 u_2 + \cdots + \gamma_{n+1} u_{n+1} > 0, \\
\cdots\cdots\cdots\cdots\cdots\cdots \\
(-1)^n (\gamma_1^{n-1} u_1 + \gamma_2^{n-1} u_2 + \cdots + \gamma_{n+1}^{n-1} u_{n+1}) > 0, \\
(-1)^{n+1} (\gamma_1^n u_1 + \gamma_2^n u_2 + \cdots + \gamma_{n+1}^n u_{n+1}) > 0.
\end{gathered} \tag{A.12}$$

Consider a point on the hyperplane $u_1 = 0$ in region D. The totality of such points will constitute an n-dimensional subspace. These points, lying in region D on the hyperplane $u_1 = 0$, will satisfy the inequalities

$$\begin{gathered}
u_2 + u_3 + \cdots + u_{n+1} > 0, \\
\gamma_2 u_2 + \gamma_3 u_3 + \cdots + \gamma_{n+1} u_{n+1} > 0, \\
\cdots\cdots\cdots\cdots\cdots\cdots \\
(-1)^n (\gamma_2^{n-1} u_2 + \cdots + \gamma_{n+1}^{n-1} u_{n+1}) > 0.
\end{gathered} \tag{A.13}$$

We previously showed that, for points lying on hyperplane L, $u_2 > 0$. Thus, in the n-dimensional subspace, $u_1 = 0$, the points lying in D satisfy the same inequalities as in (A.11), except that now, instead of the u_1 axis we have the u_2 axis, instead of the u_2 axis we have the u_3 axis, etc. On the basis of our previous assumption, an integral curve starting at one of these points could not intersect the hyperplane $u_2 + u_3 + \ldots u_{n+1} = 0$, i.e., could not intersect the hyperplane $x_1 = 0$, since, for $u_1 = 0$, $x_1 = -(u_2 + u_3 + \ldots + u_{n+1})$. We have thus shown that an integral curve lying on the hyperplane $u_1 = 0$ and in region D can not leave the half-space $x_1 < 0$. It can be shown that integral curves lying in region D "below" hyperplane L will not leave the half-space $x_1 < 0$. Consider the point $A(x_1, x_2, \ldots x_n)$ lying on hyperplane L and point $\bar{A}(\bar{x}_1, \bar{x}_2, \ldots, \bar{x}_n)$ lying on the line parallel to the x_n axis and passing through A, where $\bar{A}$ lies below A. From this, $x_1 = \bar{x}_1, x_2 = \bar{x}_2, \ldots, x_{n-1} = \bar{x}_{n-1}, x_n > \bar{x}_n$. Consider the integral curves starting at, respectively, points A and $\bar{A}$. The initial velocity, acceleration, third derivatives, etc. of these integral curves are directed towards the initial excitation. Hence, all initial derivatives up to the (n-2)'nd order are equal for the two curves, but the initial (n-1)'st derivative of the curve starting at point $\bar{A}$ is less than the corresponding quantity for the curve starting from point A. However, we have already showed that the integral curve starting from point A cannot leave the half-space $x_1 < 0$. Consequently, the integral curve starting from point $\bar{A}$ can certainly not leave this half-space.

LITERATURE CITED

[1] A. A. Fel'dbaum, "Optimal processes in automatic control systems," Automation and Remote Control (USSR) 14, No. 6 (1953).

[2] A. A. Fel'dbaum, "On the use of phase space for synthesizing optimal systems," Automation and Remote Control (USSR) 16, No. 2 (1955).

[3] A. Ia. Lerner, "On the limits on speed of automatic control systems," Automation and Remote Control (USSR) 15, No. 6 (1954).

[4] L. S. Pontriagin, "Certain mathematical problems arising in connection with the theory of optimal automatic control systems," Proceedings of the Session of the AN SSSR on Scientific Problems of Automatic Production. Basic Problems of Automatic Regulation and Control [in Russian]. (Izd. AN SSSR, 1957).

[5] G. M. Ostrovskii, "Application of nonlinear compensating devices in second-order automatic control systems," Automation and Remote Control (USSR) 17, No. 11 (1956).*

[6] A. A. Fel'dbaum, Electrical Automatic Control Systems [in Russian] (Oborongiz, 1957).

[7] A. I. Mal'tsev, Fundamentals of Linear Algebra [in Russian], (Gostekhizdat, 1948).

[8] V. V. Nemytskii and V. V. Stepanov, Quantitative Theory of Differential Equations [in Russian] (Gostekhizdat, 1950).

Received September 18, 1957

*See English translation.

CONCERNING A POSSIBILITY OF DETERMINING AN AXIAL HYDRODYNAMIC FORCE IN A VALVE

I. M. Krassov, and B. G. Turbin

(Moscow)

The paper deals with an axial hydrodynamic force that appears in valve hydraulic amplifier when the working liquid flows through it. The amplifier described may be a meter of the force. The experimental results are presented.

One of the specific characteristics of valve hydraulic amplifiers, which find wide application in automatic control systems, such as the following and others is the appearance of axial hydrodynamic forces which act on the valve from the direction of flow of the work fluid [1, 2].

The axial hydrodynamic force depends on the flow parameters of the work fluid (the drop in pressure p_0 of the fluid on the working edges of the valve, the fluid density, the valve opening $\underline{x}$) and on the constructional parameters of the amplifier (width of the through section of the valve, radial clearance between the shoulders of the valve and its sleeve, radius of curvature of the working edges of the shoulders, axial distance in the valve between the centers of the inflowing and outflowing stream, etc.). This force consists of a steady and an unsettled component and, arising only during the flow of fluid through the valve's opening, endeavours to close it, i.e., counteracts the force of the control device.

The effect of the axial hydrodynamic force on the work of the hydraulic amplifier is particularly perceptible in amplifiers having a large power amplification factor [3], such as those found in electrohydraulic servomechanisms. The output power of these is raised by increasing the pressure and consumption of the work liquid while the sensitivity is increased by utilizing low power electrical control devices. In this case the appearance of the axial hydrodynamic force imposes much more severe requirements on the electrical control devices. Thus, a study of the nature, magnitude, and effect of the axial hydrodynamic force on the operation of the hydraulic amplifier, as well as a study of methods to minimize it is of definite interest.

In the course of testing one type of two-stage hydraulic amplifier with a high power amplification factor, the feasibility of determining the magnitude of the axial hydrodynamic force from the readings of a manometer on the needle chamber was exhibited. This possibility results from the principal characteristics of the amplifier itself, a diagram of which appears in Fig. 1. In this amplifier the displacement of the needle 4 brings about a change in pressure in the pin chamber A. The difference between the pressure of the fluid on the face of the valve 1 in chamber A and the pressure of the fluid on the face of this valve in chamber B together with the force of spring 5 causes the valve to be displaced. The fluid is able to enter one or another working chamber of the output mechanism, bringing the piston of the latter into motion. When the flow commences, an axial hydrodynamic force arises on the valve and persists until the end of flow of fluid through the opening of the valve, i.e., until the end of motion of the output mechanism which is controlled by the amplifier.

We will assume that the forces acting on valve 1 are positive when they act to the left (from chamber A to chamber B); we will also assume that the opening of the valve $\underline{x}$ is positive when it is displaced to the left of its neutral position (towards chamber B).

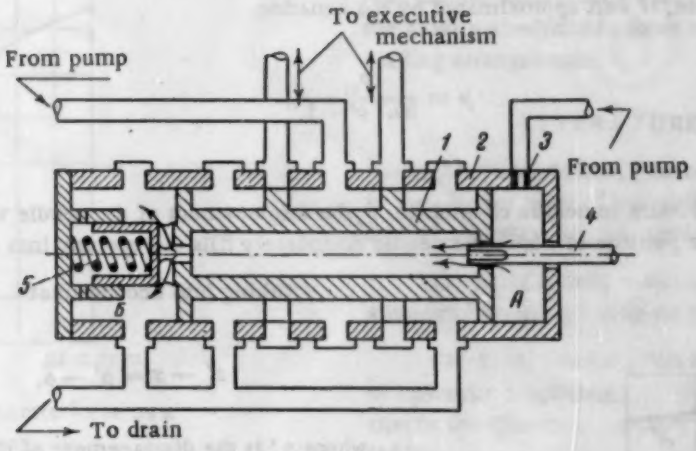

Fig. 1. Principal diagram of the hydraulic amplifier: 1) valve; 2) sleeve; 3) throttle; 4) needle; 5) spring. A) needle chamber, B) sink chamber.

Under these conditions the equilibrium equation of the valve, in the case of an established flow of fluid through it, has the form:

$$(N + cx) + F_B + R = F_A, \tag{1}$$

where N is the initial tension of spring 5, corresponding to the neutral position of the valve, c is the stiffness of the spring, x is the opening, F_A, F_B are the work fluid forces on the faces of the valve in chambers A and B, R is the steady component of the axial hydrodynamic force.

Force F_B may be assumed to be constant, whereas force F_A is defined by the equation

$$F_A = kp, \tag{2}$$

where p is the pressure in the chamber A, $k = \frac{\pi}{4}(D^2 - d^2)$ is the constructional constant of the valve (D is the diameter of the valve's shoulders, d is the diameter of the needle opening in the valve).

After the cessation of flow (caused, for example, by the stopping of the output mechanism) force R will disappear, equilibrium of the valve will be disturbed and, the position of the needle remaining unchanged, the valve will be displaced further. The pressure in chamber A will change; the equilibrium equation will take on the form:

$$(N + cx') + F_B = F'_A, \tag{3}$$

where x' is the new opening of the valve and F_A', the force due to the liquid pressure on its right face.

Subtracting Equation (3) from Equation (1) and utilizing (2), one can obtain the axial hydrodynamic force R:

$$R = k(p - p') + c(x' - x). \tag{4}$$

The difference $(x' - x)$ can be determined through the pressures p and p' with the help of the static characteristic of the first stage of amplification, which is determined experimentally. This characteristic represents the dependence of the pressure in the needle chamber on the displacement of the needle with respect to the valve and, in this particular case, is well approximated by the equation

$$p = \frac{p_{st}}{55.7\,\rho^2 + 1}, \tag{5}$$

where p_{ST} is the static pressure in needle chamber A; ρ, the displacement of the needle with respect to the valve, measured from the position at which the needle completely fills the opening into the valve.

Taking into account that

$$x' - x = \rho' - \rho, \tag{6}$$

where ρ' is the displacement of the needle in the absence of flow of work fluid through the valve, ρ is the the same but during the flow of work fluid through the valve, we will obtain utilizing (5) the following expression for determining the magnitude of $x' - x$:

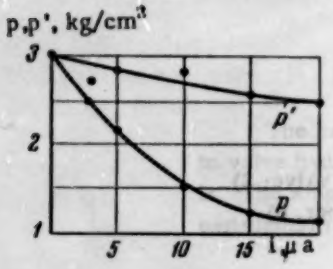

Fig. 2. Pressure in needle chamber as a function of control current. p) during and p') in absence of flow of work fluid through valve.

$$x' - x = 0{,}134\left(\sqrt{\frac{p_{st}}{p'} - 1} - \sqrt{\frac{p_{st}}{p} - 1}\right). \tag{7}$$

It follows that by measuring p and p' in the needle chamber and knowing the stiffness of the spring c and the constructional constant k, it is possible to determine from (4) and (7) the magnitude of the axial hydrodynamic force acting on the valve together with the frictional forces.

Figure 2 shows the results obtained from measurements of the pressure in the needle chamber in the presence and absence of a flow of fluid through the valve, at different control signals i causing a negative displacement of the valve. Kerosene was used as the work fluid in the experiments. The supply pressure on the entrance to the second stage of the amplifier (the valve) was equal to 50 kg/cm². The experiment was carried out for a valve having shoulders with a diameter D = 25 mm, needle opening diameter d = 2.5 mm, radial clearance equal to 0.006 mm. The stiffness of the spring 5 (Fig. 1) was equal to 3.45 kg/mm.

The experimental and calculated data necessary to determine the axial hydrodynamic force are tabulated below:

i, ma	p', kg/cm²	p, kg/cm²	$\pi(p'-p)$, kg	$c(x'-x)$, kg	R, kg
3	2.7	2.5	0.986	0.059	1.045
5	2.85	2.2	3.204	0.172	3.376
10	2.8	1.5	6.409	0.455	6.864
15	2.55	1.25	6.409	0.552	6.961
20	2.5	1.15	6.655	0.621	7.276

Figure 3 shows the relationship between the axial hydrodynamic force and the valve opening. The distribution of the experimental points indicates that the accuracy of the experiment was insufficient. On the strength of this the given relationship must be considered as approximate. From our point of view, the important fact

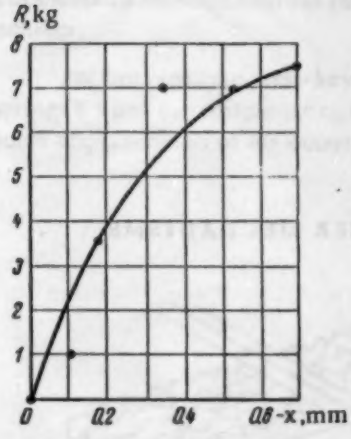

Fig. 3. Axial hydrodynamic force as a function of valve opening.

is that a two stage hydraulic amplifier of this type (needle-valve) may serve as a meter of the axial hydrodynamic force. Such a method for determining the axial hydrodynamic force eliminates all forms of loading arrangements.

LITERATURE CITED

[1] T. M. Bashta, "Reactive forces of fluid flow in the plunger pairs of hydraulic units," Stanki i Instrument (USSR), No. 11, 1956.

[2] M. Z. Litvin – Sedoi, "Hydraulic drive in automatic systems," Mashgiz (USSR), 1956.

[3] I. M. Krassov, "On the amplification factor of hydraulic amplifiers," in the collection: Automation in the Chemical Industry [in Russian] (AN USSR, (1955).

Received July 9, 1957

THE THEORY OF THE STRUCTURE OF COMBINER MECHANISMS

S. M. Iakovlev

(Moscow)

INTRODUCTION

Mechanisms which transform spatial combinations of displacements of input elements (levers, keys etc.) into displacements of output elements are widely used in telegraphy, telemechanics, centralized railroad control, the textile industry etc. Mechanical coders and decoders are examples in telegraphy and telemechanics, signal control panels in centralized railroad control (CRC), and automatic pattern-producing devices for weaving machines in the textile industry.

We assign these devices the general name of combiners. Although they are widely used, no systematic theory of their structure has so far been presented, which has made analysis and synthesis very difficult. Empirical methods have been used almost exclusively in design.

In telegraphic equipment, for instance, a set of gaps and projections is chosen for each key, and the design then checked for correct operation and absence of false signals. In signals equipment for centralized use the levers and interlocks are mainly developed in the same fashion. The numerous combinations of possible routes make the choice exceptionally difficult. The situation is no better in the textile industry.

The first attempts to rationalize analysis and synthesis have been made in CRC. A routing theory has been developed [1] which is termed mathematical because it represents the operation of combiners by symbolic expressions analogous to fractions. However, the structure of combiners is not considered systematically, so synthesis problems for CRC are still mainly solved by selection.

In 1948-9 the structure of combiners was studied systematically, and analysis and synthesis were based on Boolean algebra (algebra of logic) [2].* Here we give the same results, somewhat extended.** This theory raises some new problems demanding further study.

Structure of Two-Position Combiners

Any combiner, of no matter what design or function, has input (command) and output (effector) moving mechanical elements; input displacements are transformed to output ones. In telegraphic transmitters the input elements are key levers and the output keying mechanisms (cams), while in the decoders the input elements are selection racks or rings, and the output letter levers. In train controls the inputs are the signal levers which close routes, and the outputs the routes left open.

In the simplest case each input and output element has only two positions of rest. The mechanism is then a two-position one. The two positions are referred to as the normal and the set.

Some such mechanisms, e.g., the ST-35 transmitter in telegraphy, transform the displacements of the input elements directly into displacements of the outputs. The keying racks in the ST-35 transmitter are fitted with equilateral or right-angled triangular teeth on the key panel side, for instance (Fig. 1). When the push-button P is pressed the bottom of the lever presses on the racks and causes them to move in directions determined by the slopes of the sides of the triangles.

*The results were presented at a symposium on mathematical logic at Moscow State University in 1949.

**Certain others have also applied Boolean algebra to combiners (e.g., [3 and 7]), but in another way.

In other such mechanisms (e.g., in the Creed telegraphy transmitter) the input keys only prepare the output elements for displacement (free or lock them), while the actual displacements are effected by other components.

For instance, the press-keys P in the Creed (Fig. 2) lock the rods R and stop their displacement by the springs S when the reciprocating head H frees the rods. In railroad control panels some route levers block some displacements of the others.

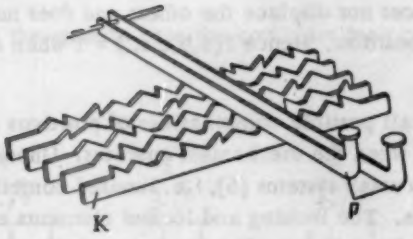

Fig. 1

Combiners of the first type differ from those of second type only in design. Any one of type one can be made to operate in two steps (preparatory, when the inputs are displaced to free or lock the outputs, and working, when the outputs are displaced by some drive mechanism) by changes in detailed construction only. This then gives us a type two mechanism of the same structure as the original mechanism.

In future we shall therefore consider only type two, in which input displacements merely prepare output ones.

In the traditional notation [1] a combiner is denoted by a kinematic system in which the input, intermediate and output elements are represented by horizontal and vertical lines (levers) hinged together via triangle links. Where coupled levers intersect a lock is shown (i.e., a part which blocks the movement). Thus Fig. 3 shows that element A locks element B, and Fig. 4 that element B locks element A. This convenient symbolism will be used in future.

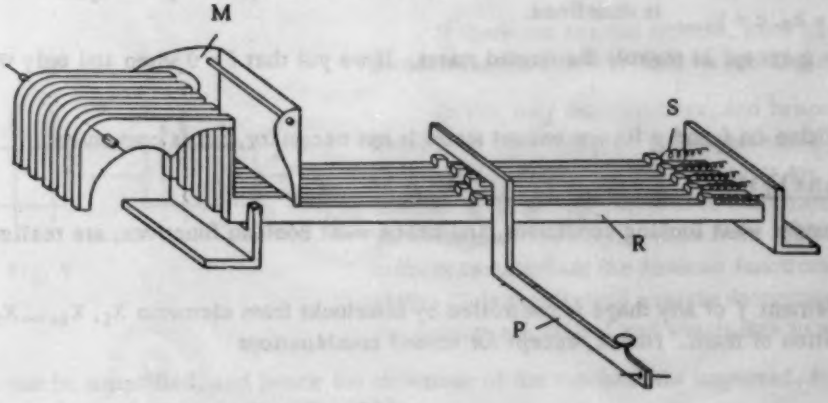

Fig. 2

Algebraic Form of the Locking Conditions

We use Boolean algebra to study two-position combiners; this algebra has been used successfully with two-position (relay) electric circuits [4] in structure studies.*

Let A, B, C,... be elements of the combiner. Let a, b, c... be variables representing their positions which take two values (0 and 1) only. Let the zero correspond only to the normal state, and unity only to the set state.

*The fundamentals of Boolean algebra are presented in ch. 1 of [4], and also (using other symbols) in [5] in the chapter on the calculus of prediction; also in [3].

Then the condition that some element X be locked in its normal position by A, B. C... can be expressed as the Boolean function f(a,b,c...) in the variables a,b,c....

Combinations of a,b,c,... correspond to combinations of A,B,C.... Suppose f(a,b,c...) = 0 if the combinations correspond to combinations which lock X in its normal position, and f(a,b,c ...) = 1 if the combinations correspond to combinations which free X for displacement to the set position.

Then the condition that some element X be locked in the set position can be expressed as the Boolean function g(a,b,c...) which is zero if the combinations correspond to combinations which lock X in the set position, and unity if the combinations correspond to combinations which free X for displacement.

In this type of mechanism the elements will be free in both positions for the same combinations of the locking elements. In other words, displacement of one element does not displace the others and does not alter the interlocks which control itself, so it can return to its original position. Hence f(a,b,c ...) = 1 when and only when g(a,b,c ...) = 1.

Fig. 3

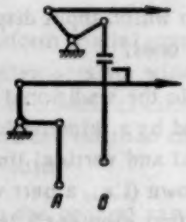

Fig. 4

Not all possible combinations of positions actually occur when the mechanism operates. Unused states occur as in relay systems [5], i.e., unused combinations of positions. The locking and locked elements exchange roles in real combiners. For example, while lever A in the set position locks B in the normal position, lever B in the set position locks A in the normal position.

f and g are undefined for the unused combinations i.e., can be chosen at will. Choice of values of the unused combinations only affects the external form of the functions and has no effect on the values for the used combinations, which are the only ones which describe the real locking conditions. The condition $f(a,b,c,\ldots)/_{a = k_1,\ b = k_2,\ c = k_3,\ldots} = 0$, where $k_1, k_2, k_3,\ldots$ are constants (i.e., zero and one) and '/' is the substitution symbol, implies that $g(a,b,c,\ldots)/_{a = k_1,\ b = k_2,\ c = k_3,\ldots}$ is undefined. Conversely, the condition $g(a,b,c,\ldots)/_{a = k_1,\ b = k_2,\ c = k_3,\ldots} = 0$ implies that $f(a,b,c,\ldots)/_{a = k_1,\ b = k_2,\ c = k_3,\ldots}$ is undefined.

Hence f = g except as regards the unused states. If we put that f = 0 when and only when g = 0, we have f = g precisely.

This condition on f and g for the unused states is not necessary, but is convenient.

Algebraic Analysis of Combiner Structure

Let us consider what locking conditions, and hence what Boolean functions, are realized by the simplest combinations.

A rigid element Y of any shape is controlled by interlocks from elements $X_1, X_2, \ldots X_m$, and is free only for one combination of them. Hence, except for unused combinations

$$f(x_1, x_2, x_3, \ldots, x_m) = g(x_1, x_2, x_3, \ldots, x_m) = \tilde{x}_1 \tilde{x}_2 \tilde{x}_3 \ldots \tilde{x}_m,$$

Fig. 5

where $\tilde{x}_i = x_i$ is set in this unique combination, and $\tilde{x}_i = \bar{x}_i$ if x_i remains in its normal state.

In the rigid kinematic scheme no displacement can occur if even one element is locked.

The situation is different if the locked element contains elastic couplings. Such a system is that of Fig. 5. Here Y has several (say, k) modes of motion, and so Y, controlled by locks from elements

$X_1, X_2, \ldots X_m$ is free not just for one combination, but for k such. Hence the locking condition is expressed by the function

$$f(x_1, x_2, x_3, \ldots, x_m) = g(x_1, gx_2, \ldots, x_m) =$$
$$= (\tilde{x}_{11}\tilde{x}_{12}\tilde{x}_{13} \ldots \tilde{x}_{1m}) + (\tilde{x}_{21}\tilde{x}_{22} \ldots \tilde{x}_{2m}) + \qquad (1)$$
$$+ (\tilde{x}_{k1}\tilde{x}_{k2} \ldots \tilde{x}_{km}) = \sum_{i=1}^{k} (\tilde{x}_{i1}\tilde{x}_{i2}\tilde{x}_{i3} \ldots \tilde{x}_{im}) = \sum_{i=1}^{k}\prod_{j=1}^{m} (\tilde{x}_{ij}).$$

In the general case the combiner may contain several stages, as shown in Fig. 6.

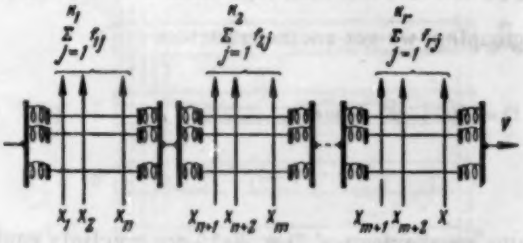

Fig. 6

If stage 1 realizes functions $f_{11}, f_{12}, f_{13}, \ldots, f_{kl_1}$, the second $f_{21}, f_{22}, \ldots, f_{2k_2}$ and the last (r th) stage $f_{r_1}, f_{r_2}, \ldots, f_{rk_r}$, the whole system clearly realizes the function

$$\prod_{v=1}^{r}\sum_{i=1}^{k} f_{vi} = \prod_{v=1}^{r}\sum_{i=1}^{k}\prod_{\gamma=1}^{m}(x_{vij}).$$

If k = 2 the hinge system of Fig. 7 can be used instead of elastic couplings.

Other ways of combining the elements can be analyzed similarly. In general, rigid couplings correspond to Boolean multiplication (logical operation 'and'), and elastic or other nonrigid couplings to Boolean addition (logical operation 'or'). Inversion (logical operation 'no') corresponds to locking for other states of inputs.

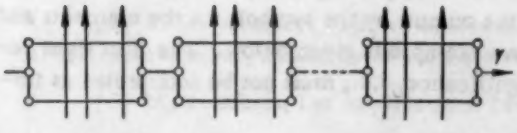

Fig. 7

If there are several outputs, each has its own Boolean function to represent its locking condition.

In this way the structures, and hence the functioning, of very complex combiners can be analyzed. The locking conditions for all outputs are written as Boolean functions appropriate to the coupling involved. To determine the output states from the input ones it suffices to calculate the Boolean functions appropriately. This rapidly and exactly determines which of the outputs are locked and which free in any input state.

The formulae can be simplified, and hence the structures of the mechanisms improved, by using algebraic transforms.

Example. Consider the mechanism of Fig. 8. We write down the condition for element X controlled by interlocks to levers A, B, C, D, E and F to operate:

$$F_X = a\bar{b}\bar{e} + \bar{e}\bar{e}\partial + a\bar{e}e + \bar{e}\partial + \bar{e}\partial\bar{e}. \qquad (2)$$

The transforms possible using Boolean algebra give

$$F_X = \bar{e}(a\bar{b}e + e\partial + ae + \partial) + \bar{e}\partial\bar{e} = \bar{e}(ae + \partial) + \bar{e}\partial\bar{e}. \qquad (3)$$

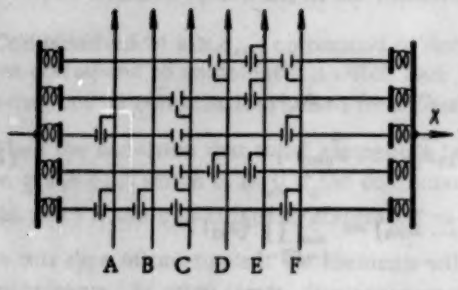

Fig. 8

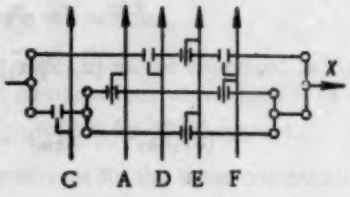

Fig. 9

The structure of the mechanism constructed from (3) is shown in Fig. 9.

Different structures corresponding to these functions can be derived, and their equivalence established.

Thus, for instance, if we transform (2) by a different regrouping, we get another structure

$$F_X = \partial(\bar{a}_0 + \bar{\partial} + \bar{\partial}\bar{e}) + \bar{a}\bar{\partial}e(\partial + 1) = \partial(\bar{\partial} + \bar{\partial}\bar{e}) + \bar{a}\bar{\partial}e, \qquad (4)$$

which satisfies the same conditions.

Figure 10 shows the structure deriving from (4). Hence the mechanisms of Figs. 8-10 are precisely equivalent, but the two latter are simpler.

Algebraic Synthesis of Combiner Structures

Use of the relations between 'and', 'or' and 'no' and the Boolean operations of multiplication, addition and inversion gives us the locking conditions for the outputs in algebraic form; these are usually given verbally. The Boolean functions are transformed to a form convenient for realization, e.g., that of (1), using identical algebraic transforms.* The general system of the mechanism is then easily sketched from the correspondence between the structures of the functions and the type of coupling between elements.

It is sometimes convenient to use the somewhat artificial device of putting the operating conditions as an algebraic expression, multiplying the Boolean functions for the outputs by the symbols for the elements and adding, as in the theory of relay contact circuits ([4], § 1.6). An example is given below. The plus signs between the Boolean functions are of logical and not structural significance, i.e., must not be interpreted as implying elastic couplings.

Any Boolean function can be represented in the disjunctive normal form as of (1) [5]. Hence this method is always sure to produce at least one solution. The number of locks is minimized by minimizing the number of letters in the Boolean functions, and the number of elastic links by minimizing the number of plus signs (Boolean additions).

Example. Let us consider the decoders used in telegraphy.

We use the artificial device indicated above and write the operation conditions as a single algebraic equation:

$$F = 1abcde + 2abcd\bar{e} + 3abc\bar{d}e + 4abc\bar{d}\bar{e} + 5ab\bar{c}de + 6ab\bar{c}d\bar{e} + 7ab\bar{c}\bar{d}e + 8ab\bar{c}\bar{d}\bar{e} + 9a\bar{b}cde + 10a\bar{b}cd\bar{e} + 11a\bar{b}c\bar{d}e + 12a\bar{b}c\bar{d}\bar{e} + 13a\bar{b}\bar{c}de + 14a\bar{b}\bar{c}d\bar{e} + 15a\bar{b}\bar{c}\bar{d}e + 16a\bar{b}\bar{c}\bar{d}\bar{e} + 17\bar{a}bcde + 18\bar{a}bcd\bar{e} + 19\bar{a}bc\bar{d}e + 20\bar{a}bc\bar{d}\bar{e} + 21\bar{a}b\bar{c}de + 22\bar{a}b\bar{c}d\bar{e} + 23\bar{a}b\bar{c}\bar{d}e + 24\bar{a}b\bar{c}\bar{d}\bar{e} + 25\bar{a}\bar{b}cde + 26\bar{a}\bar{b}cd\bar{e} + 27\bar{a}\bar{b}c\bar{d}e + 28\bar{a}\bar{b}c\bar{d}\bar{e} + 29\bar{a}\bar{b}\bar{c}de + 30\bar{a}\bar{b}\bar{c}d\bar{e} + 31\bar{a}\bar{b}\bar{c}\bar{d}e + 32\bar{a}\bar{b}\bar{c}\bar{d}\bar{e}$$

Here the figures denote the letter levers. The letters denote the corresponding selection rods, those with signs over denoting positions allowing motion, the others preventing it.

*The various identities of Boolean algebra are dealt with in § 1.7 of [4], and also in [5].

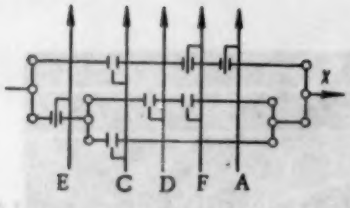

Fig. 10

In existing equipments all these combinations are distributed over the selection rods in accordance with the code used and with the positioning of the letter levers. We neglect the distribution actually used, and transform the expression analytically. We get

$$F = a(b\{c[d(1e + 2\bar{e}) + \bar{d}(3e + 4\bar{e})] + c[d(5e + 6\bar{e}) + d(7e + 8\bar{e})]\} + b\{c[d(9e + 10\bar{e}) + \bar{d} + (11e + 12\bar{e})] + c[d(13e + 14\bar{e}) + d(15e + 16\bar{e})]\} + \bar{a}(b\{c[d(17e + 18\bar{e}) + \bar{d}(19e + 20\bar{e})] + \bar{c}[d(21e + 22\bar{e}) + \bar{d}(23e + 24\bar{e})]\} + \bar{b}\{c[d(25e + 26\bar{e}) + \bar{d}(27e + 28\bar{e})] + \bar{c}[d(29e + 30\bar{e}) + \bar{d}(31e + 32\bar{e})]\}).$$

Figure 11 shows one possible design for a decoder to realize this expression.

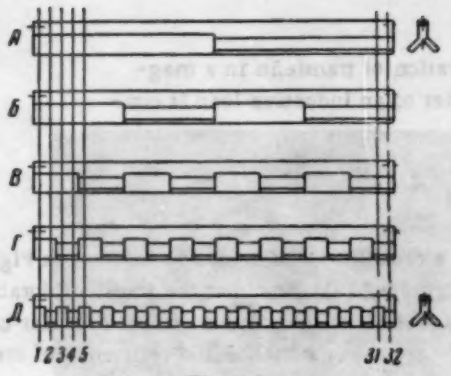

Fig. 11

In this system the rods rotate and do not move axially.

The normal position allows motion, the set position prevents it.

In conclusion we hope that this exposition of the basic theory of combiners using Boolean algebra will stimulate further developments, and the introduction of scientific methods into combiner design.

The author is indebted to G. N. Povarov for valuable discussions.

LITERATURE CITED

[1] J. Walter and J. Pavey, Automatic Train Control Devices on Railways in the West (Russian translation) (Transzheldorizdat, 1941).

[2] S. M. Iakovlev, "The structures of combiner mechanisms," Report of the Institute of Automation and Remote Control, Academy of Sciences of the USSR [in Russian] (1948).

[3] M. Touchais, Les Applications Techniques de la Logique (Dunod, Paris, 1956).

[4] V. N. Roginskii and A. D. Kharkevich, Relay Circuits in Telephony [in Russian] (Sviaz'izdat, 1955).

[5] D. Hilbert and V. Ackermann, Fundamentals of Theoretical Logic (Russian translation) (Izd. Inost. Lit., 1947).

[6] S. M. Iakovlev and M. A. Gavrilov, Authors' certificate No. 82785 of April 21, 1950.

[7] R. Higonnet and R. Gre'a Etude Logique des Circuits Electriques et des Systemes Binaires (Paris, 1955).

Received August 10, 1957

THE TRANSIENTS IN A MAGNETIC AMPLIFIER CONNECTED VIA A RECTIFIER TO AN INDUCTIVE LOAD

L. V. Safris

(Rostov-on-Don)

A method of calculating the duration of transients in a magnetic amplifier connected via a rectifier to an inductive load is considered.

INTRODUCTION

The transients in a magnetic amplifier connected via a rectifier to an inductive load (as in Fig. 1) have already been considered [1]. The deductions made there [formula (19)] show that the transient duration is determined by the load time-constant, no matter what the signal. The magnetization and rectifier characteristics were assumed ideal, with $\omega L_L \gg R_L$ (where L_L and R_L are the inductance and resistance of the load), and that the control current changes stepwise.

It is of interest to see how far this deduction can be applied if the inductors and rectifiers have nonideal characteristics.

Experiment indicates as follows.

At control currents I_θ close to maximal the rate of rise of the load current i_L is determined quite accurately by the load time-constant $\tau_L = L_L/(R_L + 2r_a)$ where r_a is the forward resistance of the bridge rectifier. This is confirmed by Fig. 2, which shows an oscillogram taken on a test model (A, appendix 1) with $\tau_L = 5.8 \times 10^{-2}$ sec.

When the control current is reduced the transient is briefer. This is confirmed by Fig. 3, which is for the same amplifier at a control current 10 times lower. Curve 1 of Fig. 4 (amplifier A) was drawn up from this oscillogram. For comparison, Curve 2 corresponds to $\tau_L = 5.8 \times 10^{-2}$ sec.

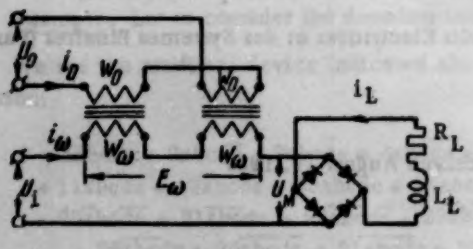

Fig. 1

The considerable divergence is explained by the back-emf induced in L_L by the current change, e_L; this acts to increase the voltage u_M acting on the rectifier bridge. This can occur by the input voltage U_1 being redistributed between bridge and output winding if the amplifier is not completely saturated ($E_\omega \neq 0$, Fig. 1). Increasing u_M reduces the transient duration (some aspects of this have been dealt with in [2], p. 669). The 'saturation angle' will not be constant throughout the transient, even if the control current changes stepwise. This is confirmed by Fig. 5, which shows u_M. The inductive load also influences the control circuit transient.

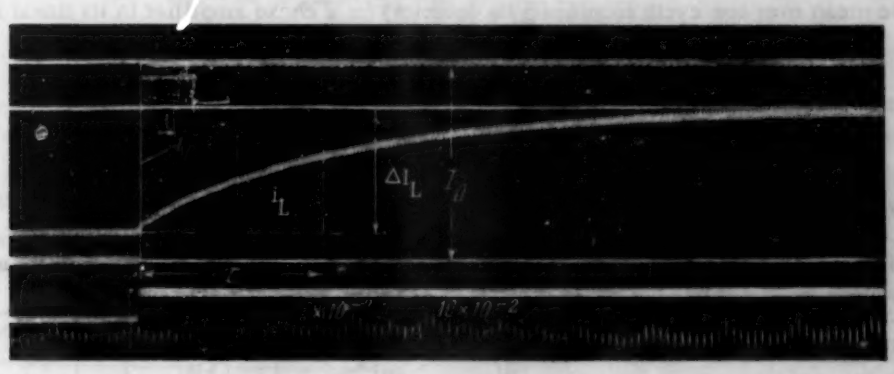

Fig. 2

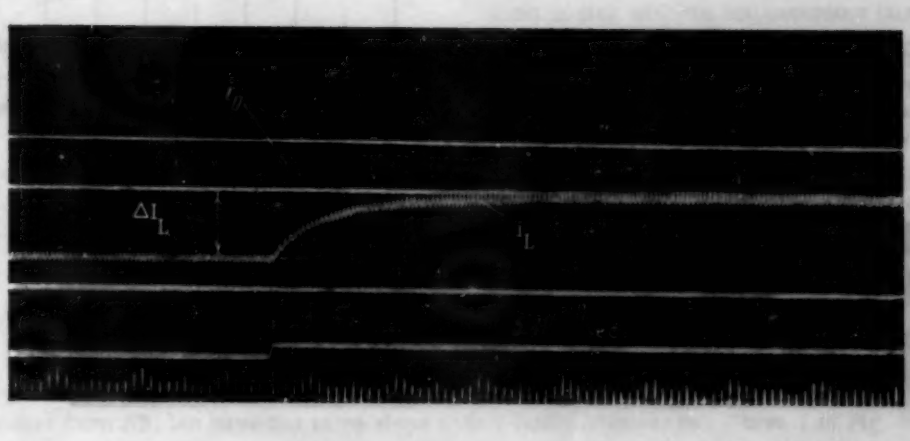

Fig. 3

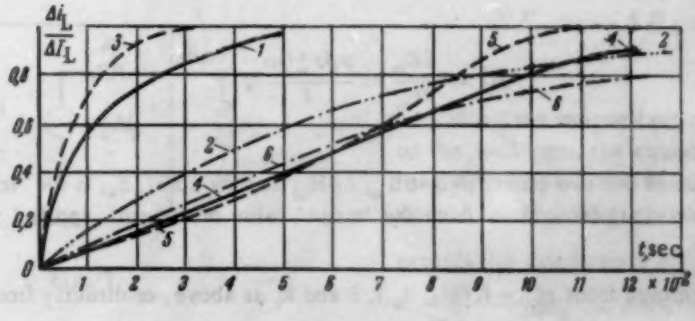

Fig. 4

Here we deduce approximate expressions to be used in transient duration calculations for the inductors and rectifiers which have nonideal characteristics, and which allow for the control circuit transient. We use the linearized magnetization characteristics method [3]. Only 'weak' signals in a choke amplifier are considered. By 'weak' are meant signals for which the current and voltage acting on the working windings in no case pass outside the rectilinear range on the magnetization characteristics, so the amplifier characteristics can be taken as constant. The bias magnetization is effected with an extra winding (not shown in Fig. 1) in series with adequately high resistance.

1. The Equivalent Circuit

It has been shown [3] that the 'instantaneous mean' a-c current change in a resistive load Δi_ω* (i.e., the arithmetic mean over one cycle recorded by a detector) for a choke amplifier in its linear range is

$$\Delta i_\omega = \frac{R_i S}{R_i + R} \Delta i_0 = k_i \Delta i_0. \tag{1}$$

Here k_i is the current gain, Δi_0 the control current change ('instantaneous mean' neglecting even harmonics), R is the total resistance (sum of the load resistance R_L and a-c winding resistance r_i; $r_i \ll R_L$ normally, so in future we assume $R \approx R_L$), S is the amplification factor, and R_i the internal resistance of the amplifier.

The amplification factor is given by

$$S = \frac{\partial I_\omega}{\partial I_0} = \sigma \frac{W_0}{W_\omega},$$

where W_0 is the number of turns on the control winding (Fig. 1), W_ω is the number of turns on the a-c winding, $\sigma = \partial H_\omega / \partial H_0$ at B_ω = const, H_ω is the 'mean' value of the a-c magnetic field component, determined from the 'mean' value of the current: $H_\omega = W_\omega I_\omega / l$, H_0 is the constant magnetic field component and l is the length of the magnetic circuit.

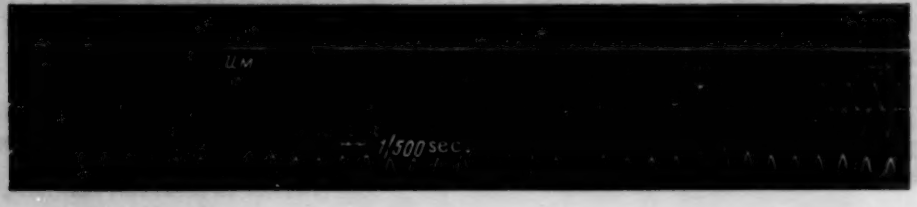

Fig. 5

The internal resistance is

$$R_i = \frac{\partial E_\omega}{\partial I_\omega} = \frac{\mu_i W_\omega^2 Q \omega}{l}.$$

Here Q is the cross-section of the two cores, $\mu_i = \partial B_\omega / \partial H_\omega$ at H_0 = const, B_ω is the 'mean' value of the a-c component of the induction, determined from the 'mean' value of the emf applied to the control winding W_ω: $B_\omega = E_\omega / \omega W_\omega Q$.

μ_i and σ are determined from $H_\omega = f_1(H_0, B_\omega)$, S and R_i as above, or directly from $I_\omega = f_2(I_0, E_\omega)$.

σ and μ_i define the magnetic properties of the inductors for a given shape of induction curve. If the range of variation in H_0, H_ω and B_ω is restricted they can be considered constant. Hence S and R_i are constant. Thus for Fig. 6 (amplifier A) we can take S = 1.05, R_i = 3500 ohms (dashed curves).

* The Δ sign indicates that the quantity can vary over the rectilinear range, and can be determined as the increase over the initial value. The mean i_ω during the transient is a time-function. This is the sense assigned to instantaneous mean, as contrasted with the steady-state ΔI_ω.

It has also [3] been shown that, no matter what the load, the control winding inductance is

$$L_0 = L_c + L_\nu = \frac{W_0^2 Q}{l}\mu_c - \frac{W_{0\nu}}{W_\omega}\frac{d(\Delta e_\omega)}{d(\Delta i_0)}. \qquad (2)$$

Here $\mu_c = \partial B_0 / \partial H_0$ at B_ω = const, $\nu = -\partial B_0 / \partial B_\omega$ at H_0 = const, L_c is the control winding inductance at zero load resistance and L_ν is the additional control winding inductance due to the load reaction.

μ_c and ν are determined from $B_0 = f_3(H_0, B_\omega)$ and are taken as constant.

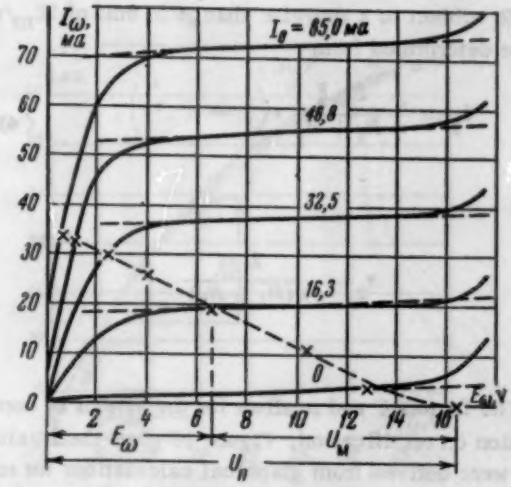

Fig. 6

The equivalent circuit shown in Fig. 7 has been drawn up from (1) and (2). It is here supposed that the delay introduced by the a-c circuit can be neglected and hence the emf is in phase with Δi_0. This assumption is based on the fact that for a resistive load the 'instantaneous mean' $\Delta i_\omega = \frac{R_i S \Delta i_0}{R_i + R}$ is almost in step with the instantaneous control current Δi_0.

In deducing (1) we assumed that the bias produced by the control signal ΔI_0 reduces ΔE_ω by an amount equal to the increase in load voltage, $R\Delta I_\omega$.

The experiments show that this remains correct in the steady state for an inductive load connected via a bridge if we take R as the input resistance of the bridge $R_M = \frac{\Delta U_M}{\Delta I_\omega}$. If E_ω and U_M were to add arithmetically, as in ideal amplifiers [1, 4], they would be related by the straight line AB of Fig. 8, and so $\Delta E_\omega = -\Delta U_M$. The curves representing the relation of ΔE_ω to ΔU_M for real amplifiers with inductive loads deviate somewhat from AB, but have the same slope over a fairly wide range. Curve 1 of Fig. 8 (amplifier A) shows $E_\omega = f_4(U_M)$, as an example. It corresponds to the load characteristic of Fig. 6, which can also be approximated by a straight line.

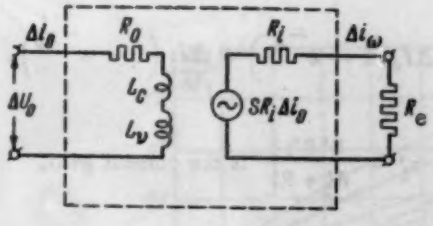

Fig. 7

We here assume that in the steady state

$$\Delta E_\omega \approx -\Delta U_M = -R_M \Delta I_\omega. \qquad (3)$$

Since the magnetization curves scarcely depend on the load type, the equivalent circuit of a choke magnetic amplifier with an inductive load can be derived from Fig. 7 by replacing R_L by R_M, at least as regards the steady state (Fig. 9a), and so $\Delta I_\omega = \frac{R_i S}{R_i + R_M}\Delta I_0$. In other words, the output circuit is replaced by a generator of emf $R_i S \Delta I_0$ and internal resistance R_i loaded by a bridge rectifier.

Figure 9a has been demonstrated correct for the a-c circuit for the steady state. For ideal amplifiers it has been shown [1, 4] that the d-c and a-c ampere-turns are equal whether the load consists of resistance with or without inductance. This follows directly from the expression for ΔI_ω, if we remember that ideal characteristics correspond to $\mu_i = \infty$, $\sigma = 1$.

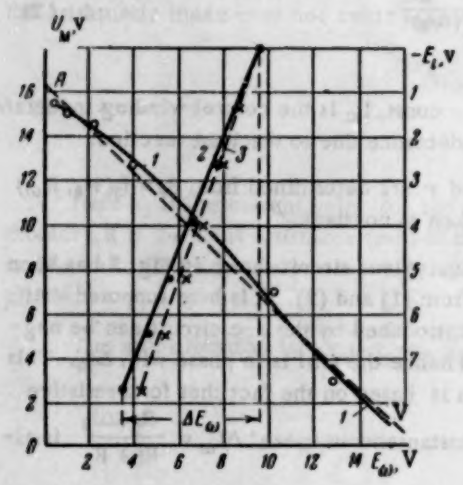

Fig. 8

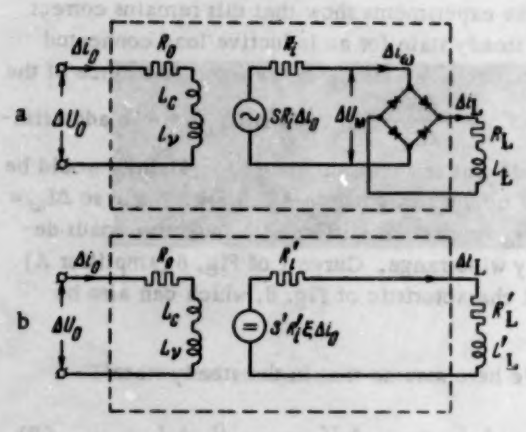

Fig. 9

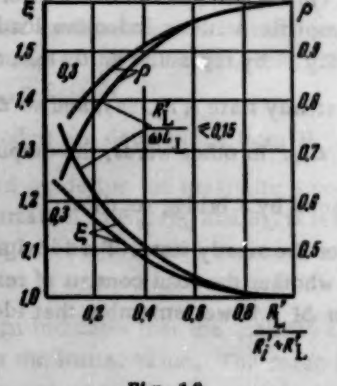

Fig. 10

We now determine whether this equivalent circuit can be used to determine the load current in the transient and steady states, provided the signals are weak.

To this end, using Fig. 9a, we determine the current $\Delta i_L = f(t)$ and compare calculation with experiment. The transforms we shall use are correct if the final results are confirmed by experiment.

We first simplify the circuit using [5], according to which the mean current in a (L_L, R_L) load connected via a rectifier to an a-c generator of internal resistance R_i subject to a stepwise change in emf of $2E_m/\pi$ can be determined from

$$i_L = \frac{2}{\pi}\frac{E_m \xi}{R_i + R_L}\cdot\left(1 - e^{-\frac{t}{\tau_e}}\right), \qquad (4)$$

where

$$\tau_e = \frac{L_L}{\rho(R_i + R_L)}.$$

The factors ξ and ρ allow for the effects of commutation on rectification. Figure 10 gives their values. these were derived from graphical calculations for sets of particular circuit parameter values. The effects of the forward and reverse resistances r_a and r_b of each arm are allowed for the recalculating R_i and R_L.

The load current in our case is

$$\Delta i_L = \frac{S' R'_i \xi \Delta I_0}{R'_i + R'_L}\left(1 - e^{-\frac{t}{\tau_e}}\right) \qquad (5)$$

$$= k'_i \Delta I_0\left(1 - e^{-\frac{t}{\tau_e}}\right) = \Delta I_L\left(1 - e^{-\frac{t}{\tau_e}}\right).$$

Here $k'_i = \frac{S' R'_i \xi}{R'_i + R'_L}$ is the current gain,

$$R'_i = \frac{(R_i + r_a)0.5r_b}{R_i + r_a + 0.5r_b},\quad R'_L = R_L' + R_a,\quad S' =$$

$$S\frac{R_i}{R_i + r_a},\quad L'_L = \frac{L_L}{\rho},$$

$$\tau_e = \frac{L'_L}{R'_i + R'_L}$$

is the equivalent time-constant of the output circuit.

Eq. (5) shows that the transients in the output are just those in a circuit consisting of an inductance L'_L and resistance $R'_1 + R'_L$ on connecting to a d-c source.

If Δi_θ is a known time-function, our assumption that S, R_1, μ_c and ν are constants means that Δi_L can be found by Laplace transform methods.

We can therefore replace this type of magnetic amplifier by the equivalent circuit of Fig. 9b. Of the two outputs (a-c and d-c in Fig. 9a), only the one to the load is here retained, as this is of direct interest to us. Hence Fig. 9b is equivalent only as regards the load circuit, and gives no indication of what occurs in the a-c circuit.

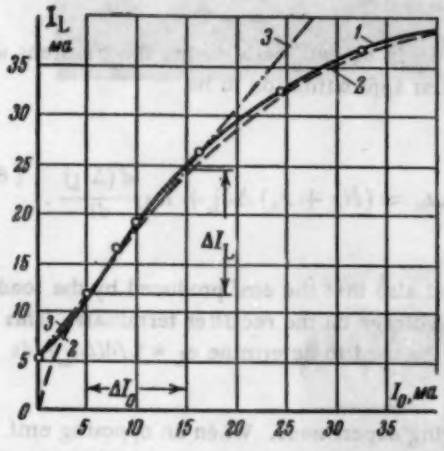

Fig. 11

To find the accuracy and applicability of (5) when deriving the steady-state Δi_L, we use Fig. 11, which shows 1) $I_L = f_5(I_\theta)$ (amplifier A), and 2) the same calculated from the graph proposed in [4] (Fig. 4) for an ideal amplifier, plus 3), which shows ΔI_L calculated from (5). In the range I_θ = 2-20 ma (5-50% of $I_{\theta max}$), which is of greatest interest to us, all three curves practically coincide. Near the maximum I_θ the divergence is large, because we have taken ξ as constant. The measured and calculated ΔI_L for other cases are given in Appendix 2.

We now consider the transient duration.

2. The Transient Duration

Three particular cases are considered.

Δi_θ varies stepwise. The transient duration will be determined by the time-constant of the output circuit τ_e, i.e., by (5). From the latter we have drawn (Appendix 2) the $\Delta i_L/\Delta I_L = f_6(t)$ curves for the models, A, B and C which differ in the inductors and rectifiers. These curves are shown in Figs. 4, 12 and 13 (curve 3). Curves 1 on these Figures were drawn up from Figs. 3, 14 and 15, which were taken under conditions corresponding to those used in the calculations. The divergence between curves 1 and 3 (at $\Delta i_L/\Delta I_L$ = 0.63) is on average 30%, and arises partly from the finite rates of change of Δi_θ and ΔB_θ, and partly from errors in measuring the oscillograms. In one case (Fig. 4) the rectifier back resistance is neglected.

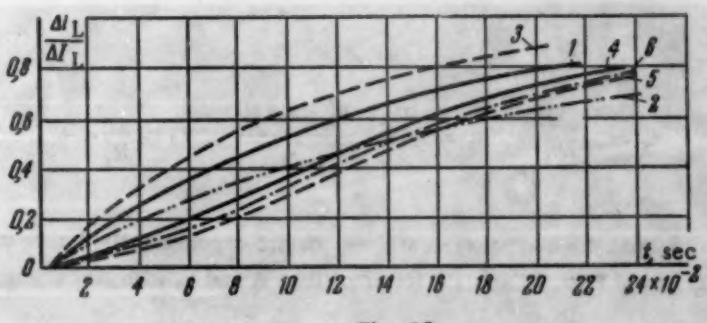

Fig. 12

The time-constants given by the oscillograms are several times smaller than τ (curves 2 on the figures), and differ more from one another the larger R'_1/R'_L.

Δu_θ varies stepwise. Here the law followed by Δi_L is determined by the parameters of the output and control circuits.

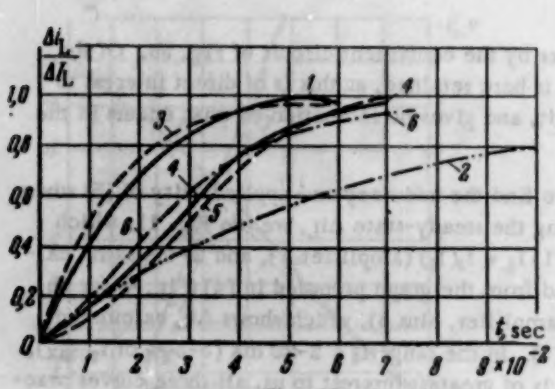

Fig. 13

The equivalent circuit of Fig. 9b shows that the transient on the output is described by

$$S' R_i' \xi \Delta i_0 = (R_i' + R_L') \Delta i_L + L_L' \frac{d(\Delta i_L)}{dt}. \quad (6)$$

The equation for the control circuit (using (2) and Fig. 9b) is

$$\Delta u_0 = R_0 \Delta i_0 + \frac{W_0^2 Q}{l} \mu_c \frac{d(\Delta i_0)}{dt} - \frac{W_0 \nu}{W_\omega \omega} \frac{d(\Delta e_\omega)}{dt}. \quad (7)$$

The Δe_ω in the ac coils during the transient we take to a first approximation to be

$$-\Delta e_\omega \approx \Delta u_M \approx (R_L' + r_a) \Delta i_L + L_L \frac{d(\Delta i_L)}{dt}. \quad (8)$$

Unlike in (3), we here assume that $R_M \Delta I_\omega \approx (R_L' + r_a) \Delta I_L$, and also that the emf produced by the load self-inductance from Δi_L is equivalent to an equal increase in the voltage on the rectifier terminals. This assumption is required because the output circuit in Fig. 9b cannot be used to determine $e_L = L/d(\Delta i_L)/dt$ ([6], p. 48).

This simplification is justified by the results from the following experiment. When an opposing emf E_L (0-8V) was connected in series with the load (amplifier A) E_ω took the value given by curve 2 of Fig. 8. The $E_\omega = f_7(E_L)$ calculated from (8) is shown by curve 3. The divergence is slight. Hence using (8) we allow of a certain inaccuracy in determining the effect of the load on the control circuit transients.

Applying the Laplace transform to (6), (7) and (8) solving we get

$$\Delta i_L = \frac{\Delta U_0}{R_0} k_i' L^{-1}\left[\frac{1}{p} \frac{1}{(\tau_c \tau_e + \tau_\nu \tau_L) p^2 + (\tau_c + \tau_\nu + \tau_e) p + 1}\right], \quad (9)$$

$$\Delta i_0 = \frac{\Delta U_0}{R_0} L^{-1}\left[\frac{1}{p} \frac{p\tau_0 + 1}{(\tau_c \tau_e + \tau_\nu \tau_L) p^2 + (\tau_c + \tau_\nu + \tau_e) p + 1}\right]. \quad (10)$$

Here

$$\tau_c = \frac{W_0^2 Q \mu_c}{l R_0}, \quad \tau_\nu = \frac{W_0 \nu (R_L' + r_a) k_i'}{W_\omega \omega R_0}, \quad \tau_L = \frac{L_L}{R_L' + r_a}. \quad (11)$$

These expressions indicate that the control current does not rise exponentially during transients. This is confirmed by the Δi_0 oscillograms of Figs. 16 and 17, for amplifiers A and B, with Δu_0 changing stepwise (Appendix 2).

Applying reverse Laplace transform we have

$$p_{1,2} = \frac{-(\tau_c + \tau_\nu + \tau_e) \pm \sqrt{(\tau_c + \tau_\nu + \tau_e)^2 - 4(\tau_c \tau_e + \tau_\nu \tau_L)}}{2(\tau_c \tau_e + \tau_\nu \tau_L)} \quad (12)$$

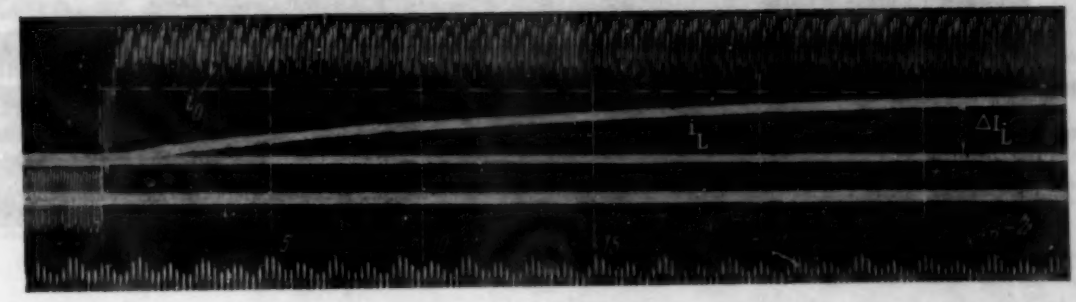

Fig. 14

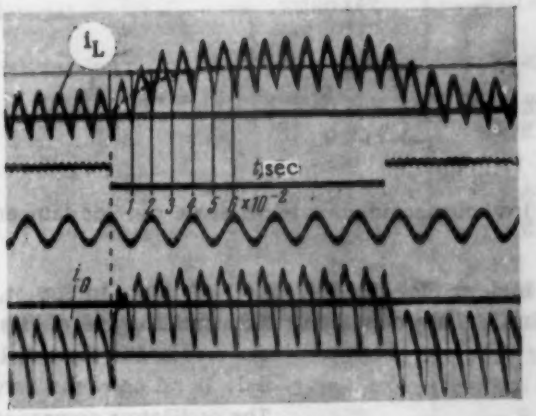

Fig. 15

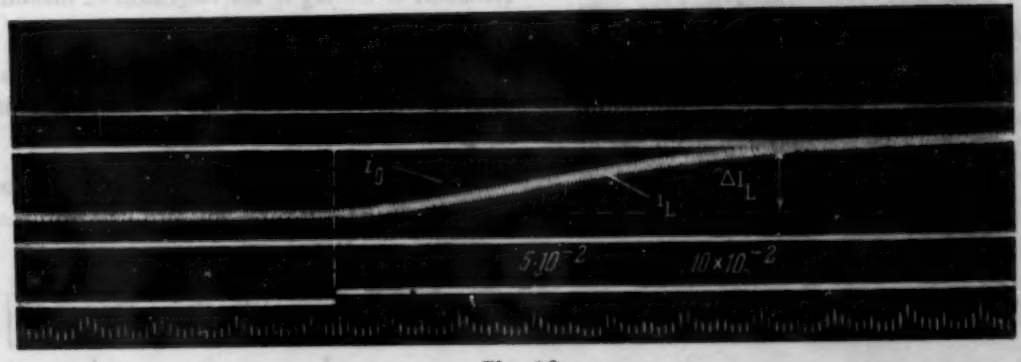

Fig. 16

Two main cases occur: p_1 and p_2 are real $(-a_1, -a_2)$ or complex $(-a \pm jb)$.

In the first case Δi_L is

$$\Delta i_L = \frac{\Delta U_0}{R_0} k_i' \left[1 + \frac{1}{a_1 - a_2}(a_2 e^{-a_2 t} - a_1 e^{-a_1 t})\right].$$

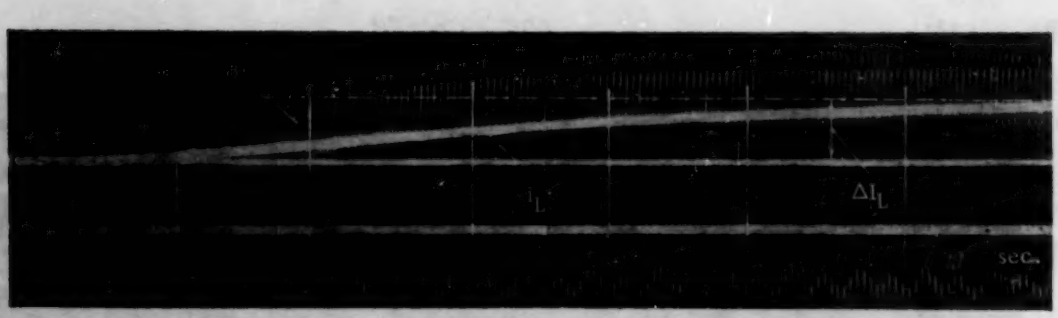

Fig. 17

If the roots are complex

$$\Delta i_L = \frac{\Delta U_0}{R_0} k_i' \left[1 - \frac{b_0}{b} e^{-\alpha t} \sin(bt - \varphi)\right], \tag{14}$$

where

$$\varphi = \arctan\frac{-b}{a}, \quad b_0^2 = a^2 + b^2 = \frac{1}{\tau_c \tau_e + \tau_v \tau_L}.$$

Hence with an inductive load connected via a rectifier we can get damped low-frequency oscillations on Δi_L.

(Fourteen) has been used to determine the $\Delta I_L/\Delta I_L = f_8(t)$ shown in Figs. 4, 12 and 13 (curves 5) for the A, B and C amplifiers (Appendix 2). They correspond to the oscillograms of Figs. 16, 17 and 18 from which the curves 4 in Figs. 4, 12 and 13 have been constructed. In all cases the curves 4 and 5 coincide adequately. The oscillatory component appears more clearly on the calculated curves than on the oscillograms.

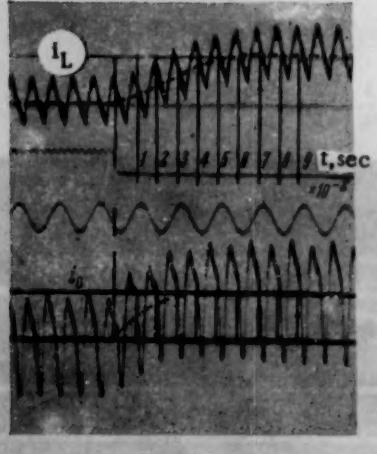

Fig. 18

The control current varies exponentially. This case is of some interest in relation to approximate estimates of the lag in the current in an inductive load from the lag in the control circuit, if known.

We assume the control circuit parameters R_θ and L_θ constant. Hence Δi_θ in response to a step voltage input will rise exponentially.

The expression for Δi_L can be derived from (9), (12) and (13) by replacing τ_c by $\tau_\theta = L_\theta/R_\theta$ and $\tau_v = 0$.

Substituting in this way, we have

$$\Delta i_L = \frac{\Delta U_\theta}{R_\theta} k_1 L^{-1}\left[\frac{1}{p}\frac{1}{(1+\tau_0 p)(1+\tau_e p)}\right], \tag{15}$$

$$p_1 = -\frac{1}{\tau_0}, \qquad p_2 = -\frac{1}{\tau_e}.$$

Applying the reverse Laplace transform we have

$$\Delta i_L = \frac{\Delta U_0}{R_0} k_i' \left[1 + \frac{1}{\tau_e - \tau_0}\left(\tau_0 e^{-\frac{t}{\tau_0}} - \tau_L e^{-\frac{t}{\tau_L}}\right)\right]. \tag{16}$$

The curves 6 corresponding to this case are shown in Figs. 4, 12 and 13 (Appendix 2). There is no great divergence between the results given by (14) and (16). We must remember here that τ_θ was taken direct from the Δi_θ oscillogram as the time corresponding to $\nabla i_\theta / \Delta i_\theta = 0.63$.

SUMMARY

1. The equivalent circuits and formulae used are confirmed by experiment.

2. The expressions for Δi_L indicate how the amplifier and rectifier parameters affect the transient duration for an inductive load and weak signals. Estimates from the load time-constant alone are useless.

3. The expressions are suitable for use until stricter and more universal methods for the purpose become available.

Appendix 1

Amplifier Descriptions

Data		Model A	Model B	Model C
Cores	Material	EN80 MZ (NIITVCh)	Permalloy	Transformer steel
	Construction	Spiral toroids	Spiral toroids	Ring toroids
	$10^{-4} Q$, $м^3$	2×0.325	2×1.5	2×1.67
	l, $м$	0.13	0.2	0.25
Windings	W_w, Turns	190	40	800
	W_0 »	200	120	600
	r_f, ohms	2×2.1	2×0.8	2×2.05
Parameters	S	1.05	3	0.55
	R_f, ohms	3500	105	1600
	$10^{-3}\ \mu_c$,	0.6	3.8	2.5
	ν	1,38	1.35	1.5
Bridge rectifier	Type	DGTs-4	Cuprous oxide	Selenium
	r_a, ohms	122	9	40
	r_b »	∞	2200	9000
Load	R_L »	186	100	320
	L_L, Henries	25	19	19
Operating conditions	Frequency, c/s	500	500	50
	U_L, v	16.2	22.5	63
	I_{op} (bias), ma	5	15	45

Appendix 2

Calculation of Δi_L

Operating conditions	Model A	Model B	Model C
R'_i, ohms	3620	103	1200
R'_L, ohms	308	109	360
$R'_L/\omega L_L$	0.004	0.0015	0.06
$R'_L/(R'_L+R'_L)$	0.078	0.51	0.23
$\Delta i_0 = \begin{cases} 0 & \text{when } t<0 \\ \Delta I_0 & \text{when } t\geqslant 0 \end{cases}$	ξ 1.33 ρ 0.63	1.07 0.93	1.18 0.8
ΔI_0, ma	5.0	30	30
$10^{-2}\tau_p$ sec. { exp. / calc.	1.2 0.8 (67%)	13.5 9.6 (71%)	1.9 1.5 (79%)
$\frac{\Delta i_L}{\Delta I_L}$ { exp.	Fig. 4 (curve 1)	Fig. 12 (curve 1)	Fig. 13 (curve 1)
$\frac{\Delta i_L}{\Delta I_L}$ { calc.	Fig. 3. Fig. 4 (curve 3)	Fig. 14. Fig. 12 (curve 3)	Fig. 15. Fig. 13 (curve 3)
R_0, ohms	6.8	4.5	134
$10^{-2}\tau_c$, sec.	0.18	1.8	0.9
$10^{-2}\tau_v$ »	3.65	4.85	0.52
$\Delta u_0 = \begin{cases} 0 & \text{when } t<0 \\ \Delta U_0 & \text{when } t\geqslant 0 \end{cases}$	$10^{-2}\tau$ sec. 5.8	16.1	4.75
	$p_{1,2}$, 1/sec. $-10.8 \pm j\,18.5$	$-8.5 \pm j\,5.7$	$-38.3 \pm j\,34$
$\tan\varphi$	−1.71	−0.67	−0.885
φ, rad	−1.04	−0.59	−0.725
b_0 1/sec.	21.6	10.3	51
b_0/b	1.17	1.8	1.5
ΔI_L, ma { exp.	7	46	14
ΔI_L, ma { calc.	6.3	43	14.5
$\frac{\Delta i_L}{\Delta I_L}$ { exp.	Fig. 4 (curve 4)	Fig. 12 (curve 4), Fig. 17.	Fig. 13 (curve 4), Fig. 18.
$\frac{\Delta i_L}{\Delta I_L}$ { calc.	Fig. 16 Fig. 4 (curve 5)	Fig. 12 (curve 5)	Fig. 13 (curve 5)
$10^{-2}\tau_0$ sec.	7	7	1.6
$\frac{\Delta i_0}{\Delta I_0} = 1 - e^{-\frac{t}{\tau_0}}$ $10^2 \frac{1}{\tau_e - \tau_0}$, $\frac{1}{\text{sec.}}$	0.16	0.38	10
$\frac{\Delta i_L}{\Delta I_L}$ calc.	Fig. 4 (curve 6)	Fig. 12 (curve 6)	Fig. 13 (curve 6)

LITERATURE CITED

[1] N. P. Vasil'eva, "Operation of a magnetic amplifier connected to a load containing resistance and inductance via a bridge rectifier," Automation and Remote Control (USSR) 15, No. 6 (1954).

[2] M. A. Rozenblat, Magnetic Amplifiers [in Russian] (Izd. Sov. Radio, 1956).

[3] L. V. Safris, "Magnetic amplifier calculation from linearized magnetization characteristics," Trudy Rostov. Inst. Inzh. Zelezh. Trans. No. (Transzheldorizdat, 1956).

[4] H. F. Storm, "Saturable reactor with inductive d.c. load," Trans. AIEE, Vol. 71, part 1, pp. 335-343, (1952).

[5] L. V. Safris, "Calculation of the current in an inductive load connected via a bridge rectifier," Trudy Rostov. Inst. Inzh. Zelezh. Trans. No. (Transzheldorizdat, 1956).

[6] V. G. Komar, The Operation of Semiconductor Rectifiers in Control Circuits [in Russian] (Gosenergoizdat, 1952).

Received April 6, 1957

THE CALCULATION OF A CHOKE MAGNETIC AMPLIFIER CONNECTED TO A SINGLE-PHASE BRIDGE RECTIFIER

N. A. Kaluzhnikov

(Kharkov)

A method for the calculation of a choke magnetic amplifier connected to a single-phase bridge rectifier as regards the a-c circuit is presented, for the case where the load has inductive and capacitative components, using the theory of the ideal 'linear' magnetic amplifier.

Practically the only papers on the calculation of a choke magnetic amplifier connected to a single-phase bridge rectifier are those of Komar [1] and Vasil'eva [2].

The calculation of a complex nonlinear circuit such as the a-c circuit in a magnetic amplifier connected to a single-phase bridge rectifier must involve some fairly major simplifications.

Here we also make some assumptions.

1. The rectifiers are ideal (forward resistance and back conductances both zero).

2. The 'natural' magnetization mode is used (impedance for even harmonics zero).

3. Core losses are neglected, and the resistance and leakage of the windings are assumed zero.

4. Only large inductances and capacitances are considered so that the load time-constant is much longer than one half-period of the supply. In other words we assume the inductance to smooth the current ideally and the capacitance the voltage. These conditions are adequately satisfied in practice by a load with $\omega L_l \geq (5-10)R_l$ and $\omega C_l \geq (5-10)/R_l$.

Here we consider two extreme cases.

1. The cores consist of a material with a rectangular magnetization curve.

2. The magnetic amplifier acts as a linearly varying inductance (linear case).

The latter case is only of interest in calculations as representing an extreme case. This type of assumption is made if the currents and voltages are assumed sinusoidal with the load operating on a-c, which is the basis of most existing calculation methods.

Real amplifiers work in modes lying between these extremes. We therefore need only consider these modes, and recommend the less favorable of them, so that normal control operation is possible under real conditions.

All load parameters (resistance, opposing emf etc.,) are assumed given, together with the bridge output current I_l.

The object of calculations on the a-c circuit is to determine the supply voltage U_c, the minimum voltage on the amplifier U_a, and the current drawn by the a-c windings I_a. These are all calculated from the load parameters and from the magnetic conditions used, which are determined by k_B equal to the ratio $U_{a\,max}/U_a$, $U_{a\,max}$ is taken as equal to U_c. The calculations are done using half-period mean voltages and currents.

All types of load are divided into two groups, namely Komar's A [1], where the impedance is inductive and 'double short circuit' operation occurs and R, where the impedance is capacitative and 'double open circuit' operation occurs.

The purely resistive load case falls between these and allows neither A nor R modes.

Operation with an Inductive Load

Figure 1 shows three circuits (a, b and c) to be considered in this section. They are ones with an emf acting in the same direction and a resistance, with an inductance plus resistance, and with an inductance plus two resistances. In all cases there is a divergence between the mean currents before and after rectification.

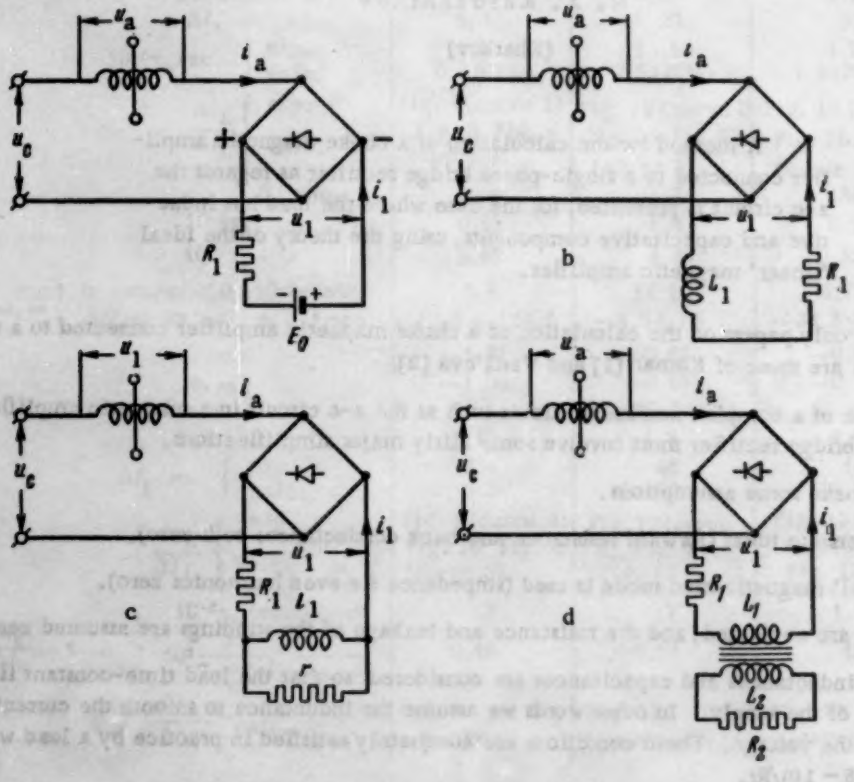

Fig. 1. Circuits using single-phase bridge rectifiers and inductive loads.

Ideal amplifier. We start with the circuit of Fig. 1 a. Figure 2 shows graphs of u_a, u_1, i_a and i_1.

The operation of the circuit falls into two sections. In the first no current at all is passed, and the line voltage is entirely taken up in magnetizing the cores. During this period a current $i_1 = E_0/R_1$ flows in the load circuit.

During the second the amplifier is completely saturated.

The circuit then presents zero impedance, and the rectifier begins to conduct at the instant of transition. The total current flowing is $i_1 = (u_1 + E_0)/R_1$, so $u_1 = i_1 R_1 - E_0$.

A more detailed description of the operation is given in [1, 2].

The mean values of these quantities are

$$U_a = \frac{1}{\pi}\int_{-\pi/2}^{\psi} u_m \cos \omega t \, d\omega t = \frac{1}{\pi} u_m (\sin \psi + 1) = U_c \frac{1+\sin\psi}{2}, \qquad (1)$$

$$U_1 = \frac{1}{\pi}\int_{\psi}^{\pi/2} u_m \cos\omega t \, d\omega t = \frac{1}{\pi} u_m (1 - \sin\psi) = U_c \frac{1-\sin\psi}{2}, \tag{2}$$

$$I_a = \frac{1}{\pi}\int_{\psi}^{\pi/2}\left(\frac{u_m}{R_1}\cos\omega t + \frac{E_0}{R_1}\right) d\omega t = \frac{1}{\pi}\frac{u_m}{R_1}(1 - \sin\psi) + \left(\frac{1}{2} - \frac{\psi}{\pi}\right)\frac{E_0}{R_1} =$$

$$= \frac{U_c}{R_1}\frac{1-\sin\psi}{2} + \left(\frac{1}{2} - \frac{\psi}{\pi}\right)\frac{E_0}{R_1}, \tag{3}$$

$$I_1 = \frac{1}{\pi}\int_{-\pi/2}^{\psi}\frac{E_0}{R_1} d\omega t + \frac{1}{\pi}\int_{\psi}^{\pi/2}\left(\frac{u_m}{R_1}\cos\omega t + \frac{E_0}{R_1}\right) d\omega t = \frac{U_c}{R_1}\frac{1-\sin\psi}{2} + \frac{E_0}{R_1}. \tag{4}$$

The expression for the two coefficients used are

$$k_B = \frac{U_c}{U_a} = \frac{2}{1+\sin\psi} \tag{5}$$

and

$$\beta = \frac{I_a}{I_1} = \frac{\frac{U_c(1-\sin\psi)}{2} + \left(\frac{1}{2} - \frac{\psi}{\pi}\right)E_0}{U_c\frac{1-\sin\psi}{2} + E_0} = \frac{1 + \left(\frac{1}{2} - \frac{\psi}{\pi}\right)\frac{E_0}{U_1}}{1 + \frac{E_0}{U_1}}. \tag{6}$$

Here

$$U_1 = I_1 R_1 - E_0 = U_c \frac{1-\sin\psi}{2}.$$

We turn now to Fig. 1c, which is the equivalent circuit with allowance for the mutual inductance (Fig. 1d) at unit coupling coefficient ($M^2/L_1L_2 = 1$). The parameters of the two circuits are [1] related by $R_1 = R_1$, $r = R_2 (L_1/L_2)$, $L_1 = L_1$.

Using Komar's results, we have $\mu_1 = i_1 R - I_1 r$ where $R = R_1 + r$. We thus get a circuit equivalent to that with a forward emf, if we put $E_0 = I_1 r$. This enables us to transfer the deductions to this circuit also. The two circuits show an essential difference in mode of operation, however. In Fig. 1a the emf does not depend on the magnetic amplifier at all, whereas in the latter case the emf depends on the amplifier current.

Hence U_a, U_1 and k_B are given by (1), (2) and (5). The expressions for I_a, I_1 and β are somewhat altered.

Since the d-c component of the voltage across the inductance is zero, we have

$$I_1 = \frac{U_1}{R_1} = \frac{U_c}{R_1}\frac{1-\sin\psi}{2}. \tag{4a}$$

For I_a we then have

$$I_a = \frac{U_c}{R_1 + r}\frac{1-\sin\psi}{2} + \left(\frac{1}{2} - \frac{\psi}{\pi}\right)\frac{I_1 r}{R_1 + r}.$$

Substituting for I from (4a), we get (after manipulation)

$$I_a = \frac{U_c}{R_1}\,\frac{1-\sin\psi}{2}\left[1-\left(\frac{1}{2}-\frac{\psi}{\pi}\right)\frac{r}{R_1+r}\right], \tag{3a}$$

$$\beta = 1-\frac{\pi+2\psi}{2\pi}\,\frac{r}{R_1+r} = \frac{1}{1+\frac{r}{R_1}}\left(1+\frac{\pi-2\psi}{2\pi}\,\frac{r}{R_1}\right). \tag{6a}$$

(Six) and (6a) are identical if $\frac{E_0}{U_1} = \frac{r}{R_1} = k_R$. (6)

Hence the graphs derived for Fig. 1c can be applied to Fig. 1a if the k_R are equal. Suppose now that k_R varies from 0 to ∞ due to change in r at R_1 = const.

For $k_R = 0$ we have a purely resistive load, and (1), (2), (4a) and (5) apply. The expressions for I_a and β simplify to

$$I_a = \frac{U_c}{R_1}\,\frac{1-\sin\psi}{2} = I_1 \text{ and } \beta = 1.$$

For $k_R = \infty$ we get the circuit of Fig. 1b. Here

$$I_a = \frac{U_c}{R_1}\,\frac{1-\sin\psi}{2}\,\frac{\pi-2\psi}{2\pi} \tag{3b}$$

$$\beta = \frac{\pi-2\psi}{2\pi}. \tag{6b}$$

The analysis therefore gives this result. For all inductive load types without exception $U_a + U_1 = U_c$ if the core material is ideal. The extreme cases are $k_R = 0$ (pure resistance load) and $k_R = \infty$ (resistance + inductance). In the first case β = 1, in the second β is maximal. All other cases are intermediate. The nonlinear distortions introduced by the load are defined by k_R, which is r/R_1 for Fig. 1c, and E_0/U_1 for Fig. 1a.

Figure 3a shows $\beta = f(k_R)$ for an 'ideal' amplifier.

Linear choke. A bridge fed via a linear input inductance is treated in the same way.

Figure 4 shows how the currents and voltages in the circuit of Fig. 1b change in time. Unlike in the preceding case, the two halves of the circuit operate independently in the first section. Here

$$u_a = u_c,\ u_1 = i_1 R_1 - E_0 = 0,\ i_1 = \frac{E_0}{R} \text{ and } i_a = \int \frac{u_c}{x_a}\,d\omega t + C = \frac{u_m}{X_a}\sin\omega t + C.$$

In the second section the law followed by the current is given by $u_c + E_0 = X_a\,\frac{di_a}{d\omega t} + i_a R_1$, where $i_a = i_1$, $u_1 = i_1 R_1 - E_0$ and $u_a = u_c - u_1 = X_a\,\frac{di_a}{d\omega t}$.

These give the instantaneous currents and voltages as

$$i_a = i_1 = \frac{u_m}{Z}\cos(\omega t - \varphi) + \frac{E_0}{R_1} + Ae^{-\frac{\omega t}{\tau}}$$

(where $Z = \sqrt{R_1^2 + X_a^2}$, $\tan \varphi = \tau = \frac{X_a}{R_1}$, and X_a is the linear input inductance);

$$u_1 = \frac{u_m}{Z} R_1 \cos(\omega t - \varphi) + AR_1 e^{-\frac{\omega t}{\tau}},$$

$$u_a = -X_a \frac{u_m}{Z} \sin(\omega t - \varphi) - \frac{X_a}{\tau} Ae^{-\frac{\omega t}{\tau}}.$$

The integration constants are given by the initial conditions $i_a(\theta) = \frac{E_0}{R_1}$ and $i_a(\psi) = \frac{E_0}{R_1}$.

This gives the choke current variation law as:

in the interval $(\psi - \pi)$ to θ, $i_{a_1} = \frac{u_m}{X_a}(\sin \omega t - \sin \theta) + \frac{E_0}{R_1}$;

in the interval θ to ψ, $i_a = i_1 = \frac{u_m}{Z}\left[\cos(\omega t - \varphi) - \cos(\theta - \varphi) e^{-\frac{\omega t - \theta}{\tau}}\right] + \frac{E_0}{R_1}$;

in the interval ψ to $(\theta + \pi)$, $i_{a_2} = \frac{u_m}{X_a}(\sin \omega t - \sin \psi) + \frac{E_0}{R_1}$.

Expressions for u_1 and u_a in the interval from θ to ψ are represented:

$$u_1 = u_m \cos \varphi \left[\cos(\omega t - \varphi) - \cos(\theta - \varphi) e^{-\frac{\omega t - \theta}{\tau}}\right],$$

$$u_a = -u_m \left[\sin \varphi \sin(\omega t - \varphi) - \cos \varphi \cos(\theta - \varphi) e^{-\frac{\omega t - \theta}{\tau}}\right].$$

The formulas for the mean currents and voltages are

$$I_1 = \frac{E_0}{R_1} + \frac{1}{\pi}\int_{\theta}^{\psi}\left(i_1 - \frac{E_0}{R_1}\right) d\omega t = \frac{E_0}{R_1} + \frac{U_c}{R_1}\frac{\sin \psi - \sin \theta}{2}, \tag{7}$$

$$I_a = \frac{E_0}{R_1} + \frac{1}{\pi}\int_{\theta}^{\psi}\left(i_1 - \frac{E_0}{R_1}\right) d\omega t +$$

$$+ \frac{1}{\pi}\int_{\alpha}^{\theta}\left(i_{a_1} - \frac{E_0}{R_1}\right) d\omega t + \frac{1}{\pi}\int_{\psi}^{\pi+\alpha}\left(i_{a_2} - \frac{E_0}{R_1}\right) d\omega t =$$

$$= I_1 - \frac{U_c}{R_1}\frac{1}{\tau}\left[\frac{\theta - \alpha}{2}\sin \theta + \frac{\pi + \alpha - \psi}{2}\sin \psi + \frac{\cos\theta - \cos\psi - 2\cos\alpha}{2}\right], \tag{8}$$

$$U_1 = I_1 R_1 - E_0 = U_c \frac{\sin \psi - \sin \theta}{2}, \tag{9}$$

$$U_a = \frac{1}{\pi}\int_{\alpha}^{\theta} u_c \, d\omega t + \frac{1}{\pi}\int_{\theta}^{\delta} u_a \, d\omega t - \frac{1}{\pi}\int_{\delta}^{\psi} u_{xp} \, d\omega t -$$

$$- \frac{1}{\pi}\int_{\psi}^{\pi+\alpha} u_c \, d\omega t = U_c\left[\tau \cos \delta + \frac{\sin \psi + \sin \theta}{2}\right], \tag{10}$$

$$I_B = \frac{2}{2\tau \cos \delta + \sin \psi + \sin \theta}, \tag{11}$$

$$\beta = \frac{I_a}{I_1} = 1 - \frac{\frac{U_c}{R_1}\frac{1}{\tau}\left[\frac{\theta-\alpha}{2}\sin\theta + \frac{\pi+\alpha-\psi}{2}\sin\psi + \frac{\cos\theta-\cos\psi-2\cos\alpha}{2}\right]}{\frac{E_0}{R_1} + \frac{U_c}{R_1}\frac{\sin\psi-\sin\theta}{2}}. \qquad (12)$$

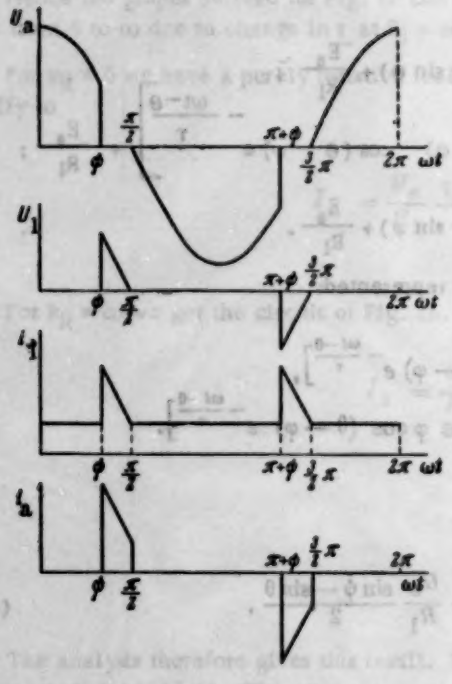

Fig. 2

The angles ψ, δ and α are given by $i_1(\psi) = \frac{E_0}{R_1}$, $u_a(\delta) = 0$, $i_{a1}(\alpha) = 0$.

The resulting transcendental equations for the angles are:

$$\cos(\psi - \varphi) = \cos(\theta - \varphi)\, e^{-\frac{\psi-\theta}{\tau}}, \qquad (13)$$

$$\sin(\delta - \varphi) = \frac{\cos(\theta-\varphi)}{\tau}\, e^{-\frac{\delta-\theta}{\tau}}, \qquad (14)$$

$$\sin\alpha = \frac{\sin\theta - \sin\psi}{2}. \qquad (15)$$

In deducing the last equation we have also used the condition $i_a(\theta + \pi) = -\frac{E_0}{R_1}$, which gives $\frac{E_0}{R_1} = \frac{\sin\theta + \sin\psi}{2}\frac{u_m}{X_a}$. This latter, when transformed, gives a relation important to the subsequent analysis:

$$\tau = \frac{\pi}{2}\frac{U_c}{E_0}\frac{\sin\theta + \sin\psi}{2}.$$

Substituting for U_C from (9), we finally get

$$\tau = \frac{\pi}{2}\frac{U_1}{E_0}\frac{\sin\psi + \sin\theta}{\sin\psi - \sin\theta}. \qquad (16)$$

Equations (9) – (11) and (13) – (15) continue to apply to the circuit of Fig. 1c.

(Seven), (8), (12) and (16) are somewhat altered:

$$I_1 = \frac{U_1}{R_1} = \frac{U_c}{R_1}\left(\frac{\sin\psi - \sin\theta)}{2}\right), \qquad (7a)$$

$$I_a = I_1 - \frac{U_c}{R_1}\frac{R_1}{R_1 + r}\frac{1}{\tau}\left[\frac{\theta-\alpha}{2}\sin\theta + \frac{\pi+\alpha-\psi}{2}\sin\psi + \frac{\cos\theta-\cos\psi-2\cos\alpha}{2}\right], \qquad (8a)$$

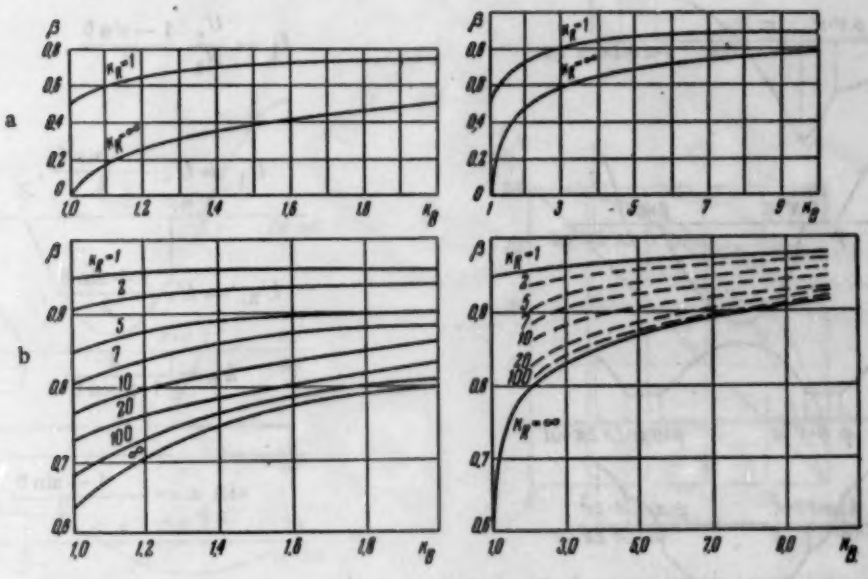

Fig. 3

$$\beta = 1 - \frac{\frac{R_1}{R_1 + r}\frac{1}{\tau}\left[\frac{\theta - \alpha}{2}\sin\theta + \frac{\pi + \alpha - \psi}{2}\sin\psi + \frac{\cos\theta - \cos\psi - 2\cos\alpha}{2}\right]}{\frac{\sin\psi - \sin\theta}{2}}, \tag{12a}$$

$$\tau = \frac{\pi}{2}\cdot\frac{R_1}{r}\cdot\frac{\sin\psi + \sin\theta}{\sin\psi - \sin\theta}. \tag{16a}$$

Also $\tau = \frac{X_a}{R_1 + r}$. This gives the required relation between the circuit parameters and θ and ψ.

Let us consider the limiting cases r = 0 and r = ∞.

When r = 0, we get on passing to the limit that

$$U_1 = U_c\cos\varphi, \quad U_a = U_c\sin\varphi, \quad I_1 = I_a = \frac{U_c}{R_1}\cos\varphi \text{ and } \beta = 1.$$

We consider the second case, which corresponds to the circuit of Fig. 1b, in somewhat more detail (Fig. 5 illustrates the processes occurring).

Here $\tau = 0$ and $\varphi = 0$ when r = ∞. Now (13), in which the RHS becomes zero, gives $\cos(\psi - \varphi) = 0$ or $\psi = \frac{\pi}{2} - \varphi = \frac{\pi}{2}$. Hence $\sin\psi = \cos\varphi = 1$.

(Sixteen) then becomes

$$\tau_L = \frac{X_a}{R_1} = \frac{\pi}{2}\cdot\frac{1 + \sin\theta}{1 - \sin\theta} \tag{16b}$$

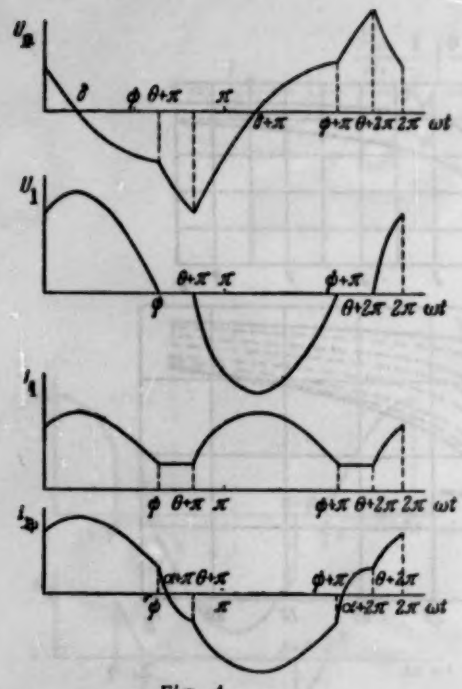

Fig. 4

(τ_L is the time constant for the circuit of Fig. 1b).

The other equations also become

$$I_1 = \frac{U_c}{R_1}\,\frac{1-\sin\theta}{2}, \qquad (7b)$$

$$U_1 = U_c\,\frac{1-\sin\theta}{2}, \qquad (9b)$$

$$U_{a_1} = U_c\,\frac{1+\sin\theta}{2}, \qquad (10b)$$

$$k_B = \frac{2}{1+\sin\theta}, \qquad (11b)$$

$$\sin\alpha = -\,\frac{1-\sin\theta}{2}, \qquad (15b)$$

$$I_a = I_1 - \frac{U_c}{R_1}\,\frac{1}{\pi}\,\frac{1-\sin\theta}{1+\sin\theta}\left[(\theta-\alpha)\sin\theta + \left(\frac{\pi}{2}+\alpha\right) + \cos\theta - 2\cos\alpha\right], \qquad (8b)$$

$$\beta = 1 - \frac{2}{\pi}\,\frac{(\theta-\alpha)\sin\theta + \left(\frac{\pi}{2}+\alpha\right) + \cos\theta - 2\cos\alpha}{1+\sin\theta}. \qquad (12b)$$

Let us summarize the results. For a linear choke $U_a + U_l = U_c$ applies only if an inductive resistance is connected to the bridge output. The deviation from this law increases as k_R falls, and becomes maximal for a pure resistance load, to which applies the law $U_a^2 + U_l^2 = U_c^2$.

As regards β, the position is the same as for an ideal amplifier, i.e., β falls as k_R increases.

The worst of the two extreme modes is, as regards the voltage equations, the ideal case, since $U_a = U_c - U_l$ is the minimum U_a which can occur in the circuit for given U_c and U_l. In no case can U_a be lower than this calculation gives in a real amplifier. A real amplifier will therefore not have a performance below the calculated one.

The error in U_a is minimal for a load consisting of a resistive inductance (in both cases the law is $U_a = U_c - U_l$) and maximal for a purely resistive load.

The β for a linear inductance was derived above. This has also to be estimated in the calculation, since for a given I_l the I_a will increase with ($I_a = \beta I_l$). The most reliable calculation is that which gives the highest current for a given I_l.

Figure 3b shows $\beta = f(k_B)$ for k_R = var and a linear inductance.

Figure 6 shows the load curves in relative units for $k_R = 0$, 1 and ∞, where $I_{l\,max} = \frac{U_c}{R_l}$.

Operation Into a Capacitative Bridge

This type of circuit shows a divergence between the mean voltages before and after the bridge. Three such circuits, to be considered here, are shown in Fig. 7.

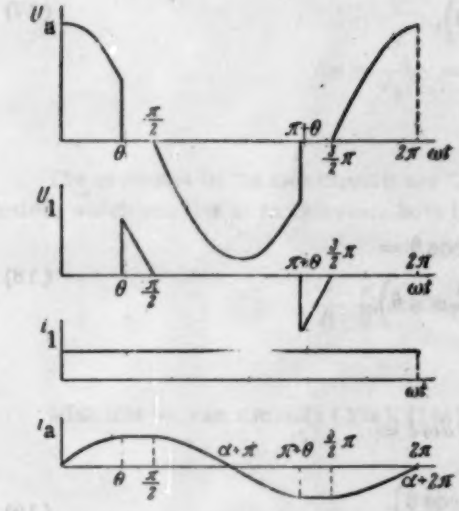

Fig. 5.

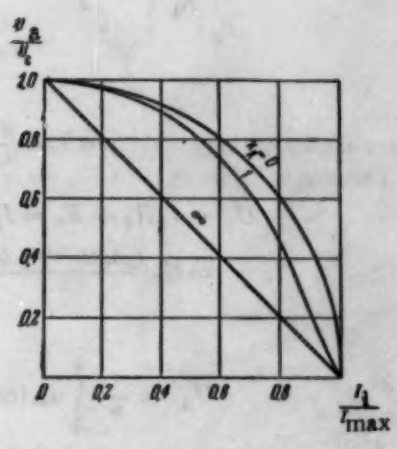

Fig. 6. Load curves for an amplifier working into a bridge rectifier with an inductive load.

As before, we start with an ideal amplifier.

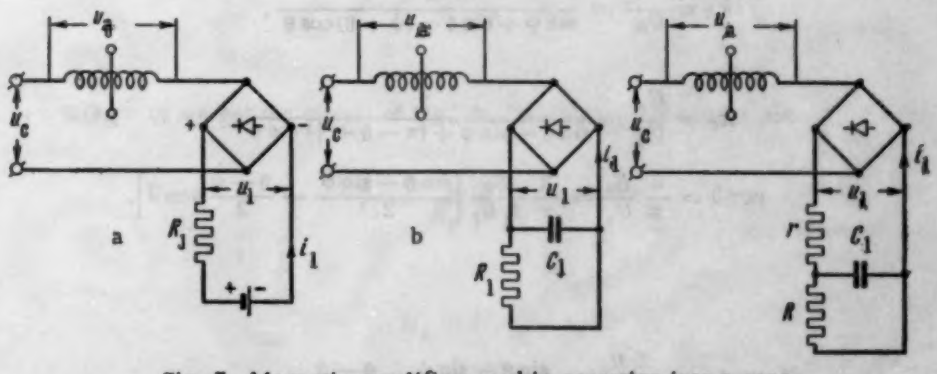

Fig. 7. Magnetic amplifiers used in operation into a capacitative bridge.

Ideal Magnetic Amplifier

Let us first consider the circuit with the opposing emf and pure resistance (Fig. 7a).

Figure 8a shows how u_a, u_1 and i_a vary.

The operation splits up into three sections. In the first (from $-\pi/2$ to $-\theta$) the rectifier does not conduct because of the battery ('double open circuit').

From $-\theta$ to ψ the line voltage is distributed between the amplifier and the rectifier; no current flows because the amplifier is unsaturated (core flux increasing), so $u_a = u_c - E_\theta$.

From ψ to θ the amplifier is saturated and all excess voltage $(u_c - E_\theta)$ acts on R_1 $\left(i_1 = \frac{u_c - E_\theta}{R_1}\right.$, $u_1 = u_c + E_\theta = i_1 R_1 + E_\theta$).

The mean values of I_1, U_1 and U_a are

$$I_1 = I_a = \frac{1}{\pi}\int_{\psi}^{\theta} \frac{u_m \cos\omega t - E_0}{R_1}\, d\omega t = \frac{1}{\pi}\int_{\psi}^{\theta} \frac{u_m}{R_1}(\cos\omega t - \cos\theta)\, d\omega t =$$

$$= \frac{U_c}{R_1}\left(\frac{\sin\theta - \sin\psi}{2} - \frac{\theta - \psi}{2}\cos\theta\right), \tag{17}$$

where

$$\cos\theta = \frac{E_0}{u_m} = \frac{2}{\pi}\,\frac{E_0}{U_c};$$

$$U_1 = I_1 R_1 + E_0 = I_1 R_1 + \frac{\pi}{2} U_c \cos\theta =$$

$$= U_c\left(\frac{\sin\theta - \sin\psi}{2} + \frac{\pi - \theta + \psi}{2}\cos\theta\right); \tag{18}$$

$$U_a = \frac{1}{\pi}\int_{-\theta}^{\psi} u_m(\cos\omega t - \cos\theta)\, d\omega t =$$

$$= U_c\left(\frac{\sin\psi + \sin\theta}{2} - \frac{\psi + \theta}{2}\cos\theta\right). \tag{19}$$

The expressions for k_B and k_C, and one for k_R as a function of θ and ψ, which is required later on, are

$$k_B = \frac{U_c}{U_a} = \frac{2}{\sin\psi + \sin\theta - (\psi + \theta)\cos\theta}, \tag{20}$$

$$k_c = \frac{U_c}{U_1} = \frac{2}{\sin\theta - \sin\psi + (\pi - \theta + \psi)\cos\theta},$$

$$\cos\theta = \frac{2}{\pi}\,\frac{E_0}{U_c} = \frac{2}{\pi}\,\frac{E_0}{I_1 R_1}\left[\frac{\sin\theta - \sin\psi}{2} - \frac{\theta - \psi}{2}\cos\theta\right], \tag{21}$$

so

$$k_R = \frac{I_1 R_1}{E_0} = \frac{\sin\theta - \sin\psi}{\pi\cos\theta} = \frac{\theta - \psi}{\pi}. \tag{22}$$

Consider now the circuit of Fig. 7c. In this case [1] $u_1 = i_1 r + I_1 R$. Hence all deductions for the previous circuit can be transferred to this one if E_0 is replaced by $I_1 R$ and R_1 by r in (17) – (22).

Putting $r + R = R_1$ for Fig. 7c, we have

$$I_1 = \frac{U_c}{R_1}\,\frac{R_1}{r}\left(\frac{\sin\theta - \sin\psi}{2} - \frac{\theta - \psi}{2}\cos\theta\right). \tag{17a}$$

Since $U_1 = I_1 (r + R) = I_1 R_1$ [1], then

$$U_1 = U_c\,\frac{R_1}{r}\left(\frac{\sin\theta - \sin\psi}{2} - \frac{\theta - \psi}{2}\cos\theta\right). \tag{18a}$$

Equation (19) and (20) remain unchanged, while (21) and (22) become

$$k_c = \frac{U_c}{U_1} = \frac{r}{R_1} \frac{2}{\sin\theta - \sin\psi - (\theta - \psi)\cos\theta}, \tag{21a}$$

$$k_R = \frac{I_1 r}{I_1 R} = \frac{r}{R} = \frac{\sin\theta - \sin\psi}{\pi\cos\theta} - \frac{\theta - \psi}{\pi}. \tag{22a}$$

The processes in the two circuits are the same if the k_R are equal. In addition to this important conclusion, which enables us to calculate both in the same way, we get a futher useful expression:

$$\frac{r}{R}\frac{\pi}{2}\cos\theta = \frac{\sin\theta - \sin\psi}{2} - \frac{\theta - \psi}{2}\cos\theta.$$

With this we can simplify (17a), (18a) and (21a):

$$I_1 = \frac{U_c}{R_1}\frac{R_1}{R}\frac{\pi}{2}\cos\theta, \tag{17a'}$$

$$U_1 = U_c \frac{R_1}{R}\frac{\pi}{2}\cos\theta, \tag{18a'}$$

$$k_c = \frac{R}{R_1}\frac{2}{\pi}\frac{1}{\cos\theta}. \tag{22a'}$$

When $r = 0$ ($k_R = 0$) we get the circuit of Fig. 7b, for which the formulae are

$$I_1 = \frac{U_c}{R_1}\frac{\pi}{2}\cos\theta, \tag{17b}$$

$$U_1 = U_c \frac{\pi}{2}\cos\theta, \tag{18b}$$

$$U_1 = U_c(\sin\theta - \theta\cos\theta) \tag{19b}$$

(the last derives from (19) by putting $\varphi = \theta$),

$$k_B = \frac{1}{\sin\theta - \theta\cos\theta}, \tag{20b}$$

$$k_c = \frac{2}{\pi}\frac{1}{\cos\theta}. \tag{21b}$$

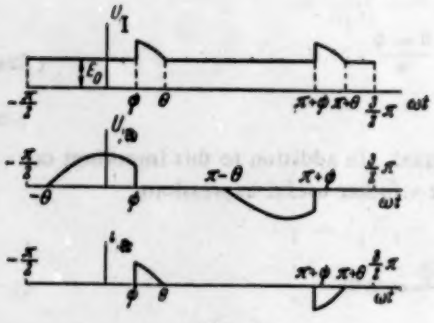

Fig. 8a

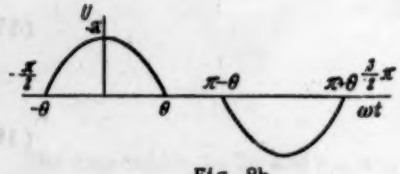

Fig. 8b

Figure 8b shows how u_a varies; u_1 equals E_0 throughout here. Then i_a takes the form of pulses of infinite amplitude and infinitesimal duration. It flows at $\omega t = \theta$, $\pi + \theta$, $2\pi + \theta$ and etc. The mean value over a half-period is U_1/R_1.

When $R = 0$ ($k_R = \infty$) we get the pure resistance case. Hence Fig. 7b has the maximum nonlinearity, which becomes less as k_R increases.

The result of this analysis is the $k_C = f(k_B)$ curves of Fig. 9 for k_R = var, with which the a-c circuit of a magnetic amplifier can be calculated for given load parameters.

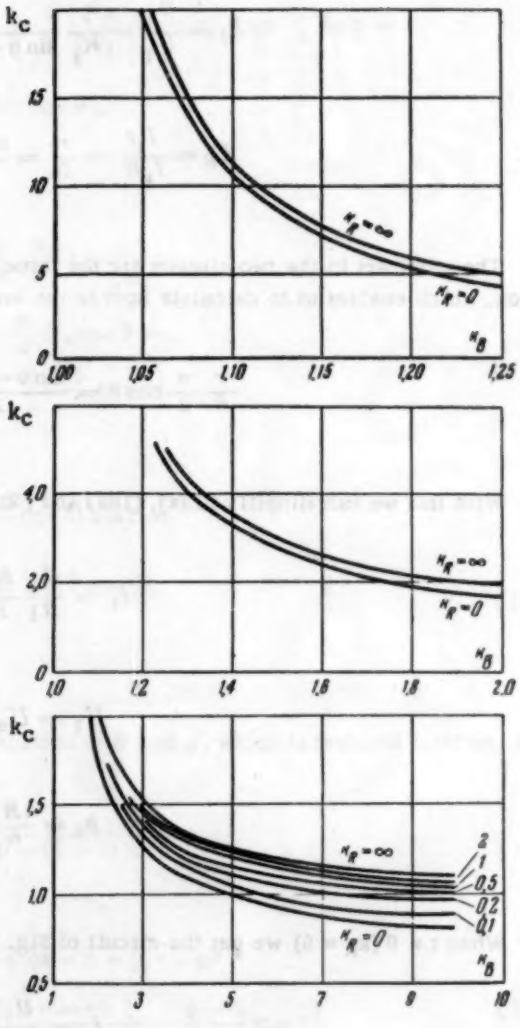

Fig. 9

Linear Inductance

The inductance is connected to the input of a bridge which has a resistive load plus opposing emf. Two cases occur, namely, continuous and discontinuous current flow. The u_a, u_1 and i_a curves for both cases are shown in Fig. 10.

The current is found by solving

$$X_a \frac{di_a}{d\omega t} + R_1 i_a = u_m \cos \omega t - E_0.$$

The initial condition is $i_a(-\theta) = 0$, where θ is defined by $\cos \theta = \frac{E_0}{u_m} = \frac{2}{\pi} \frac{E_0}{U_C}$. This gives

$$i_a = \frac{U_m}{Z} \left[\cos(\omega t - \varphi) - \cos(\theta + \varphi) e^{-\frac{\omega t + \theta}{\tau}}\right] - \frac{E_0}{R_1}\left(1 - e^{-\frac{\omega t + \theta}{\tau}}\right), \quad i_1 = |i_a|,$$

where $$Z = \sqrt{X_a^2 + R_1^2} \text{ and } \tau = \frac{X_a}{R_1} = \tan\varphi.$$

u_1 and u_a take the forms

$$u_1 = i_a R_1 + E_0, u_a = X_a \frac{di_a}{d\omega t} = u_m\left[-\sin\varphi\sin(\omega t - \varphi) + \cos\varphi\cos(\theta+\varphi)e^{-\frac{\omega t+\theta}{\tau}}\right] - E_0 e^{-\frac{\omega t+\theta}{\tau}}$$

(for more detail see [5]).

The mean values of I_1, U_1 and U_a are

$$I_1 = I_a = \frac{1}{\pi}\int_{-\theta}^{\psi} i_a\, d\omega t = \frac{U_c}{R_1}\left[\frac{\sin\psi + \sin\theta}{2} - \frac{\psi+\theta}{2}\cos\theta\right], \tag{23}$$

$$U_1 = \frac{1}{\pi}\int_{-\theta}^{\psi} u_1 d\omega t = U_c\left[\frac{\sin\psi + \sin\theta}{2} + \frac{\pi-\psi-\theta}{2}\cos\theta\right], \tag{24}$$

$$U_a = \frac{1}{\pi}\int_{-\upsilon}^{\delta} u_a\, d\omega t - \frac{1}{\pi}\int_{\delta}^{\psi} u_a\, d\omega t = U_c\tau(\cos\delta - \cos\theta). \tag{25}$$

Here ψ and δ are found from $i_a(\psi) = 0$ and $u_a(\delta) = 0$, which give us transcendental equations

$$\cos(\psi-\varphi) = \cos(\theta+\varphi)e^{-\frac{\psi+\theta}{\tau}} + \frac{\cos\theta}{\cos\varphi}(1 - e^{-\frac{\psi+\theta}{\tau}}), \tag{26}$$

$$\sin(\delta-\varphi) = \frac{\cos(\theta+\varphi)e^{-\frac{\delta+\theta}{\tau}}}{\tau} - \frac{\cos\theta}{\sin\varphi}e^{-\frac{\delta+\theta}{\tau}} \tag{27}$$

The expressions for k_B, k_C and k_R are

$$k_B = \frac{1}{\tau(\cos\delta - \cos\theta)}, \tag{28}$$

$$k_c = \frac{2}{\sin\psi + \sin\theta + (\pi - \psi - \theta)\cos\theta},$$

$$\cos\theta = \frac{2}{\pi}\frac{E_0}{U_c} = \frac{2}{\pi}\frac{E_0}{I_1 R_1}\left(\frac{\sin\psi + \sin\theta}{2} - \frac{\psi+\theta}{2}\cos\theta\right), \tag{29}$$

$$k_R = \frac{I_1 R_1}{E_0} = \frac{\sin\psi + \sin\theta}{\pi\cos\theta} - \frac{\psi+\theta}{\pi}. \tag{30}$$

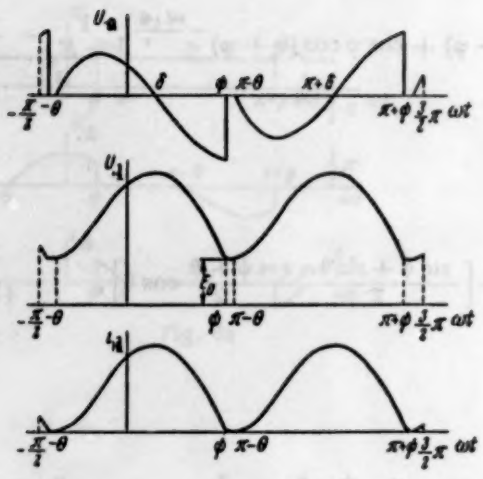

Fig. 10a

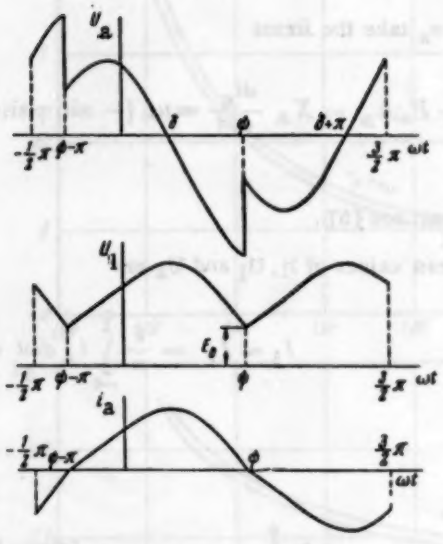

Fig. 10b

In the second case, when the current flows in the inductance throughout the half-period, the expressions change to

$$i_a = \frac{u_m}{Z}\left[\cos(\omega t - \varphi) + \cos(\psi - \varphi)\, e^{-\frac{\omega t + \pi - \psi}{\tau}}\right] - \frac{E_0}{R_1}\left(1 - e^{-\frac{\omega t + \pi - \psi}{\tau}}\right),$$

$$i_1 = |i_a|,\quad u_1 = i_1 R_1 + E_0,$$

$$u_a = u_m\left[-\sin\varphi \sin(\omega t - \varphi) - \cos\varphi \cos(\psi - \varphi)\, e^{-\frac{\omega t + \pi - \psi}{\tau}}\right] - E_0 e^{-\frac{\omega t + \pi - \psi}{\tau}}.$$

These formulae are obtained by putting $\theta = \pi - \psi$:

$$I_a = I_1 = \frac{1}{\pi}\int_{\psi-\pi}^{\psi} i_a\, d\omega t = \frac{U_c}{R_1}\left(\sin\psi - \frac{\pi}{2}\cos\theta\right), \tag{23'}$$

$$U_1 = \frac{1}{\pi}\int_{\psi-\pi}^{\psi} u_1 d\omega t = U_c \sin\psi, \tag{24'}$$

$$U_a = \frac{1}{\pi}\int_{\psi-\pi}^{\delta} u_a\, d\omega t - \frac{1}{\pi}\int_{\delta}^{\psi} u_a\, d\omega t = U_c\tau(\cos\delta - \cos\theta). \tag{25'}$$

The following formulae also alter somewhat

$$\cos(\psi - \varphi) = \frac{\cos\theta}{\cos\varphi}\,\frac{1 - e^{-\frac{\pi}{\tau}}}{1 + e^{-\frac{\pi}{\tau}}}, \tag{26'}$$

$$\sin(\delta - \varphi) = -\frac{\cos(\psi - \varphi)}{\tau} e^{-\frac{\pi+\delta-\psi}{\tau}} - \frac{\cos\theta}{\sin\varphi} e^{-\frac{\pi+\delta-\psi}{\tau}}, \tag{27'}$$

$$k_c = \frac{1}{\sin\psi}, \tag{29'}$$

$$k_R = \frac{2\sin\psi}{\pi\cos\theta} - 1. \tag{30'}$$

The boundary between the two cases is found by putting $\psi + \theta = \pi$ (30). Then we have

$$\tan\theta = \frac{\pi}{2}(1 + k_R). \tag{31}$$

Considering now Fig. 7c, and using the above expressions, we get the formulae applying to this case only:

$$I_1 = \frac{U_c}{R_1}\frac{R_1}{r}\left[\frac{\sin\psi + \sin\theta}{2} - \frac{\psi+\theta}{2}\cos\theta\right],$$

$$U_1 = I_1 r + E_0 = I_1 r + \frac{\pi}{2} U_c \cos\theta = U_c \frac{R_1}{r}\left(\frac{\sin\theta + \sin\psi}{2} - \frac{\psi+\theta}{2}\cos\theta\right), \tag{30a}$$

$$k_R = \frac{r}{R} = \frac{\sin\psi + \sin\theta}{\pi\cos\theta} - \frac{\psi+\theta}{\pi}.$$

The last of these gives

$$\frac{\sin\psi + \sin\theta}{2} - \frac{\psi+\theta}{2}\cos\theta = \frac{r}{R}\frac{\pi}{2}\cos\theta,$$

so the expressions for I_1 and U_1 can be simplified to

$$I_1 = \frac{U_c}{R_1}\frac{R_1}{R}\frac{\pi}{2}\cos\theta, \tag{23a}$$

$$U_1 = U_c \frac{R_1}{R}\frac{\pi}{2}\cos\theta, \tag{24a}$$

$$k_c = \frac{R}{R_1}\frac{2}{\pi}\frac{1}{\cos\theta}. \tag{29a}$$

Equations (25) – (28) retain their forms for this load type.

If the switching is continuous the relationships also alter somewhat:

$$I_1 = \frac{U_c}{R_1}\frac{R_1}{r}\left(\sin\psi - \frac{\pi}{2}\cos\theta\right) = \frac{U_c}{R_1}\sin\psi = \frac{U_c}{R_1}\frac{R_1}{R}\frac{\pi}{2}\cos\theta, \tag{23a'}$$

$$U_1 = U_c \frac{R_1}{r}\left(\sin\psi - \frac{\pi}{2}\cos\theta\right) = U_c \sin\psi = U_c \frac{R_1}{R}\frac{\pi}{2}\cos\theta, \qquad (24a')$$

$$k_R = \frac{r}{R} = \frac{2\sin\psi}{\pi\cos\theta} - 1, \qquad (30a')$$

$$\cos\theta = \frac{2}{\pi}\frac{R}{R_1}\sin\psi,$$

$$k_c = \frac{R}{R_1}\frac{2}{\pi}\frac{1}{\cos\theta} = \frac{1}{\sin\psi}. \qquad (29a')$$

We now consider Fig. 7b, whree $k_R = 0$. Figure 11 shows how the voltages and currents vary in time; the relevant equation is

$$X_a \frac{di_a}{d\omega t} = u_m \cos\omega t - E_0,$$

the solution of which, subject to the condition $i_a(-\theta) = 0$, will be

$$i_a = \frac{u_m}{X_a}[\sin\omega t + \sin\theta - \cos\theta(\omega t + \theta)],$$

where

$$\cos\theta = \frac{I_1 R_1}{u_m} = \frac{E_0}{u_m}.$$

The voltages are found from $u_a = u_c - E_0$ ($u_a = u_m \cos\omega t - I_1 R_1$) and $u_1 = I_1 R_1 = \text{const}$.

For this load type we get, without integrating, U_1 and I_1.

$$U_1 = I_1 R_1 = U_c \frac{\pi}{2}\cos\theta, \qquad (23b)$$

$$I_1 = \frac{U_c}{R_1}\frac{\pi}{2}\cos\theta. \qquad (24b)$$

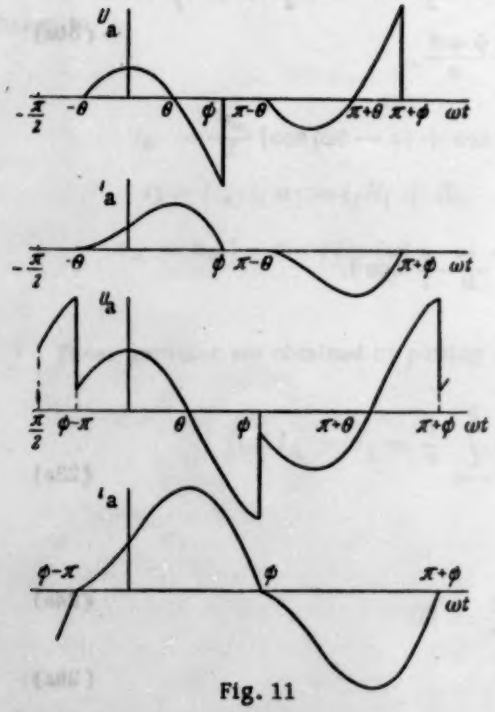

Fig. 11

U_a and the coefficients are given by

$$U_{a\cdot} = \frac{4}{\pi}\int_0^{\theta} u_m(\cos\omega t - \cos\theta)\, d\omega t = 2U_c(\sin\theta - \theta\cos\theta), \qquad (25b)$$

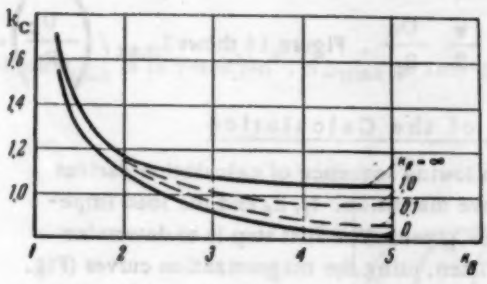

Fig. 12

$$k_B = \frac{1}{2(\sin\theta - \theta\cos\theta)}, \qquad (28b)$$

$$k_c = \frac{2}{\pi\cos\theta}. \qquad (29b)$$

If the switching is continuous the expressions for U_1 and I_1 remain in force, while U_a is found by integrating:

$$U_a = \frac{2}{\pi}\int_{\theta}^{\psi} u_m(\cos\theta - \cos\omega t)\, d\omega t = U_c[\sin\theta - \sin\psi + (\psi - \theta)\cos\theta] \qquad (25b')$$

and

$$k_B = \frac{1}{\sin\theta - \sin\psi + (\psi - \theta)\cos\theta}. \qquad (28b)$$

To determine ψ we use the condition that

$$\frac{u_m}{\pi}\int_{\psi-\pi}^{\theta}(\cos\omega t - \cos\theta)\, d\omega t = \frac{u_m}{\pi}\int_{\theta}^{\psi}(\cos\theta - \cos\omega t)\, d\omega t.$$

This gives $\sin\psi = \frac{\pi}{2}\cos\theta$ $(\psi > \theta)$.

The boundary between the modes occurs at

$$\operatorname{tg}\theta = \frac{\pi}{2}. \qquad (31b)$$

Figure 12 shows the results as $k_c = f(k_B)$ for k_R = var.

Figure 13 shows the load curves for a magnetic amplifier with a capacitative load, with $k_R = 0$ (Fig. 7b), $k_R = 0.1$ (Fig. 7c) and $k_R = \infty$ (pure resistance load), for an ideal amplifier and for a linear choke.

The curves of Fig. 13 show that the calculated U_a is least for the ideal amplifier. These curves should therefore be used to give a reliable design. The extent of the error can be estimated by comparing the curves for a given value of k_R.

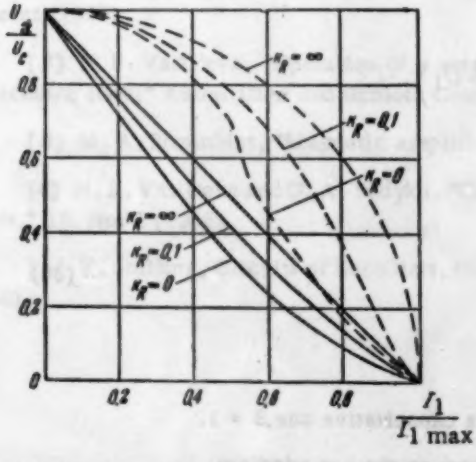

Fig. 13. Load curves for a magnetic amplifier with a capacitative load connected to a bridge rectifier. The full lines are for an ideal amplifier, and the dashed for a linear input choke.

These curves are drawn in relative units, $\frac{U_a}{U_c}$ and $\frac{I_1}{I_{1\max}}$, where

$$I_{1\max} = \frac{U_c}{R}\frac{R}{R}\cdot\frac{\pi}{2}(\cos\theta)_{\max} =$$

$$= \frac{U_c}{R_1}(1 + k_R)\frac{\pi}{2}(\cos\theta)_{\max}$$

The value of $(\cos\theta)_{max}$ is given by (22) with $\psi = -\theta$ (i.e., the amplifier is assumed completely saturated throughout the conducting section of the half-cycle). This gives $k_R = \frac{2}{\pi}(\tan\theta - \theta)$, which is used to calculate $(\cos\theta)_{max}$.

For a capacitative load (Fig. 7b) $(\cos\theta)_{max} = 1$ and $I_{1\,max} = \frac{\pi}{2}\frac{U_c}{R_1}$. Figure 14 shows $I_{max} / \left(\frac{U_c}{R_1}\right) = f(k_R)$.

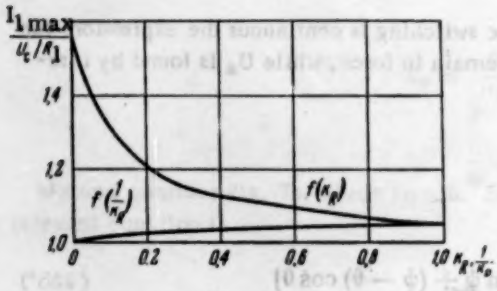

Fig. 14

Sequence of the Calculation

The following sequence of calculation derives from the above discussion. I_1, E_θ and the load impedance must be given. The first step is to determine U_1 and k_R. Then, using the magnetization curves (Fig. 15), we select the two working points (1 and 2) which correspond to the maximum load current and to $I_a = 0$.

The first should be chosen at the knee in the curve; the choice of the second (of coordinates B_{min} $H_{\sim max}$) depends on the purpose of the amplifier (see, for example, [4]).

Then U_c, U_a and I_a are calculated from

$$U_c = k_c U_1, \tag{32}$$

$$U_a = \frac{U_c}{k_B}, \tag{33}$$

$$I_a = \beta I_1. \tag{34}$$

For an inductive load k_c is found from

$$k_c = \frac{k_B}{k_B - 1}. \tag{35}$$

(this formula is easily derived using

$$U_c = U_{a1} + U_1 = \frac{U_c}{k_B} + U_1\Big).$$

k_c is determined from Fig. 9 for a capacitative load.

k_B is calculated from

$$k_B = \frac{B_{max}}{B_{min}}, \tag{36}$$

where B_{max} and B_{min} correspond to the points in Fig. 15.

For an inductive load we select β from Fig. 3b, whereas for a capacitative one, $\beta = 1$.

We can now calculate the steel volume and the number of turns on the a-c winding:

$$V_{st} = \frac{U_a I_a}{4fB_{min}H_{\sim max}} \cdot 10^6, \text{ cm}^3, \tag{37}$$

$$W_{\sim} = \frac{U_a \, 10^4}{4 f S_{st} B_{min}}, \qquad (38)$$

where B_{min} is in v-sec/m^2, $H_{\sim max}$ in amp-turns/m, and S (core section) in cm^2.

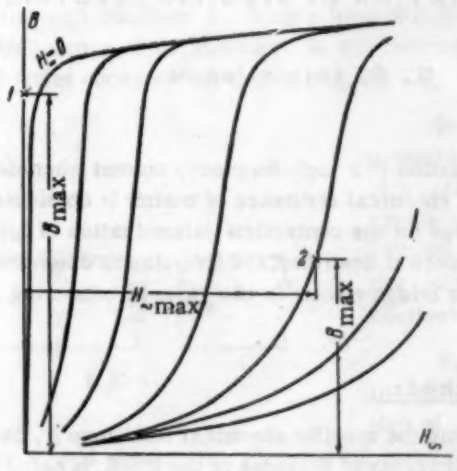

Fig. 15

In conclusion, we observe that as the operation is highly reliable the dimensions are somewhat overestimated, so the method cannot be recommended for high-power amplifiers, particularly if transformer steel is used.

The resistance of the rectifier can be allowed for approximately from its voltage-current characteristics. The resistance calculated for the maximum load current should be added to R_1. A more precise method is given in [1]. The resistance of the windings can be added to R_1 in the same way.

LITERATURE CITED

[1] V. G. Komar, The Operation of Semiconductor Rectifiers in Control Circuits [in Russian] (Gosenergoizdat, 1952).

[2] N. P. Vasil'eva, "Operation of a magnetic amplifier into a bridge rectifier connected to a resistive inductance load," Automation and Remote Control (USSR) 15 No. 6 (1954).

[3] M. A. Rozenblat, "Magnetic amplifiers," Radiotekhnika, 1953, No. 2.

[4] N. P. Vasil'eva and O. A. Sedykh, "Calculation of magnetic amplifiers with complex (impedance) loads," 16, No. 1 (1955).

[5] V. Shilling, Circuits of Rectifiers, Inverters and Frequency Converters [in Russian] (Gosenergoizdat, 1950).

Received April 19, 1956

CONTACTLESS DETERMINATION OF SPECIFIC ELECTRICAL RESISTANCE

G. G. Iarmol'chuk

The utilization of a high-frequency current when determining the specific electrical resistance of matter is considered. The circuit of a bridge for the contactless determination of specific electrical resistance is described, and formulae to determine the sensitivity of the bridge circuit in two cases of measuring are given.

1. Physical Principles of Methods

The contactless method of measuring the specific electrical resistance ρ, developed at the Institute of Automation and Remote Control of the Academy of Sciences of the USSR, is based on the utilization of eddy currents which arise in a conducting material when the latter is placed in an alternating magnetic field.

The alternating magnetic field is set up by an induction coil which is supplied with a high frequency current. A body placed in the magnetic field of the coil changes the latter's parameters. This change in the coil's parameters depends on the geometrical dimensions of the body and its specific resistance ρ. The coil's parameters may be measured by any known method.

Let us examine this phenomenon more closely. Figure 1 shows a uniform cylinder of a meterial having a specific resistance ρ, lying in a high frequency magnetic field. Circulating currents are induced in the body of the cylinder in planes perpendicular to the vector of the magnetic field H.

Due to the skin effect, the current distributes itself nonuniformly through the cross section of the specimen. The greatest current density is found on the surface of the cylinder. The distribution of the current density through the cross section of the test piece is shown in Fig. 2, where q_0 is the surface current density, δ is the skin depth, $\frac{1}{2}D$ is the radius of the cylinder.

Fig. 1

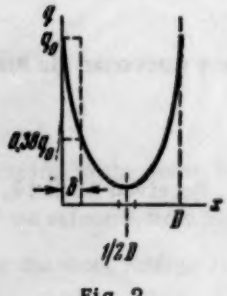

Fig. 2

Since the use of such a curve is difficult, the effective action of the current in the body of the cylinder is replaced by the current density q_0, spreading in the cylinder to a depth δ.

In accordance with known data [1-3], the skin depth is

$$\delta = 503 \sqrt{\frac{\rho}{\mu f}}\ mm, \qquad (1)$$

where ρ is the specific electrical resistance of the material in ohm mm^2/m, μ is the magnetic permeability of the material, f is the current frequency in cps.

For nonmagnetic materials (of which more will be said later) $\mu = 1$ and formula (1) takes on the form:

$$\delta = 503\sqrt{\frac{\rho}{f}}\ \text{мм}. \tag{2}$$

The current induced in the body of the cylinder sets up its own magnetic flux, which is determined by the skin depth δ and the dimensions of the cylinder. Hence the cylinder may be considered to be hollow, having a specific resistance ρ and wall thickness δ. Such a body will have its own resistance R_2 and inductive reactance ωL_2, where L_2 is the inductance of the cylinder. In this case the cylinder may be represented by an equivalent circuit, consisting of series connected R_2 and L_2 (Fig. 3).

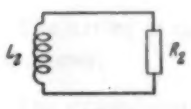

Fig. 3

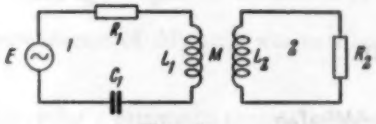

Fig. 4

Such a representation of the phenomenon occuring in the body of the cylinder reduces it to a case which is studied in the theory of coupled electrical circuits. In this case, the cylinder and the induction coil, in whose field the cylinder is located, are effectively, inductively coupled circuits.

Figure 4 shows the circuit diagram of inductively coupled circuits. Circuit 1 consists of a coil, having a inductance L_1, connected in series with a resistance R_1 and capacitance C_1, where E is the current source. Circuit 2 represents the equivalent circuit of the cylinder, where M is the mutual inductance between the two circuits.

From theory [4] is known that, in the presence of the mutual inductance M, the effect of the second circuit on the first is to change the resistive and reactive components of the first circuit.

The effective impedance of the equivalent circuit, i.e., the impedance with the effect of circuit 2 on circuit 1 taken into account, will be

$$Z_{1oe} = R_1 + \frac{\omega^2 M^2 R_2}{|Z_2|^2} + j\left(X_1 - \frac{\omega^2 M^2 X_2}{|Z_2|^2}\right), \tag{3}$$

where Z_2 is the effective impedance of circuit 2, $Z_2 = R_2 + jX_2$, $X_1 = \omega L_1$, $X_2 = \omega L_2$.

In Equation (3) the second term on the right side represents the magnitude of the added resistance.

$$\Delta R_1 = \frac{\omega^2 M^2 R_2}{|Z_2|^2} = \frac{\omega^2 M^2 R_2}{R_2^2 + (\omega L_2)^2}. \tag{4}$$

If the skin depth δ is small compared with the dimensions of the cylinder, then the inductance of such a cylinder will be affected very slightly by the magnitude of ρ, which affects the skin depth, while the resistance R_2 will be proportional to $\sqrt{\rho}$.

In fact, R_2, for $\delta << \frac{D}{2}$, may be calculated from the formula

$$R_2 = \rho\frac{\pi D}{\delta h}. \tag{5}$$

Substituting the expression for δ from Equation (2) into (5), we obtain

$$R_2 = \frac{\rho\pi D\sqrt{f}}{503h\sqrt{\rho}\,10^3} = \frac{P\sqrt{\rho f}}{5.03\times 10^5 h}. \tag{6}$$

Here D and h are expressed in millimeters, $P = \pi D$ is the circumference of the cylinder.

Thus the magnitude of the resistance R_2 of the cylinder will depend on the specific resistance of the cylinder's material, which in its turn will bring about a change in the magnitude ΔR_1, i.e., the transfered resistance in circuit 1.

To find the conditions for a maximum ΔR_1, let us differentiate (4) with respect to R_2 and equate it to zero:

$$\frac{d(\Delta R_1)}{dR_2} = \frac{\omega^2 M^2 [(\omega L_2)^2 - R_2^2]}{[R_2^2 + (\omega L_2)^2]^2} = 0, \tag{7}$$

Thus we find that ΔR_1 is a maximum when $R_2 = \omega L_2$.

It follows that ΔR_1 is a function of the expression $R_2/\omega L_2$.

Let us set $R_2/\omega L_2 = n$; then $R_2 = n\omega L_2$.

Substituting this expression for R_2 in formula (4):

$$\Delta R_1 = \frac{\omega^2 M^2 \omega L_2 n}{(\omega L_2)^2 (n^2 + 1)},$$

and thus

$$\frac{\Delta R_1 L_2}{\omega M^2} = \frac{n}{n^2 + 1}. \tag{8}$$

Figure 5 shows the dependence of $\frac{\Delta R_1 L_2}{\omega M^2}$ on n. It is apparent from the curve that the maximum occurs at n = 1.

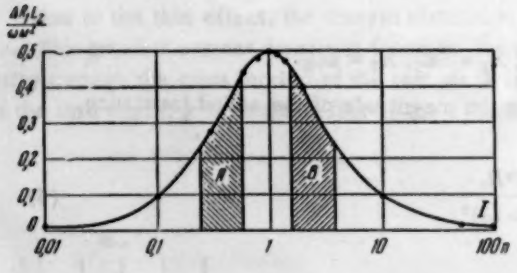

Equation (4), when ΔR_1 is a maximum for a given ω, M, and L_2, may be rewritten as:

$$\Delta R_{1\,\max} = \frac{\omega M^2}{2L_2}. \tag{9}$$

The more the R_2 will differ in the sample from the inductive reactance ωL_2, the more the transferred resistance ΔR_1 will differ from $\Delta R_{1\max}$.

In the measurement of ρ for samples having equal dimensions, and considering ωL_2 constant at least within range of the measured ρ's, a single valued solution requires that either the left or the right branch of the curve in Fig. 5 be utilized. From the point of view of greater sensitivity it is recommended that either region A or region B be used (Fig. 5).

The point of inflection occurs where $R_2 = \omega L_2$. Substituting the expression for R_2 from Equation (6), we obtain

$$\frac{P\sqrt{\rho f}}{5{,}03 \times 10^5 h} = \omega L_2. \tag{10}$$

From Equation (10) it is possible to obtain the value of ρ_{cr}, i.e., the value of ρ corresponding to the point of inflection in the curve of the transferred resistances:

$$\rho_{cr} = L_2^2 \left(\frac{h}{P}\right)^2 f 10^{13} \frac{\text{ohm} \cdot mm^2}{m}. \qquad (11)$$

From Equation (11) it is possible to determine that critical frequency, for a given value of ρ, which corresponds to the point of inflection in the curve:

$$f_{cr} = \frac{\rho}{L_2^2} \left(\frac{P}{h}\right)^2 10^{-13} \text{ cps}. \qquad (12)$$

In Equations (11) and (12) L_2 is expressed in henries, P and h in mm, f in cps, and ρ in ohm mm^2/m.

The nature of the dependence of ΔR_1 on h was verified experimentally. Measurements were carried out on a Q-meter.

The experimental curve for a prismatic sample, measuring 5 × 6 × 24 mm, at a frequency of 150 kc, is given in Fig. 6.

The dependance of the position of the point of inflection in the curve of the transferred resistance, on frequency can be seen in Fig. 7, where values of the figure of merit $Q = 1/\omega CR$ are plotted along the ordinate. As R increases, Q decreases. Hence the maximum transferred resistance corresponds, at a given frequency, to the lowest value of Q. The curves are given for prismatic specimens measuring 5 × 6 × 24 mm, for different values of ρ and for different frequencies. It is apparent from the curves that, with increase in frequency, the minimum Q moves in the direction of larger ρ, which agrees with the condition for obtaining ΔR_{1max} ($R_2 = \omega L_2$).

From the curves it may be also seen that for a sample measuring 16 × 20 × 50 mm, at a frequency of 1 Mc the minimum Q occurs at a much larger value of ρ than for a sample measuring 5 × 6 × 24 mm.

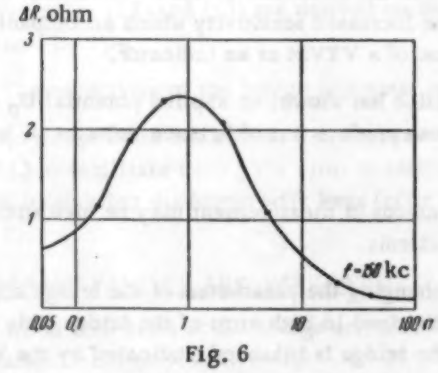

Fig. 6

From what has been said, we can establish rules which must be followed to obtain single-valued measurements.

If the rising portion of the curve in Fig. 5 (region A) is used in the measurements, then the maximum value ρ_{max}, for a given frequency, must be less than the value of ρ_{cr}. For the dropping part of the curve (region B), we must accordingly have $\rho_{min} > \rho_{cr}$.

Insofar as, with increase in frequency, the point of inflection in the curve [cf. Equation (12)] moves in the direction of larger ρ, then the current frequencies must be so chosen that the point of inflection of the curve falls within a controllable region, enclosed by ρ_{min} and ρ_{max}. Using formula (12) we find the frequencies $f\rho_{min}$ and $f\rho_{max}$, at which the point of inflection of the curve will correspond to ρ_{min} and ρ_{max}.

For measuring purposes, any frequencies may be used (from a single-valuedness point of view) except those lying between $f\rho_{min}$ and $f\rho_{max}$. Hence for region A the frequency must be greater than $f\rho_{max}$, while for region B – less than $f\rho_{min}$.

Thus the conditions for single-valuedness require that the following restrictions be observed in measuring ρ: for region A (Fig. 5) $\rho_{max} < \rho_{cr}$ and $f > f\rho_{max}$, for region B – $\rho_{min} > \rho_{cr}$ and $f < \rho_{min}$.

2. Methods of Measuring the Specific Resistance

The physical basis of the contactless method of measuring ρ which was discussed above, shows that the problem is reduced to the measurement of the transferred resistance in the coil circuit. This resistance may be measured by any of the well-known methods; in particular, bridge circuits may be used.

The bridge circuit shown in Fig. 8 was used at the Institute of Automation and Remote Control to check the specific resistance of small samples [5] using the contactless method. The following symbols are introduced in this diagram:

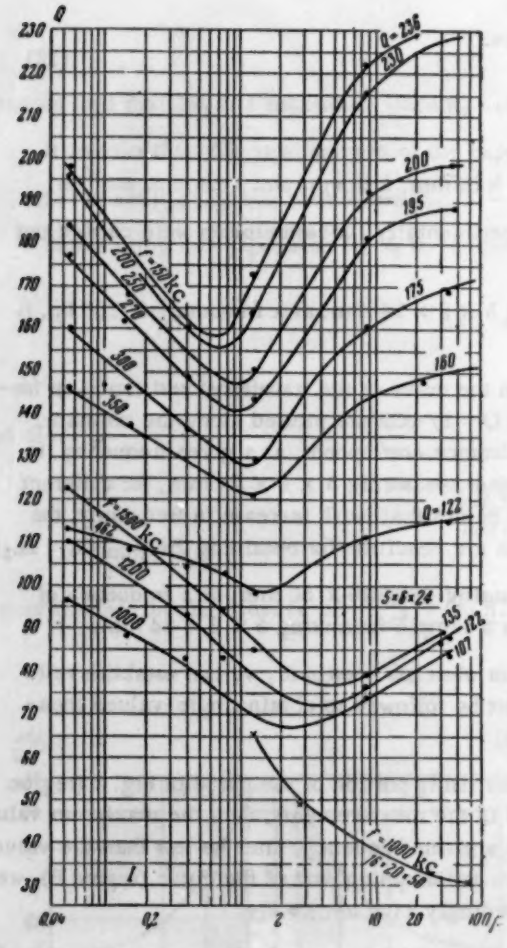

Fig. 7

L_1' is the variable inductance in balancing arm of the bridge, L_2' is the measuring coil having inductance L_2, r_1 and r_2 are variable resistances, C_3 and C_4 are variable air-gap capacitors, T_p is a coreless transformer for isolating the bridge circuit from the VTVM circuit, KV is a vacuum tube voltmeter, U_p is an applied source voltage of 7-8 volts at a frequency $f \approx 1$ Mc, L_1 and L_2 are filament lamps. The balance conditions for the bridge are:

$$\frac{r_1}{r_2} = \frac{C_4}{C_3} = \frac{L_1'}{L_2'}. \tag{13}$$

From the balance conditions we can write

$$L_2'C_4 = L_1'C_3. \tag{14}$$

Equality (14) is independent of the frequency ω.

If we pick a value of ω such that $\omega^2 L_2' C_4 = \omega^2 L_1' C_3 = 1$, then conditions of series resonance will exist in both arms of the bridge.

The use of the resonance effect is convenient to the extent that the increased sensitivity which accompanies it permits the use of a VTVM as an indicator.

As practice has shown, an applied potential $U_p = 7$v and $f = 1$Mc can produce out of balance voltages of tens of volts.

Two methods of measurement may be used with the given bridge circuit.

1. By changing the parameters of the bridge arms, resonance is obtained in both arms of the bridge (this is determined from the filament lamps L_1 and L_2) at the same time as the bridge is balanced (indicated by the VTVM). Then a master sample, having a known resistance, corresponding to one of the limits of the ρ being measured, is introduced into measuring coil L_2'. The deflection on the VTVM is noted. Next, the sample in coil L_2' is replaced by another master sample having the same dimensions but having a specific resistance corresponding to the second limit of the ρ being measured. The new voltmeter deflection is noted. Following this, all samples having the same dimensions as the two master samples have a ρ obtained from the formula:

$$\rho_x = \frac{U_x - U_1}{U_2 - U_1}(\rho_2 - \rho_1) + \rho_1, \tag{15}$$

where U_1 and ρ_1 are respectively, the out of balance voltage corresponding to first master sample, and the latter's specific resistance, U_2 and ρ_2 – the same for the second master sample, U_x and ρ_x – the same for the test sample.

Formula (15) is derived on the assumption that U is a linear function of ρ in the established limits of measurements, and that this holds true for samples which, when placed in the test circuit, produce voltmeter deflections greater than those corresponding to the master samples.

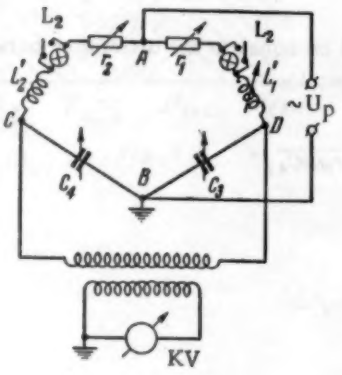

Fig. 8

2. For the initial calibration of the bridge a master sample is chosen which has a specific resistance ρ_1 lying beyond the limits of the ρ expected for the samples to be measured. In this case either $\rho_1 > \rho_{max}$, or $\rho_1 < \rho_{min}$ where ρ_{min} and ρ_{max} are the assigned limits of measurement.

Next, sample ρ_1 is replaced by another master sample with specific resistance ρ_2. The value ρ_2 is chosen so that the range of measured ρ is bounded by ρ_1 and ρ_2, i.e., if $\rho_2 < \rho_{min}$, then $\rho_2 > \rho_{max}$, but if $\rho_1 > \rho_{max}$, then $\rho_2 < \rho_{min}$ (Fig. 9).

When the master sample having ρ_2 is introduced, the bridge is unbalanced and a voltmeter reading is registered. Following this, the resistance of every unknown sample ρ_x can be determined from the formula

$$\rho_x = \rho_1 + \frac{U_x}{U_2}(\rho_2 - \rho_1)\frac{\text{ohm}\cdot\text{mm}^2}{\text{m}}, \tag{16}$$

if $\rho_2 > \rho_1$, and

$$\rho_x = \rho_1 - \frac{U_x}{U_2}(\rho_1 - \rho_2), \tag{17}$$

if $\rho_2 < \rho_1$.

Formulas (16) and (17) are derived on the assumption that the voltmeter readings are proportional to the difference $\rho_1 - \rho_2$.

The sensitivity of the bridge is greater in the second method than in the first.

As was pointed out above, filament lamps L_1 and L_2 are included in the arms containing the inductances L_1' and L_2' to facilitate tuning the arms to resonance. At resonance the lamps glow. The sensitivity may be increased by shorting the lamps with keys (after resonance is achieved) and thus decrease the resistance in arms 1 and 2.

3. Sensitivity of the Bridge

When both arms of the bridge are tuned to resonance, and if conditions (13) are met, then the bridge will be balanced. Let us pick $C_3 = C_4$.

If the second method of measurement is used, i.e., if the bridge is calibrated using the master sample ρ_1, the bridge will be put out of balance when the master sample is replaced by a test sample having a different ρ. In the absence of current in the indicator loop (diagonal CD in Fig. 8) the voltage across capacitor C_3 will be equal to (at voltage resonance):

$$U_{BD} = \frac{U_p}{r_1}\frac{1}{j\omega C_3}, \tag{18}$$

where r_1 is the total resistance in the arm ADB, U_p is the voltage delivered by source of potential, C_3 is the value of capacitance. Analogously for branch ACB

$$U_{BC} = \frac{U_p}{r_2} \frac{1}{j\omega C_4}, \tag{19}$$

where r_2 is the resistance of arm ACB.

The voltage U_g across the detector diagonal of the bridge will be equal to the difference between the voltage drops (ignoring the effect of the current in the detector diagonal):

$$U_g \approx U_{BD} - U_{BC} = U_p \left(\frac{1}{r_1 j\omega C_3} - \frac{1}{r_2 j\omega C_4} \right).$$

Since $C_3 = C_4$ by choice, then

$$U_g \approx \frac{U_p}{j\omega C_3} \left(\frac{1}{r_1} - \frac{1}{r_2} \right). \tag{20}$$

When the master sample in coil L_2' is replaced by a sample with a different value of ρ, the resistance in arm ABC will become equal to $r_2' = r_2 + \Delta r_2$, where Δr_2 is the change in the transferred resistance in the circuit of L_2' due to change of sample.

In this case expression (20) takes on the form:

$$U_g \approx \frac{U_p}{j\omega C_3} \left(\frac{1}{r_1} - \frac{1}{r_2 + \Delta r_2} \right).$$

When the bridge is balanced with the master sample in the circuit of L_2, the equality $r_2 = r_1$ exists and one can write

$$U_g \approx \frac{U_p}{j\omega C_3} \left[\frac{\Delta r_2}{r_1 (r_1 + \Delta r_2)} \right]. \tag{21}$$

The bridge sensitivity is $\overline{S} = \dfrac{\partial U_{CD}}{\partial \Delta r_2}$.

Taking the derivative of (21) with respect to Δr_2, we find

$$\overline{S} = \frac{U_p}{j\omega C_3} \frac{1}{(r_1 + \Delta r_2)^2}. \tag{22}$$

If $r_1 >> \Delta r_2$ then we can assume that S does not depend on Δr_2 and remains constant, while the voltage U_g, according to equation (21), will be proportional to Δr_2. The scale will be linear. Usually the sensitivity increases with decrease in r_1, i.e., with increase of Q-factor of the induction coils L_1' and L_2'. In fact, taking the modulus of formula (22) we get

$$S = |\overline{S}| = \frac{U_p}{\omega C_3 r_1} \frac{1}{r_1 \left(1 + \frac{\Delta r_2}{r_1}\right)^2} = \frac{U_p Q_1}{r_1 \left(1 + \frac{\Delta r_2}{r_1}\right)^2}, \tag{23}$$

where $Q_1 = 1/\omega C_3 r_1$ is the Q factor of circuit ADB.

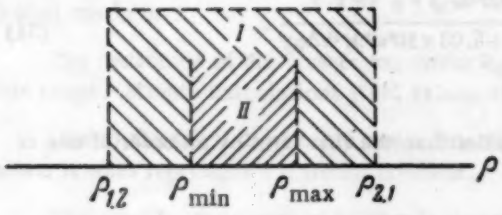

Fig. 9

To determine the dependence of S on ρ we substitute (6) in (4):

$$\Delta r_2 = \frac{\omega^2 M^2 \frac{P\sqrt{\rho f}}{5.03 \times 10^5 h}}{\left(\frac{P\sqrt{\rho f}}{5.03 \times 10^5 h}\right)^2 + (\omega L_2)^2}. \tag{24}$$

The calculations may be simplified by determining the bridge sensitivity S under the condition of maximum transferred resistance, i.e., under condition (7). In such a case Equation (27) can be rewritten in the following form:

$$\Delta r_2 = \frac{\omega^2 M^2 5.03 \times 10^5 h}{2P\sqrt{\rho f}} \tag{25}$$

When a sample having a specific resistance ρ is replaced in the measuring coil by another sample with specific resistance $\rho + \Delta\rho$, the change in the circuit's resistance becomes equal to the difference between the transferred resistances:

$$\Delta r_2' = \frac{5{,}03 \times 10^5 \omega^2 M^2 h}{2P\sqrt{f}} \left(\frac{1}{\sqrt{\rho}} - \frac{1}{\sqrt{\rho + \Delta\rho}}\right). \tag{26}$$

The expression $\frac{1}{\sqrt{\rho}} - \frac{1}{\sqrt{\rho + \Delta\rho}}$ in (26) is approximately equal to:

$$\frac{1}{\sqrt{\rho}} - \frac{1}{\sqrt{\rho + \Delta\rho}} \approx \frac{\Delta\rho}{2\rho\sqrt{\rho}}. \tag{27}$$

Let us introduce the symbol

$$A = \frac{5.03 \times 10^5 \omega^2 M^2 h}{4P\sqrt{f}}. \tag{28}$$

Then we will have

$$\Delta r_2' = A \frac{\Delta\rho}{\rho\sqrt{\rho}}. \tag{29}$$

We substitute the value of $\Delta r_2'$ from (29) into (21) to express the potential across the measuring diagonal of the bridge:

$$U_g = \frac{U_0 A}{j\omega C_2} \frac{\Delta\rho}{r_1(r_1\rho\sqrt{\rho} + A\Delta\rho)}. \tag{30}$$

To find the modulus of the bridge sensitivity as a function of $\Delta\rho$, we take the derivative of expression (30):

$$S_\rho = \left|\frac{\partial U_g}{\partial \Delta\rho}\right| = \frac{U_p 5.03 \times 10^5 \omega^2 M^2 h r_1 \rho \sqrt{\rho}\, 4P\sqrt{f}}{\omega C_3 r_1 (4P\sqrt{f} r_1 \rho \sqrt{\rho} + 5.03 \times 10^5 \omega^2 M^2 h \Delta\rho)^2}. \quad (31)$$

If, in the denominator, the second term in brackets is smaller than the first term by an order of one or two (as a result of the smallness of M^2), then

$$S_\rho \approx \frac{U_p \pi \sqrt{f}\, M^2 h 5.03 \times 10^5}{2C_3 r_1^2 P\rho \sqrt{\rho}}. \quad (31')$$

Equation (31') can be rewritten in a different form by introducing the figure of merit $Q_1 = 1/\omega C_3 r_1$:

$$S_\rho = \frac{U_p h \pi \sqrt{f}\, \omega Q_1 5.03 \times 10^5 M^2}{2 r_1 P \rho \sqrt{\rho}}. \quad (32)$$

Maximum sensitivity occurs when $R_2 = \omega L_2$. Replacing in Equation (32) $\frac{P\sqrt{\rho f}}{5.03 \times 10^5 h} = R_2$ by ωL_2 and M^2 by $k^2 L_1 L_2$, we obtain

$$S_{\rho\max} = \frac{U_p k^2 \omega L_1 Q_1}{4 r_1 \rho}. \quad (33)$$

It follows from Equation (33) that to increase the sensitivity it is profitable to increase the inductance of the measuring coil, the Q-factor and the coupling coefficient. The sensitivity increases as well with decrease in r_1.

All the conclusions are arrived at on the assumption that the distributed capacitance of the inductive coils is small and can be ignored when compared to the capacitance C_3.

In practice, the bridge sensitivity S_ρ varies by fractions of a volt to several volts per unit of specific resistance, depending on actual conditions. Such a sensitivity permits the use of a VTVM as an indicator without an intermediate amplifier.

The transformer (cf. Fig. 8) is used in the circuit mainly as an isolating element. However, the bridge sensitivity may be increased by increasing the transformation ratio of the output transformer.

4. Range of Application of the Described Method [9-12]

The described method may be used to measure small samples of nonmagnetic materials having a volume of 20-30 mm^3. The measurement of ρ for such samples by usual methods using a dc source, presents great difficulties.

The method may be used as the basis for the development of apparatus for the determination of the ρ of materials in ingots, manufactured objects, etc. It is also useful in the design of automatic sorters of items by their specific resistance. Using phase discriminators one can control the dimensions of the items, determine the presence of logitudinal cracks appearing on the surface of the items, and thereby control the quality of production, etc.

It is possible to devise an absolute method of determining ρ by measuring the transferred ΔR_1 and ΔL_1 once a method is developed for the accurate determination of the magnitudes R_2 and L_2 in relation to the frequency and the dimensions of the samples.

5. An Apparatus Using the Contactless Method for the Sorting of Carbon Brushes by Their Specific Resistance

The specific resistance of electric carbon brushes according to GOST 2332-43 varies between 0.05 and 60 ohm mm^2/m.

The resistance of the brushes to current R_{shch} depends on ρ and their dimensions. It also varies over a wide range. Simple calculations yield values of R_{shch} for brushes in the range from 1×10^{-5} to 1×10^{-2} ohms.

Due to the small dimensions and resistances of the brushes, the measurement of the specific resistance of carbon brushes represents a difficult problem.

The specific resistance of brushes is measured either by the method of separated circuits or by a bridge method. However, the variation of the current density along the cross section of the brush, as a result of the effect of the quality of contact between the brush and the connecting plates, which arises in the method of separated circuits, or else the contact resistance between the current.carrying plates and the brush, introduce significant variations which affect the magnitude of the experiment errors in the method. Practice shows that these errors may sometimes reach values of 100% of the resistance being measured.

Neither is the problem of control in mass production solved by the rho-apparatus developed at a branch of the research institute for electric cells and electrocarbon, which is based on the method of divided circuits [7].

These difficulties in measurement (control) were overcome by using the above-described contactless method of measuring the specific resistance. Models of the bridge described in part 2 were built for this purpose. A photograph of one of these units is shown in Fig. 10. The measuring coil into which the brush being measured is placed can be seen on the right. A single unit comprises the bridge and a single-tube high frequency signal generator. Power is derived from a regulated rectifier which is fed from 220 volt mains. The signal generator frequency is chosen between 0.6 and 1 Mc for different models of the apparatus.

Results of measurements made with the different models were found to be easily reproducible and the sorting speeds were high.

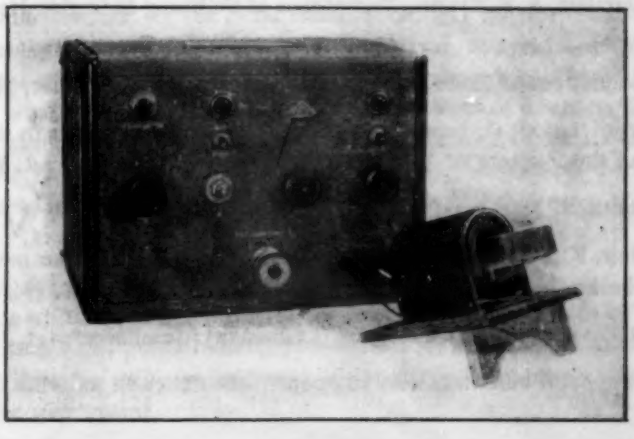

Fig. 10

The inadequacies of the bridge include the necessity for a preliminary warm-up before measurement, and the necessity of determining the specific resistance of the master brushes in a laboratory by an absolute method (amalgam or rho-apparatus) for each type of brush being controlled.

The results of control-measurement on the given equipment sometimes diverge from the results obtained using dc current methods owing to different laws governing the evolution of the mean measured value. However, the results are much more reproducible on this equipment than on old methods.

The apparatus is used to control stocks of brushes prior to their copper plating. However, on principle, the method may be applied to the control of copper plated brushes, without ruining them.

The equipment will work either if the brush is introduced into the measuring coil or if it is placed on the face of the coil, thus facilitating the design of an automatic sorter.

When brushes are produced to the third grade of accuracy, the theoretical rejection error is approximately 8%, of which 5% is due to the effect of the tolerance in the length of the brush.

The circuit of the apparatus is simple, and it is suitable for manufacture in a factory KIP. The most difficult part of the work involved in assembling the bridge is the initial tuning of the high-frequency bridge. Equipment of this type has been used successfully for over a year and a half at one factory producing carbon brushes.

SUMMARY

The theoretical conditions which were discussed in the paper point up the possibility of utilizing, for control purposes, currents, which make it unnecessary to have contacts between the object being measured and the elements of the measuring circuit. The developed models of a device for the sorting of objects by their specific resistance have shown their advantages over sorting equipment using a dc current.

This method may be used in production for the continuous control of some parameters which determine the quality of the product: the specific resistance, diameters of objects, the presence of longitudinal cracks, the wall thickness of thin-walled cylinders, etc.

This method can be recommended for the development of automatic control and sorting equipment, and in some cases it may serve as the basis for developing pickups for application in automatic regulating systems.

LITERATURE CITED

[1] V. P. Vologdin, Inductive Casehardening [in Russian] (Oborongiz, 1947).

[2] G. I. Babat, G. V. Dershvarts, A. D. Svenchanskii and M. Ia. Smelianskii, Industrial Electrical Ovens [in Russian] (Gosenergoizdat, 1948).

[3] K. Z. Shepeliakovskii, S. E. Ryskin, Techniques of Utilizing Induction Heating [in Russian] (Mashgiz, 1949).

[4] B. P. Aseev, Foundations of Radio Engineering [in Russian] (Sviaz'izdat, 1947).

[5] N. N. Shumilovskii and G. G. Iarmol'chuk, "Automation of processes in the production of electrocarbon products, "Report of the Institute of Automation and Remote Control Acad. Sci. USSR (1953).*

[6] "Brushes for Electrical Machines," GOST, 2332-43.**

[7] Ia. G. Davidovich, K. M. Rozin and A. S. Fialkov, "Equipment for the measurement of specific resistance," Zavodskaia Laboratoria, No. 6, 1955.

[8] G. G. Ginkin, Radio Engineering Handbook [in Russian] (Gosenergoizdat, 1948).

[9] P. Zijlstra, "Ein apparat zum nachweis von oberflächenrissen in metalldrähten," Philips Technische Rundschau, No. 1, 1949.

[10] F. Förster, "Theoretische und experimentelle grundlagen der zerstorungsfreien wertstoffprüfung mit wirbelstromverfahren," Zeitschrift für Metallkunde, Bd. 43, 1952, Bd. 45, 1954.

[11] H. Staats, "Now a useful nondesdructive testing tool" Materials and Methods, Vol. 38, No. 4, 1953.

[12] R. Hochschild, "Eddy current testing. A new tool makes inspection automatic," Control Engineering (October, 1954).

Received April 25, 1957

*In Russian.

**As in original – Publisher's note.

A LINEAR INDUCTION POTENTIOMETER FOR INDUSTRIAL USE

O. I. Aven, S. M. Domanitskii and Io. M. Pul'er

(Moscow)

A description is given of an induction potentiometer with a linear dependence between the output voltage and the shaft rotation in a range close to ±90°. A method of computation is given, and also an experimental method for investigating similar potentiometers. Experimental results are provided. The potentiometer described could serve as a standard for industrial types.

INTRODUCTION

The slide-wires which find such broad use in industrial automatic devices have essential inadequacies. The presence of sliding contacts, which contribute to the unreliability of the slide-wire functioning, also affect the reliability of the apparatus of which the slide-wire is a component. In spite of its apparent simplicity, the accurate preparation of slide-wires is quite complex. The use of slide-wires together with contact-less apparatus in, for example, the positioning feedback loop of a contact-less executive mechanism [1], leads in fact to a de-emphasis of the contact-less parts of the devices. The inadequacies of slide-wires necessitated the search for a means of constructing contact-less devices which still possessed characteristics analogous to those of slide-wires.

In contemporary apparatus destined for use in industrial automatic control systems, there are sometimes used, instead of slide-wires, selsyns or inductive transducers. However, selsyns have a maximum rotational angle, corresponding to the linear portion of their characteristic, of about ±15-20°, which can only be extended to ±50-60° by adding special windings, which frequently leads to all sorts of troubles. Small-size inductive transducers are usually manufactured with forward motion and are designed for small disturbances. Moreover, there is a transformation of the forward motion to a rotary one which complicates the kinematics of the apparatus. Thus, there are no contemporary contact-less variable transducers of the rotary type for industrial use which possess large rotational angles (180-240°).

The present paper describes an induction potentiometer designed, in particular, to replace slide-wires in control and regulation systems which have a maximum rotational angle of 180° (±90°). It should be mentioned that the inductive system on which this potentiometer is based allows a maximum angle of 240° (±120°) to be obtained. The problem in developing this potentiometer was to make it universal, suitable for use in secondary tools, regulators and executive mechnisms.

With this problem for a starting point, the following special requirements were formulated for the potentiometer.

1. The potentiometer should function in equalizing designs, similar to the schematic of Fig. 1.

2. The potentiometer must be designed for an ac source voltage of 50 hertz frequency.

3. The potentiometer's output voltage must correspond to the input parameters of the standard industrial control system amplifiers.

4. For rotational angles close to 180° (±90°) or 240° (±120°), the error in amplitude must not exceed 0.5%.

5. The phase angle between the input and output voltages must not depend on the angle of potentiometer shaft rotation.

6. In construction and dimensions, the potentiometers should be compatible with control and regulation devices (executive mechanisms, regulators, secondary tools, etc.).

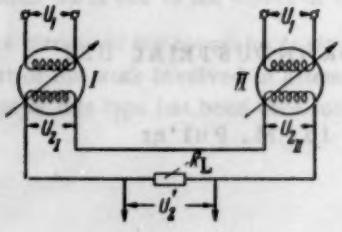

Fig. 1

Potentiometer Construction

The induction system described in [2] was taken as the basis for the functioning of our industrial linear induction potentiometer.

Figure 2 gives the physical design of the linear induction potentiometer with a ± 90° range of shaft rotation. On the same figure is provided the design of the magnetic link, with the principal dimensions noted, and an indication of the fluxes, Φ_1 and Φ_2 for different magnetic flux paths, as determined by the given positioning of the windings and the choice of the current direction.

There is a pair of windings W_{21} and W_{22} on the potentiometer rotor, and an analogous pair W_{11} and W_{12} on the stator.

The primary windings W_{11} and W_{12} comprising the exciting winding, upon rotation of the rotor in the range ± 90°, change their orientation with respect to windings W_{21} and W_{22}, comprising the secondary winding. At this, the flux in the secondary winding changes from zero to a maximum value, at some phase angle. The secondary winding is loaded by load resistor z_{2L}.

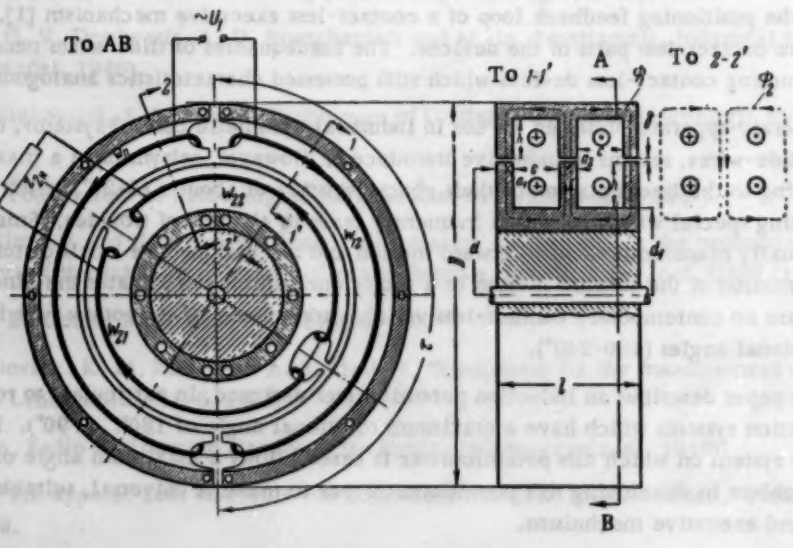

Fig. 2. Physical design of the potentiometer.

The construction of the potentiometer is clarified by the overall view (Fig. 3). In the slots of the non-magnetic housing of the stator 1 are embedded the blocks at the back of the stator 2 composed of drawn sheets of electrical steel. These sheets are bonded to CF. The layer of adhesive serves simultaneously as insulation between the laminas. Also inserted in the stator housing are the lateral 3 and intermediate 4 disc block which, together with the back, make up the III-shaped magnetic stator. The stator winding 5 is wound on a former and inserted in the stator assembly.

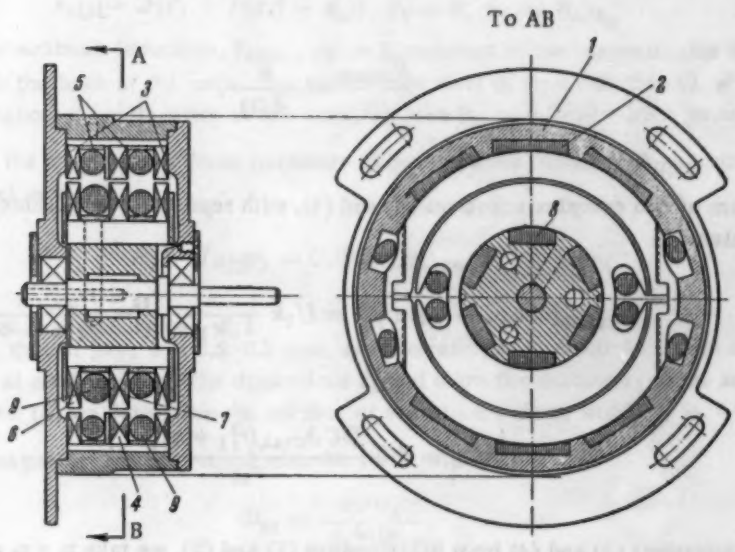

Fig. 3. Overall view of the potentiometer.

The rotor is assembled the same way as the stator and, analogously to the stator, has the III-shaped magnetic characteristic (8, 6 and 7 are, respectively, the rotor back, side and middle disc blocks). The rotor winding 9 is also wound on a former and inserted in the rotor assembly, the winding endings being led along the uncovered shaft. The potentiometer construction is intended to allow the mechanization of the winding on the stator and rotor.

It should be mentioned that, as shown in [2], there is the possibility of so laying out the primary and secondary windings on the stator that one may obtain a completely contact-less system for arbitrary angle of rotation. However, in a system with windings of the rotor, with rotation angles less than 360°, it is possible to have the winding endings made of flexible conductor, thus securing a contact-less system. The construction of a potentiometer with windings on both rotor and stator, in comparison with a design having windings only on the stator, possesses a host of advantages – effective utilization of copper and steel by virtue of the complete encircling of the primary and secondary windings along their entire length. This latter fact accounts for a minimum of end effect, thus increasing the effective angle of rotation, and permitting a high degree of magnetic symmetry in the system. This in turn effects a much higher accuracy of potentiometer behavior.

Method of Potentiometer Calculation

The method for carrying out the engineering calculations for the potentiometer is based on the given technical requirements. We make use of the basic relationships given in [2]. Below is given the method for computing an induction potentiometer for the case where one is given the supply voltage U_1 the maximum amplitude of the secondary voltage U_{2max} the load resistance z_{2L} and $(\pm \delta U_2)_{max}$ the active component of the maximum potentiometer error (coinciding in phase with U_1), taken as the ratio of U_{2max} with respect to unity.

From the results of the computations are determined the physical dimensions of the potentiometer, the number of turns and the conductor diameter for the primary and secondary windings. The magnitude of the primary and secondary currents is found, as well as the output voltage when the potentiometer is loaded.

The computations are carried out in the following sequence.

1. We find the ratio of the number of turns, $k = w_2/w_1$, of the secondary and primary potentiometer windings and also the inductive reluctance x_θ. Using Relationships (1) and (2), which appear in [2],

$$(\pm \delta U_2)_{\max} = 0.25 \mathrm{Re}\left[\frac{2jx_0k^2}{z_{2H}\bar{A}(1)}\right], \tag{1}$$

$$\frac{\dot{U}_{2\max}}{U_1} = \frac{k}{\bar{A}(1)}, \tag{2}$$

we obtain the system of two complex equations (3) and (4), with repsect to the argument of $\dot{U}_{2\max}$ (the angle Φ_2) and the coefficient k:

$$U_{2\max}(\cos\varphi_2 + j\sin\varphi_2) = \dot{U}_1 k \frac{r_{2l} + jx_{2l}}{1.3r_1 + j(1.3x_{2l} + 1.38\gamma)}, \tag{3}$$

$$\gamma = k^2 x_0 = 2.6 \frac{(\delta U_2)_{\max}(r_{2l}^2 + x_{2l}^2)}{x_{2l}}. \tag{4}$$

For deriving Equations (3) and (4) from Relationships (1) and (2), we take $r_1 = r_2 = 0$, $x_{1s} \approx 0.3x_0$ and $x_{2s} \approx 0.3x_0k^2$. Moreover in the expression for $\bar{A}(1)$ in Equation (1), we take $z_{2L} = \infty$. Then

$$\bar{A}(1) = \left(\frac{z_{2s}}{z_{2l}} + 1\right)\left(\frac{z_{1s}}{2jx_0} + 1\right) + \frac{z_{1s}k^2}{z_{2l}} = 1.3.$$

The following notation was employed in giving the previous equations: $z_{1s} = 2(r_1 + jx_{1s})$ is the total reactance of the primary winding (stator), $z_{2s} = 2(r_2 + jx_{2s})$ is the total reactance of the secondary winding (rotor), $z_{2L} = r_{2L} + jx_{2L}$ is the total load reactance, r_1 and x_{1s} are the active and inductive reactance of one coil of the stator winding, r_2 and x_{2s} are the active and inductive reactance of one coil of the rotor winding, r_{2L} and x_{2L} are the active and reactive load reactance, and w_1 and w_2 are the number of turns in the stator and rotor windings.

From Equations (3) and (4) we obtain

$$k = \frac{U_{2\max}}{U_1}\sqrt{\frac{(1.3r_{2l})^2 + (1.3x_{2l} + 1.38\gamma)^2}{r_{2l}^2 + x_{2l}^2}}. \tag{5}$$

Here, γ is immediately determined for (4) and, in its turn,

$$x_0 = \frac{\gamma}{k^2}. \tag{6}$$

It should be mentioned that if $z_{2L} = \infty$, or r_{2L}, then Equation (1) reduces identically to zero. In this case, one has only Equation (2) for a starting point, together with (3) and (5), which are derived from it, from which it is clear that, for $\gamma = 0$, the value of the reactive reluctance can be arbitrary. As will be shown below, x_0 in this case is determined from practical rational relationships deriving from the geometry of the induction system and the given current requirements.

2. We find the current of the unloaded potentiometer:

(7)

$$I_{1UL} = \frac{U_1}{z_{1UL}} = \frac{U_1}{2{,}6x_0},$$

where

$$z_{1UL} = 2[r_1 + j(x_{1s} + x_0)],\ r_1 = 0,\ x_{1s} \approx 0{,}3x_0.$$

3. We assign the maximum induction, B_{max}, which is obtained in the magnetizable disc in the section immediately adjacent to the back of the rotor. For transformer steel of type E42 (E4AA), which will essentially render negligible the influence of nonlinearity of the steel, we take B_{max} = 2000 – 3000 gauss.

4. We determine the magnetizing force necessary to generate the induction B_{max}, not taking into account the reactance of the steel sections:

$$F_1 = I_{1UL} w_1 = 0.8 \times 2B_{max.} \left(\frac{d_1}{d}\right) \delta. \tag{8}$$

The magnitude of the air gap, δ = 0.2-0.3 mm, and the ratio, d_1/d = 0.6-0.8, were chosen from considerations of the physical configuration (the dimensions d_1 and d are the diameters of the stator bore, as shown in Fig. 2). From Equation (8) we determine the number of turns in the stator winding: $w_1 = F_1/I_{1UL}$.

5. We find the magnetic flux connected with the stator winding:

$$\Phi_{01} = \frac{10^8 U_0}{4.44 f w_1}. \tag{9}$$

Here, $U_0 = I_{1UL}x_0 = I_{1UL}z_{1UL}/2.6 = U_1/2.6$.

6. We determine the width of the blocks a_2 and a_1 (Fig. 2), of the stator and rotor magnetic conductors, as a function of the diameter d, given by physical considerations:

$$a_2 = \frac{\Phi_{01}}{B_{max.} \tau k_c} \left(\frac{d}{d_1}\right),\quad a_1 \approx \frac{a_2}{2} \tag{10}$$

(it is desirable that $a_1 > 10\delta$).

Here, $\tau = \pi d/2$, $k_C \approx 0.9$ is the charging coefficient of the steel blocks.

7. We compute the cross-sectional area of the backs of the stator and rotor magnetic conductors:

$$S_{st.} = S_r = \frac{\Phi_{01}}{B_{max.}}, \tag{11}$$

from which the basis dimensions of the backs may be found.

8. We determine the area $S_1 = I_{1UL}/\Delta$ (and the diameter, d_1) of the stator winding conductors by starting from the given current density, Δ.

9. We find the height h of the aperture (Fig. 2) by taking the width of the aperture to be $c \approx 2a_1$:

$$h = \frac{S_{ap}}{c} \approx \frac{S_1 w_1}{2k_M a_1}. \tag{12}$$

Here, S_{ap} is the aperture area, $k_C \approx 0.3$-0.35 is the charging coefficient of the aperture copper.

10. Knowing all the magnetic conductor dimensions we determine, from known formulae, the active reactance of one stator coil.

11. We find the number of turns of the rotor winding, $w_2 = kw_1$, the area of conductor S_2 and the reactance of one rotor coil r_2.

12. After the determination of the winding data, the current and voltage in various regimens, taking into account the ohmic resistance of the windings and the influence of the load, are found from Formulae (13), (14) and (15) given in [2].

The relations referred to will be complex, thus allowing the determination both of the real values of the current and the voltage, and also their phase displacement.

The current in the stator winding

$$\dot{I}_1 = \frac{\dot{U}_1}{z_{1s} + 2jx_0\left[1 - \frac{2jx_0k^2}{z_2 + 2jx_0k^2}\left(\frac{\alpha}{\alpha_{max}}\right)^2\right]}, \tag{13}$$

where α / α_{max} is with respect to the angle of rotation,

$$z_2 = z_{2s} + z_{2l} = 2(r_2 + jx_{2s}) + z_{2l}$$

The current in the rotor winding

$$\dot{I}_2 = \frac{2jx_0k\dot{I}_1}{z_2 + 2jx_0k_2}\frac{\alpha}{\alpha_{max}}. \tag{14}$$

The magnitude of the stator and rotor winding currents without loading, and short-circuited, may be found from Expressions (13) and (14) if one takes, respectively, $z_2 = \infty$ and $z_2 = z_{2s}$.

The voltage across the load

$$\dot{U}_2 = \frac{\frac{\alpha}{\alpha_{max}}}{\left(\frac{z_{2s}}{z_{2l}}+1\right)\left(\frac{z_{1s}}{2jx_0}+1\right) + \frac{z_{1s}k^2}{z_{2l}} + \frac{2jx_0k^2}{z_{2l}}\left[1 - \left(\frac{\alpha}{\alpha_{max}}\right)^2\right]}\dot{U}_1k. \tag{15}$$

Here, α is the angular rotation of the potentiometer rotor, α_{max} is the maximum angular rotation of the potentiometer rotor.

The magnitude of $\underline{k}$, and the active part of the maximum error $(\delta U_2)_{max}$ may also be specified from Expression (5) and (1).

In the cases where $z_{2L} = \infty$ or $z_{2L} = r_{2L}$, the computation is carried out in the following manner. The magnitude of the required current I_{1UL} and the diameter $\underline{d}$ are given from practical considerations once U_1, U_{2max} and z_{2L} are known. The number of turns w_1 may be found from Equation (8), and the reluctance x_0 from the expression, $x_0 = U_1/2.6I_{UL}$. Further computations are carried out in the same order as above, taking into account the rational relationships in the geometry of the potentiometer, $a_1 > 10\delta$, $c/a_1 \approx 2$, $a_2/a_1 \approx 2$, $d_1/d = 0.6\text{-}0.8$.

EXPERIMENTAL METHODS

Below are given the results of experimental investigation of the linear induction potentiometer. The potentiometers were calculated on the following data: $U_1 = 80$ volts, $U_{2max} = 7$ volts. They had the following dimensions: D = 70 mm, d = 50 mm, $a_1 = 3$ mm, $a_2 = 4$ mm, $\delta = 0.3$ mm. Photographs of a disassembled potentiometer are given in Fig. 4.

The linear induction potentiometers were investigated both as individual components, and as functioning parts of equalizing designs. As shown by experiment, the empirical curves, $I_{1UL} = f(\alpha)$, $I_{1SC} = f(\alpha)$ and $I_{2SC} = f(\alpha)$, for individual potentiometers, have the same character as the computed curves constructed from Equations (13) and (14). The maximum discrepancy for the currents, I_{1UL} and I_{1SC}, nowhere exceeded 10-12% and for the current I_{2SC}, nowhere exceeded 5-7%. Satisfactory agreement with computed values was also given by the empirical curves for the phase displacements, $\varphi_{1UL} = f(\alpha)$, $\varphi_{2UL} = f(\alpha)$, $\varphi_{1SC} = f(\alpha)$ and $\varphi_{2SC} = f(\alpha)$, where φ_{1UL} is the angular displacement between the primary current $\dot{I}_{1UL}$ and voltage, $\dot{U}_1$, vectors, φ_{2UL} is the angle between vectors $\dot{U}_1$ and $\dot{U}_{2UL}$. φ_{1SC} is the angle between $\dot{U}_1$ and $\dot{I}_{1SC}$ and φ_{2SC} is the angle between

$\dot{U}_1$ and $\dot{I}_{2SC}$. The angles φ_{1UL} and φ_{2UL} do not, in fact, depend on the position of the potentiometer rotor. The magnitude of the angles was measured by means of a Ts50 vectormeter. The maximum deviation between the experimental and the computed values was 5° for φ_{1UL} and φ_{1SC} and 12-15° for φ_{2UL} and φ_{2SC}.

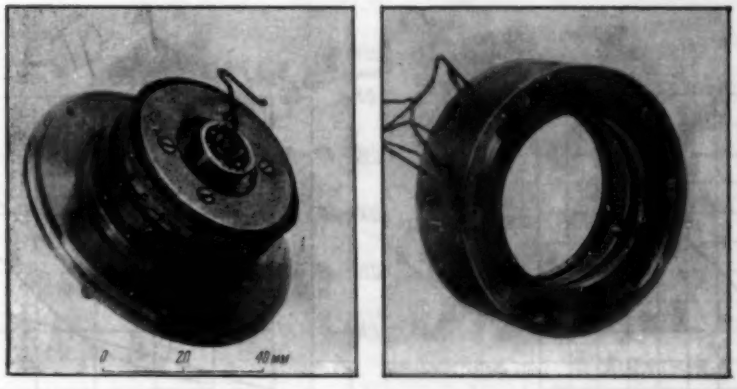

Fig. 4.

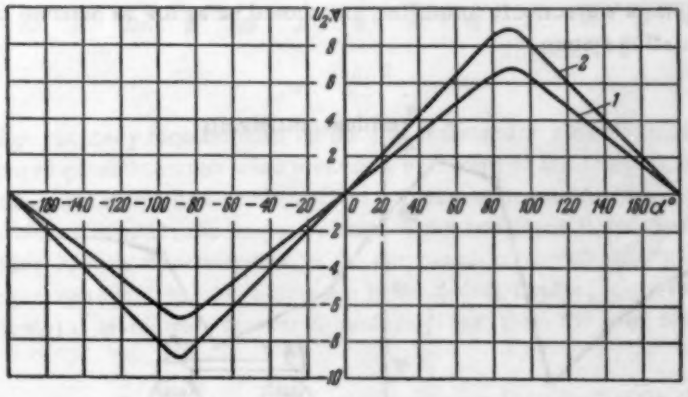

Fig. 5

Figure 5 shows the dependence of the secondary voltage on the angle of rotor rotation for one potentiometer, with load resistance R_L = 500 ohms (curve 1) and $R_L = \infty$ (curve 2). The minus sign for voltage U_2 is conventionally chosen so as to show phase variation of the output voltage from 180°.

Figure 6 gives the initial portion of the curve for $R_L = \infty$. The angle of rotation was established with a high degree of accuracy by means of an optical graduating device. The minimum "residual" voltage, U_{2min}, corresponding to the angle $\alpha = 0$, for different potentiometers was measured at from 12 to 35 millivolts, comprising 0.2-0.5% of U_{2max}. It is necessary to mention that the residual voltage contained fundamentally the higher harmonics. The relationship between the voltage at the fundamental harmonic and the voltage at the higher harmonics in the curve of the secondary voltage, U_{2min}, depends only on the quality of the magnetic material, and on the care with which the potentiometers are prepared. The composition and magnitude of the higher harmonics depends, in significant measure, particularly on the quality of heat treatment of the steel plates of the magnetic conductors, but the magnitude of the residual voltage at the fundamental harmonic also depends on the accuracy of the preparation and assembly of the potentiometers. Figure 7 gives the dependence of U_{2min}, U_{2max} and U_{2min}/U_{2max} for one of the potentiometers on the supply voltage U_1. As is

clear from Fig. 7, for small and large values of supply voltage, the quantity U_{2min}/U_{2max} increases. This stems from the fact that, for weak and for strong fields, the influence of the nonlinearity in the steel characteristic is greater, thanks to which the difference in e.m.f.'s of the potentiometer rotor winding coils is increased.

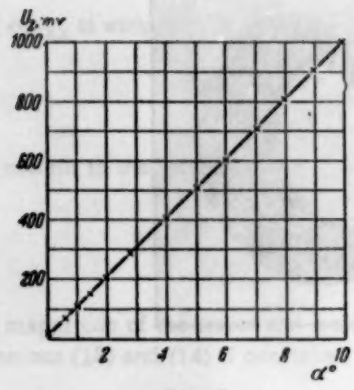

Fig. 6

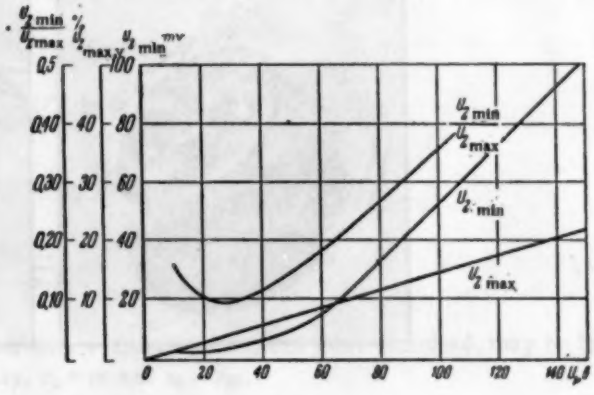

Fig. 7

For various regulators, particular interest inheres in the magnitude of the "residual" unequalized voltage, corresponding to the actual adjusted state of the potentiometer rotor in an equalizing circuit. This voltage is fed to the input of the regulator's electronic amplifier, and should be as low as possible in order to minimize the static error of the regulating system.

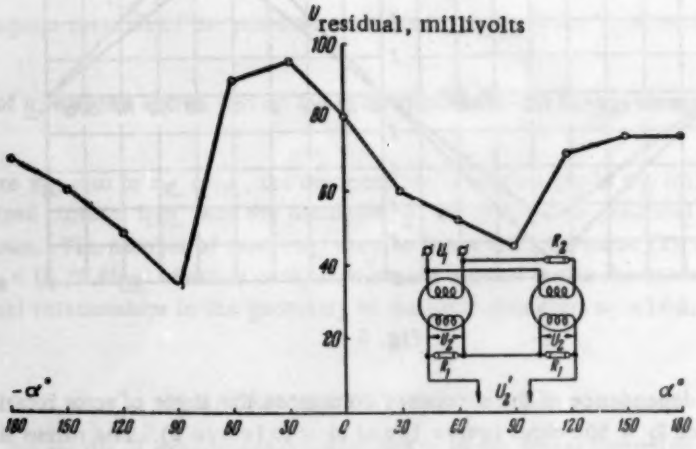

Fig. 8

Figures 8 and 9 give the curves $U_{res} = f(\alpha)$, taken from equalizing circuits for $U_1 = 80$ volts and $R_L = \infty$. In the first case, the stator windings of two potentiometers were connected in parallel. The rotor windings were loaded with a resistance, $R_1 = 10$ kilohms. In order that the rotor winding voltages coincide in phase a resistor $R_2 = 140$ ohms was connected in series with the stator winding of one of the potentiometers. For the series-connected stator windings (Fig. 9), one of its windings, with the same purpose, was shunted by a resistor $R_2 = 330$ kilohms.

In the potentiometers under consideration, the output voltage U_2 and the corresponding voltage U_2' were displaced about 45° from the line voltage. In order that the voltage supplied to the equalizing circuit's phase-sensitive electronic amplifiers coincide with the line voltage, it was necessary to place a phase-displacing RC network at the output of the circuits of Figs. 8 and 9. For taking off the curves of Figs. 8 and 9, one of the

potentiometers was turned to the angular position corresponding to $\alpha = 0$, and the rotor of the second potentiometer was adjusted each time so that a minimum value of the voltage U_{res} was obtained. As is clear from Figs. 8 and 9, the maximum values of U_{res} were, respectively, 95 millivolts and 145 millivolts. For the parallel-connected stator windings, the characteristics of the unbalanced voltage $U_2' = f(\alpha)$ in the compensation circuit (Fig. 10) were also taken off. This curve is rectilinear throughout the entire working range of the unbalancer which, given a linear amplifier, guarantees that the sensitivity will be independent of the angular rotation of the potentiometer.

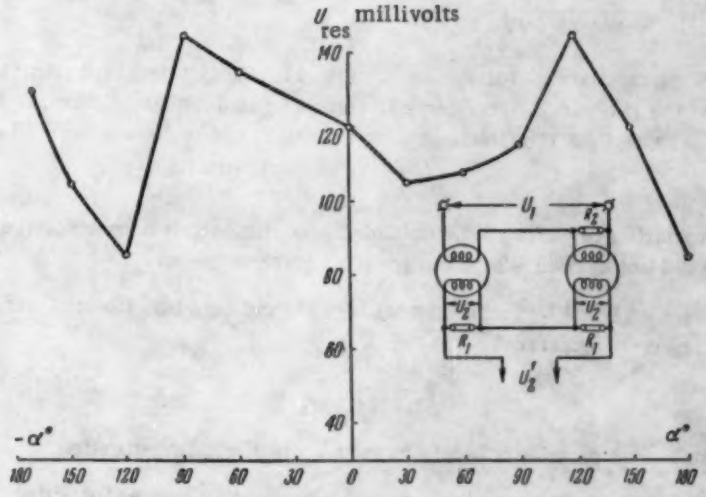

Fig. 9

Because of the high accuracy requirements on the linear induction potentiometers, the amplitude and phase errors of the prepared potentiometers were measured by means of the compensating circuit shown in Fig. 11. This circuit is a somewhat simplified version of the compensating circuit of a particular measuring instrument [3]. In the circuit of Fig. 11, the output voltage of the test piece is compensated by the voltage drop U_e across the test divider R_e, which corresponds to the computed magnitude of the induction potentiometer's output voltage, and by the voltage drop, ΔU across the linear (wire) divider, R_d. The compensated unbalance voltage ΔU (in amplitude) is taken from divider R_d and, in phase, from the rotor rotation of the phase-shifter PS.

On the basis of the results thus measured, the amplitude error is immediately obtained

$$\Delta U_2\% = \frac{R_d}{R_{e\,max}} 100\%.$$

The phase error is found from the relationship

$$\Delta\varphi \approx \tan\Delta\varphi = \frac{|\Delta U_2| \sin\beta}{|U_e| \pm |\delta U| \cos} \cdot \bullet$$

Here, β is the angular rotation of the phase-shifter rotor, R_{emax} is the resistance of the test divider corresponding to the compensating current for $U_2 = U_{2max}$, R_d is the divider resistance necessary to compensate the output voltage for a definite angular rotation of the induction potentiometer rotor.

It was demonstrated by the error measurements that, even for relatively crude preparation of the potentiometers, it is possible to guarantee an amplitude error of the first harmonic not exceeding $\pm 0.5\%$ of U_{2max} in a range of 150-160°. The amplitude error decreases with a lowering of the working range of the potentiometer.

• As in original (cos). Editor.

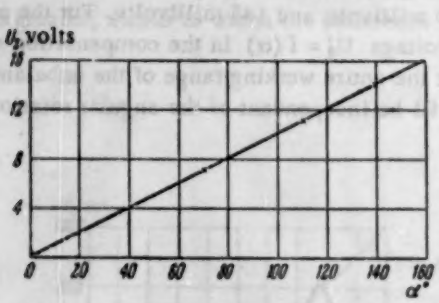

Fig. 10. Dependence of the unbalanced voltage on the angle of rotation, for the two parallel-connected potentiometers shown in Fig. 9: R_1 = 10 kilohms, R_2 = 140 ohms, R_L = ∞.

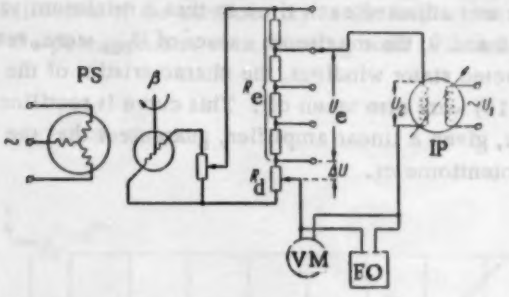

Fig. 11. Circuit designed to measure potentiometer error: PS is the phase-shifter, IP is the induction potentiometer, VM is the vacuum-tube voltmeter, EO is the electronic oscillograph.

The phase error (variation of phase of the unloaded potentiometer's output voltage as a function of the rotor's angular rotation) did not exceed ± 30' even for the worst test pieces.

The errors cited were affected by technological factors and could be lowered were the potentiometers prepared with a higher degree of accuracy.

SUMMARY

The following conclusions may be drawn from the results of our investigation.

1. Adoption of the magnetic system allows for the production of linear induction potentiometers for industrial use, satisfying established technological requirements for working angles up to ± 90°, with corresponding linear characteristics.

2. The computed values for current and voltage for actual potentiometers working in various regimens coincide satisfactorily with the experimental data.

3. The working characteristics of these potentiometers are superior to those of known contact-less position transducers currently used in industry with respect to the range in which linearity prevails, symmetry, and small residual unbalanced voltage in compensating circuits, as affected by the phase error of the potentiometers.

4. Investigation of the linear induction potentiometers herein described showed their suitability for use in automatic control systems.

5. The use of contact-less induction potentiometers increases the reliability, durability and accuracy of industrial automatic control system.

Appendix

Example of a Linear Induction Potentiometer Calculation

Below is given an example of the calculations illustrative of the above method for potentiometers supplied by a standard source.

Given: U_1 = 127 volts, U_{2max} = 12 volts, δU_{2max} = ± 0.005 and z_{2L} = (1000 + j1000) ohms. To be determined are the basic physical parameters, and the electrical parameters of the potentiometer.

1. The ratio of the number of turns, according to (5):

$$k = \frac{12}{127}\sqrt{\frac{(1.3 \times 1000)^2 + (1.3 \times 1000 + 1.38 \times 26)^2}{1000^2 + 1000^2}} = 0.125.$$

Here, γ is obtained from (4)

$$\gamma = 2.6\frac{0.005\,(1000^2 + 1000^2)}{1000} = 36.$$

2. Inductive reluctance;

$$x^0 = \frac{\gamma}{k^2} = \frac{26}{0.12^2} = 1680 \text{ ohms}$$

3. Current in the unloaded potentiometer (7)

$$I_{1UL} = \frac{127}{1680 \times 2.6} = 0.029\ a.$$

4. We take B_{max} = 2500 gauss, δ = 0.02 cm, d_1/d = 0.8 and d = 5 cm.

5. Magnetizing force of the air gap (8)

$$F_1 = 0.8 \times 2 \times 2500 \times 0.8 \times 0.02 = 64\ a.$$

6. Number of turns of the stator winding

$$W_1 = \frac{F_1}{I_{1UL}} = \frac{64}{0.029} = 2200.$$

7. Magnetic flux linked with the stator winding (9),

$$\Phi_{01} = \frac{127 \times 10^8}{2.6 \times 4{,}44 \times 50 \times 2200} = 10^4 \text{ mks}$$

8. Block width according to (10)(taking k_c = 0.9)

$$a_2 = \frac{10^4 \times 2 \times 1.25}{2500\pi \times 0.9} \approx 0.7\ см, \qquad a_1 = 0.35\ см.$$

9. Cross-sectional area of the magnetic conductor backs, according to (11)

$$S_{st} = S_{yd} = \frac{10^4}{2500} = 4\ см^2.$$

10. Area of the copper stator winding, for Δ = 3.5 amp/mm^2,

$$S_1 = \frac{I_{1UL}}{\Delta} = \frac{0.029}{3.5} = 0.0083\ мм^2.$$

We take d_1 = 0.1 mm, S_1 = 0.0078 mm^2.

11. Height of one stator according to (12), where we take k_c = 0.35,

$$h_1 = \frac{0.007810^{-2} \times 2200}{2 \times 0.35 \times 0.35} = 0.7\ см.$$

12. Active reactance of the stator coils:

$$r_1 = \rho \frac{l_1 w_1}{S_1} = \frac{1}{57} \frac{0.179 \times 2200}{0.0078} = 885 \text{ ohms}$$

where $l_1 \approx \pi (d + h_1) = \pi (5 + 0.7) = 17.9$ cm.

13. Number of turns of the rotor winding

$$w_2 = k w_1 = 0.125 \times 2200 = 274.$$

14. The dimensions of the rotor aperture are taken equal to those of the stator aperture

$$h_2 = 0.7 \text{ см.} \qquad c = 0.7 \text{ см.}$$

15. Area of the rotor winding, for $k_M = 0.25$

$$S_2 = \frac{S_{ap} \cdot k_M}{274} = \frac{7 \times 5 \times 0.25}{274} \approx 0.0445 \text{ мм}^2.$$

We take $d_2 = 0.23$ mm, $S_2 = 0.0415$ mm^2.

16. Active reactance of the rotor coils:

$$r_2 = \rho \frac{l_2 w_2}{S_2} = \frac{1}{57} \frac{0.135 \times 274}{0.0415} \approx 16.5 \text{ ohms}$$

where $l_2 = \pi (d - h_2) = \pi (5 - 0.7) = 13.5$ cm

17. Current in the stator winding (13) for $\alpha = \alpha_{max}$

$$\dot{I}_1 = \frac{127}{2(885 + j0.3 \times 1680) + 2j1680 \left[1 - \frac{2j\,1680 \times 0.125^2}{1033 + j\,1008 + 2j1680 \times 0.125^2}\right]} =$$

$$= 0.0272 e_a^{-j66.5},$$

where

$$z_2 = 2(16.5 + j0.3 \times 1680 \times 0.125^2) + 1000 + j \times 1000 \approx 1033 + j \times 1008.$$

18. Current in the rotor winding (14) for $\alpha = \alpha_{max}$

$$\dot{I}_2 = \frac{2j1680 \times 0.125 \times 0.0272\, e^{-j66.5^\circ}}{2(16.5 + j0.3 \times 1680 \times 0.125^2) + 1000 + j1000 + 2j1680 \times 0.125^2} = 0.0077 e^{-j21^\circ}.$$

19. Voltage across the load (15) for $\alpha = \alpha_{max}$

$$\dot{U}_2 = \dot{I}_2 z_{21} = 0.0077 \cdot e^{-j21^\circ} 1415 e^{j45^\circ} = 10.8\, e^{j24^\circ} \text{ v}$$

As is clear from this last expression, the secondary voltage was obtained close to the given one. If necessary, the magnitude of $\underline{k}$ may be specified by Equation (5), taking into account the active reactance of the stator and rotor windings.

The computations for the induction potentiometer were carried out by Engineer B. B. Bulanovol.

LITERATURE CITED

[1] O. I. Aven, E. D. Demidenko, S. M. Domanitskii and E. K. Krug, "An electrical servo-mechanism with speed regulation," Automation and Remote Control (USSR) 17, 3 (1956).*

[2] Iu. M. Pul'er, "Linear induction potentiometers," Automation and Remote Control (USSR) 17, 7 (1956).*

[3] Iu. M. Pul'er, "Instrument for measuring amplitude and phase errors in ac computing systems," Izmeritel'naia Tekhnika 1956, No. 6.

Received July 20, 1957

*See English translation.

TELEMETERING COMPENSATION DEVICE FOR LINEAR TRANSFERENCE

A. A. Kol'tsov and L. F. Kulikovskii

(Kuibyshev)

An inductive servosystem for linear transference that may be used in automatic and remote control devices is described. A brief theoretical analysis and construction data for the system employed by the Kuibyshev Industrial Institute are given.

One of the many possible applications of ferrodynamic measuring mechanisms with independent excitation and linear displacement of the moving part* is the combined utilization of two such measuring mechanisms, forming a telemetering unit for measuring both small and large displacements or other quantities which can be transformed into displacements.

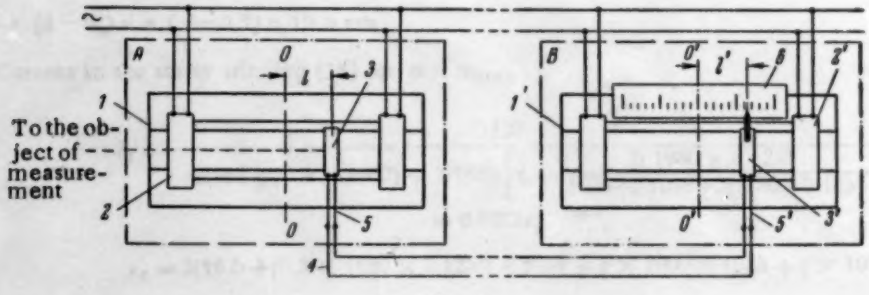

Fig. 1

The telemetering unit, represented schematically in Fig. 1, consists of two parts – the master system A and the receiving system B. The magnetic circuits of systems 1 and 1' are made of sheet electrical steel. Each magnetic circuit consists of an assembly of three rods – one central and two side ones (Fig. 2). The excitation windings 2 and 2' (Fig. 1), fed from the ac supply, are placed in the side rod grooves. Frameless coils 3 and 3', which encircle the central rod, are placed in the uniform airgaps of the magnetic circuit. By means of special devices these coils are able to move along straight lines. The output terminals of both systems are interconnected by line 4, whereas the coils are connected to the terminals by means of light flexible conductors 5 and 5' or by sliding contacts.

The coil of the master system is connected mechanically to the objects whose displacement it is required to measure. The coil of the receiving system is supplied with a pointer and the indication on scale 6 gives the value of the measured displacement.

The unit works in the following way. The excitation windings of each system produce magnetic fluxes,

*The measuring mechanism was proposed and developed by L. F. Kulikovskii and A. A. Kol'tsov. An experimental model was made at the laboratory of the "Automatic, Remote-Control and Measuring Instruments and Devices" Faculty of the Kuibyshev Industrial Institute.

equal in amplitude and directed toward each other. Hence magnetic induction in the airgaps of the system will remain constant along the whole of their length (Fig. 3), but the induction in the center rod will change in the plane of the coils according to a linear law (Fig. 4):

$$B_c = k_c l, \tag{1}$$

where k_c is the proportionality factor, l is the distance of the plane under consideration from the neutral lines 0-0 (0'-0').

Fig. 2

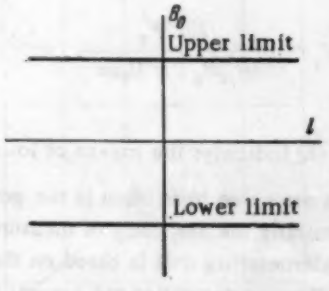

Fig. 3

The relationships shown in Figs. 3 and 4 are fully confirmed experimentally.

If coil 3 (Fig. 1) is displaced by the measured object through a length l from the neutral line 0-0, an emf will be induced in the coil

$$E_l = 2\omega w B_0 a l, \tag{2}$$

where ω is the angular supply frequency, w is the number of turns in the coil, B_δ is the magnetic induction in the airgap, α is the dimension of the core (Fig. 2), and l is the coordinate of the coil.

At the same time an emf will be generated in coil 3', which remained in the initial position

$$E_{l'} = 2\omega w' B'_0 a' l'; \tag{3}$$

as the result of this, a current will flow in the circuit connecting the two coils

$$I = \frac{E_l - E_{l'}}{Z}, \tag{4}$$

where Z is the impedance of this circuit.

Equality in (4) is achieved by adjusting the excitation current phases of systems 1 and 1' until they coincide.

For stable functioning of the system impedance, Z must be inductive.

Figure 5 is a vector diagram which shows that the interaction between the magneitc induction in the airgaps of the master and receiving systems and component I_B of current I, which is in phase (or antiphase) with the magnetic induction, will produce a force acting on the free sides of coils 3 and 3'.

Force F acting on coil 3' will cause its displacement, which will continue until there arises in the coil an emf E'_l, equal in amplitude but opposite in phase to emf E_l. The balancing of the two emf's operating in the coil circuit leads to the disappearance of current I and the stopping of coil 3', whose position at l' indicates the unknown displacement, since the value of emf E'_l is proportional to displacement l' (3). In other words, the coils of the two systems will always assume similar positions with respect to the neutral lines, i.e., $l/l' = \text{const}$. This means that the master and receiving systems can in general have different dimensions. The coil displacement equation, obtained in the normal way, has the following form:

$$m\frac{d^2l'}{dt^2} + p\frac{dl'}{dt} + \frac{\omega x [2B'_0 a' w']^2}{Z^2} l' + F'_\tau = 2\omega B_0 a l w \frac{x [2B'_0 a' w']}{Z^2}, \tag{5}$$

where m is the mass of coil 3' and the parts attached to it, p is the damping coefficient, x is the inductive reactance of the coil circuits, F'_T is the friction force which impedes the movement of coil 3'.

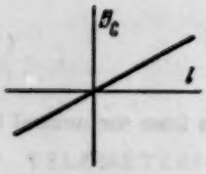

Fig. 4

When coil 3' movement, which can be oscillatory or aperiodic depending on the degree of damping:

$$\beta = \frac{p}{\frac{4B'_0 a' w'}{Z}\sqrt{m\omega x}}, \qquad (6)$$

comes to an end, the coordinates of the receiving coil will be given by the expression

$$l' = \frac{B_0 nw}{B'_0 a' w'} l \pm \frac{Z^2}{\omega x\,[2B'_0 a' w']^2} F'_T. \qquad (7)$$

The second term of Equation (7) represents the absolute error of measurement which will only equal zero when $F'_T = 0$. The last condition cannot be achieved; and it only remains to strive for a minimum friction force, whose value is determined by the weight of the coil and attached details, the material and quality of finish of the bearing surfaces and those of the guiding wires or sliding contacts.

The relative nominal error due to friction is given by the expression

$$\gamma_{F'_T} = \frac{25Z^2 F'_T}{\omega l'_N B'_0 a' w' B_0 aw}. \qquad (8)$$

Formula (8) indicates the means of lowering $\gamma_{F'_T}$.

Since the error due to friction is the governing factor in determining the accuracy of measurement, the design of the telemetering unit is based on the assumption that the following quantities are known: the length of the receiving unit scale $2l'_N$, the nominal error of measurement K, the coefficient n which is greater than one and accounts for errors other than those due to friction, the friction force F'_T, the impedance of the coil circuits Z (arg $Z = \pi/4$) and the frequency f of the excitation voltage.

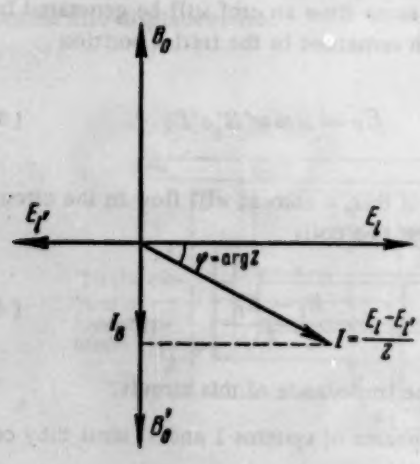

Fig. 5

Formula (9)

$$E_N = 29.8\sqrt{\frac{nfl'_N Z F'_T}{K}} \qquad (9)$$

gives the emf induced in the receiving coil when it is fully deflected. This emf must be equal to the one induced in the coil of the master system when it is also fully deflected.

Since the nominal measured displacement l_{xN} is given, the quantity characterizing the master system is known to us

$$B_0 aw = \frac{E_N}{4\pi f l_{xN}} \qquad (10)$$

as well as that for the receiving system

$$B_0' n' w' = \frac{E_N}{4\pi f l_N'} . \qquad (11)$$

When the dimensions of the magnetic circuit are determined, the number of turns in the coils and the number of ampere turns in the excitation windings do not present any difficulties if the following relationships are also used

$$B_0 = \frac{c}{2l_N} B\sigma,$$

$$c = a, \quad I_B w_B = k_1 \frac{B_0(\delta + \Delta)}{\sigma \mu_0}, \qquad (12)$$

where B is maximum permissible value of magnetic induction in the material of the magnetic circuit, σ is the coefficient of the magnetic flux utilization [1], c is the dimension of the magnetic circuit (Fig. 2), $I_B W_B$ is the number of excitation ampere turns per winding, δ is the air gap, Δ is the gap in the butt joints between the central and side rods of the magnetic circuit, and k is the coefficient accounting for the reluctance of steel.

Experiments conducted with a working model of this unit demonstrated the high efficiency of the magnetic circuit shown in Fig. 2; the magnetic flux utilization coefficient was equal to 0.7.

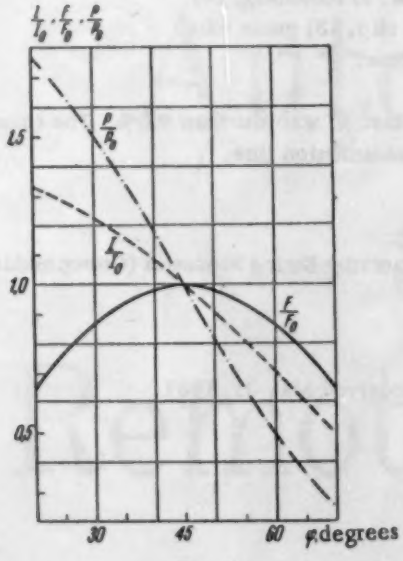

Fig. 6

The ac resistance of the coils and their lead-in wires can be considered as purely resistive; hence the impedance of the transmission line will be given by the formula

$$Z_L \leqslant \sqrt{\left[\frac{Z}{\sqrt{2}} - (r_w' + r_w)\right]^2 + \frac{Z^2}{2}}, \qquad (13)$$

where r_w' and r_w are the resistances of the receiving and master coils and their lead-in wires, respectively.

Figure 6 shows that there is a good reason for departing from condition arg Z = $\varphi = \pi/4$ when r = const., and for increasing the angle φ somewhat, since a small decrease in the controlling force F causes a large decrease in the power P and current I of the coil circuit. This increase in the angle is possible, of course, if the resulting impedance modulus does not exceed that of Z, which was used for calculations.

The working model of the telemetric unit consisted of two similar systems (Fig. 7), each of which had the following characteristics:

height of the magnetic circuit 60 mm;

length of the magnetic circuit 180 mm;

cross section of the central rod a × c = 20 × 20 mm²;

airgaps δ = 3 mm;

length of scale $2l'_N$ = 120 mm;

magnetic circuit material: sheet electric steel E42;

excitation winding (each bobbin) had a number of turns w_B = 411; wire used: enamelled, 0.47 mm diameter; excitation frequency f = 50 cps.

induction in the airgap B_0 = 0.08 v sec /m^2 at excitation current of 0.75 amp; moving coil (frameless) had a number of turns W = 500, of enamelled 0.11 mm diameter wire. friction force F_T^* = 0.08 g.

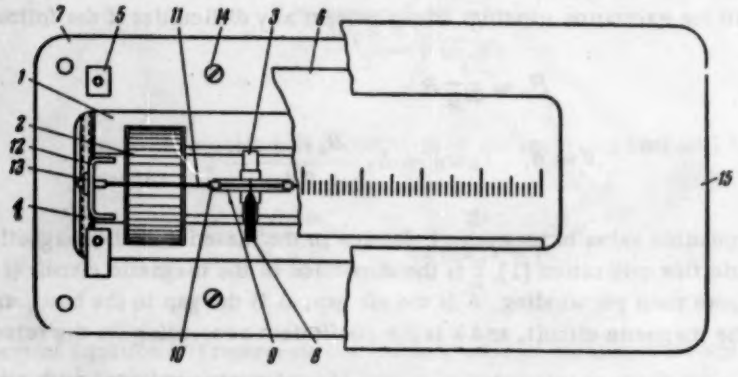

Fig. 7. Telemetering unit receiving system: 1) magnetic circuit, 2) excitation bobbin, 3) moving coil, 4) clamping bolt, 5) scale fixing bracket, 6) scale, 7) mounting plate, 8) pointer, 9) mounting, 10) roller, 11) guiding wire, 12) guide wire fixing clip, 13) guide wire tensioning device, 14) core fixing screw, 15) case.

With a coil-circuit impedance of 270 ohms, the error due to friction was less than 0.5%. The required value of angle φ was obtained by inserting an inductance into the transmission line.

LITERATURE CITED

[1] L. F. Kulikovskii, Electrical Measuring Instruments for Observing Boring Processes (Gostoptekhizdat, 1952).*

Received May 31, 1957

*Gostoptekhizdat – State Fuel Tech. Press – Publisher's note.